STRUCTURAL PERFORMANCE OF INCLINED SHEAR KEY IN STEEL-CONCRETE COMPOSITE CONSTRUCTION

By

RONI DEY

Student ID: 17MEQE006P

A thesis submitted in partial fulfilment of the requirements for the degree of

MASTER of ENGINEERING in EARTHQUAKE ENGINEERING

Institute of Earthquake Engineering Research

CHITTAGONG UNIVERSITY OF ENGINEERING AND TECHNOLOGY

APRIL 2024

This project titled **"Structural Performance of Inclined Shear Key in Steel-Concrete Composite Construction"** submitted by **Roni Dey**, Student ID. No. **17MEQE006P**, Session: **2017-2018** has been accepted as satisfactory in partial fulfilment of the requirements for the degree of **Master of Engineering in Earthquake Engineering [M. Engg. (EQE)]** on 25th April, 2024.

Board of Examination

Prof. Dr. Md. Rabiul Alam — Chairman
Department of Civil Engineering — (Supervisor)
Chittagong University of Engineering & Technology

Prof. Dr. Md. Moinul Islam — Member
Director — (Ex-Officio)
Institute of Earthquake Engineering Research
Chittagong University of Engineering & Technology

Dr. Shafayat Bin Ali — Member
Research Assistant Professor
Institute of Earthquake Engineering Research
Chittagong University of Engineering & Technology

Prof. Dr. Md. Robiul Awall — Member
Department of Civil Engineering — (External)
Rajshahi University of Engineering & Technology

Declaration of Candidate

I hereby declare that the work contained in this thesis has not been previously submitted to meet requirements for an award at this or any other higher educational institution. To the best of my knowledge and belief, the Thesis contains no material previously published or written by another person except where due reference is cited. Furthermore, the Thesis complies with PLAGIARISM and ACADEMIC INTEGRITY regulation of CUET.

RONI DEY
17MEQE006P
Institute of Earthquake Engineering Research
Chittagong University of Engineering & Technology (CUET)

Declaration by the Supervisor

This is to certify that **RONI DEY** has carried out this research work under my supervision, and that he has fulfilled the relevant Academic Ordinance of the Chittagong University of Engineering and Technology, so that he is qualified to submit the following Thesis in the application for the degree of MASTER of ENGINEERING in EARTHQUAKE ENGINEERING. Furthermore, the Thesis complies with the PLAGIARISM and ACADEMIC INTEGRITY regulation of CUET.

DR. MD. RABIUL ALAM

Professor

Department of Civil Engineering

Chittagong University of Engineering & Technology

Acknowledgement

All the praise goes to the Almighty GOD, the most powerful, magnificent and merciful, for the successful completion of this project.

The author would like to express deep gratitude to the honourable supervisor, Dr. Md. Rabiul Alam, Professor, Department of Civil Engineering, CUET for his continuous supervision, proper guidelines, suggestions and encouragement throughout the research work.

The Author expresses deep gratitude to Prof. Dr. Md. Moinul Islam, Director, Institute of Earthquake Engineering Research for motivations, encouragement and continuous support.

Special Thanks to the CUET authority & Engr. Md. Serajul Islam, the honourable Chief Engineer, CUET for giving me the opportunity of higher education along with my job and elevating my knowledge level.

Immeasurable gratitude to all the faculty members of the Institute of Earthquake Engineering Research (IEER) for their proper guidelines and endless support.

Thanks to all the officials and staffs of the institute for their co-operation.

.

Abstract

The use of steel-concrete composite structures is growing in popularity within the construction sector. In steel-concrete composite structure full composite action between steel and concrete is developed using shear connector. Shear connector transfer the transverse shear developed at the interface of steel and concrete. Headed shear stud is the most common type of shear connector which is conventionally welded perpendicularly to the flange surface of the steel beam with zero inclination. Some of the shear connectors unconsciously get welded at an inclined angle during this process. Design equations are not available for inclined shear key in the current design codes like Eurocode 4, CSA S4-14, BNBC-2020, AASHTO LRFD. Here an attempt has been made to investigate the structural performance of inclined shear key in steel-concrete composite construction. A numerical finite element model of push out test of steel-concrete composite structure as per Eurocode is developed using FEA software ANSYS. The developed FE push-out test model for a 19 mm perpendicularly placed headed shear stud is validated and its results are compared with the previous experimental test. The ultimate shear resistance of a perpendicularly welded headed shear stud obtained from FE analysis is found to be very close to that calculated using the BNBC-2020 & AASHTO LRFD recommended design equations. The ultimate shear resistance of 15, 30 & 45-degree inclined headed shear stud is found to be increased by 15 %, 17.33 % & 24 % respectively for the inclination of headed shear stud along the direction of loading and decreased by 56 %, 42.57 % & 46.93 % respectively for inclination opposite to the direction of loading. For inclination along the direction of loading, 15-degree & 30-degree inclined Headed shear stud exhibits ductile behaviour with maximum slip value 10.79 mm & 7.97 mm respectively but for 45-degree inclination headed shear stud is found to be brittle with maximum slip value 3.95 mm. Headed shear studs are

found to be brittle for all the angles of inclination opposite to the direction of loading having maximum slip less than 6 mm, which is the Eurocode 4 recommended minimum threshold for ductile behaviour. Hence, headed shear stud shall be welded to the flange surface very carefully in steel-concrete composite construction. Only if the direction of loading is known, inclined shear keys may be a better choice for enhanced composite action of steel concrete composite structures.

বিমূর্ত

নির্মাণ খাতে স্টীল-কনক্রিট কম্পোজিট স্ট্রাকচারের জনপ্রিয়তা ক্রমাগত বৃদ্ধি পাচ্ছে। স্টিল-কনক্রিট কম্পোজিট স্ট্রাকচারে সিয়ার কানেকটর ব্যবহার করে সম্পূর্ণ কম্পোজিট কার্যক্ষমতা তৈরী করা হয়। সিয়ার কানেকটর স্টিল ও কনক্রিট এর সংযোগস্থলে তৈরী সিয়ার ফোর্স কে স্থানান্তর করে। সিয়ার কানেকটর ওয়েলডিং এর মাধ্যমে স্টিল বিমের সাথে সংযোগ করা হয়।সাধারনত প্রচলিত নিয়মে সিয়ার কানেকটর গুলো স্টিল বিমের উপর উলম্বভাবে কোন ধরনের কৌনিক বিকৃতি ছাড়া ওয়েলডিং করা হয়। কিন্তু ওয়েলডিং এর সময় অসাবধানতা বশত কিছু কিছু সিয়ার কানেকটর কিছুটা হেলানো হতে পারে। প্রচলিত কোডগুলো যেমন ইউরো কোড, বিএনবিসি,কানাডিয়ান কোড বা এস্টো এল আর এফ ডি তে এ ধরনের হেলানো সিয়ার কানেকটরের সিয়ার ধারণ ক্ষমতা নির্ণয় করার কোন সূত্র নেই।এখানে এনসিস সফটওয়্যার এর মাধ্যমে এ ধরনের হেলানো হেডেড সিয়ার কানেকটরের কার্যক্ষমতা নির্ণয় করার প্রচেষ্টা চালানো হয়েছে।প্রথমে তৈরীকৃত নিউমেরিকেল মডেলের গ্রহনযোগ্যতা যাচাই করার জন্য প্রাপ্ত ফলাফলকে পূর্বের ল্যাব টেস্টের ফলাফলের সাথে তুলনা করা হয়েছে।এর পর একই ধরনের ম্যাটারিয়ালস ও অন্যান্য শর্ত প্রয়োগ করে ১৫ ডিগ্রি, ৩০ ডিগ্রি ও ৪৫ ডিগ্রি হেলানো সিয়ার কানেকটর এর জন্য মডেল প্রস্তুত করা হয়েছে। গবেষণার ফলাফলে দেখা গেছে, স্টিল বিমে যে দিক থেকে বল প্রয়োগ করা হয় সিয়ার কানেকটর ঐ দিকে হেলানো থাকলে কানেকটর এর সিয়ার ধারণক্ষমতা ১৫,৩০ ও ৪৫ ডিগ্রি হেলানো কানেকটরের জন্য যথাক্রমে প্রায় ১৫%,১৭.৩৩% ও ২৪% পর্যন্ত বৃদ্ধি পেতে পারে।অন্যদিকে সিয়ার কানেকটর গুলো, স্টিল বিমে যে দিক থেকে বল প্রয়োগ করা হয় তার বিপরীত দিকে হেলানো থাকলে কানেকটরের সিয়ার ধারণক্ষমতা ১৫,৩০ ও ৪৫ ডিগ্রি হেলানোর জন্য যথাক্রমে প্রায় ৫৬%,৪২.৫৭% ও ৪৬.৯৩% পর্যন্ত হ্রাস পায়।এছাড়া বলের অভিমূখে ১৫ ডিগ্রি ও ৩০ ডিগ্রি হেলানো সিয়ার কানেকটর ডাকটাইল আচরণ করে ও ৪৫ ডিগ্রি হেলানো সিয়ার কানেকটর ভঙ্গুর প্রকৃতির আচরণ করে। বলের বিপরীত দিকে ১৫ ডিগ্রি,৩০ ডিগ্রি ও ৪৫ ডিগ্রি হেলানো সিয়ার কানেকটরের প্রত্যেকটি ভঙ্গুর প্রকৃতির আচরণ করে।তাই সিয়ার কানেকটরের ওয়েল্ডিং সতর্কতার সাথে করতে হবে। শুধুমাত্র বলের অভিমূখ নিশ্চিত হওয়া গেলে হেলানো সিয়ার কানেকটর ব্যবহার করে এর অতিরিক্ত সিয়ার ধারণক্ষমতা ও ডাকটিলিটি কাজে লাগানো যেতে পারে।

Table of Contents

Abstract v
বিমূর্ত vii
Table of Contents viii
List of Figures xii
List of Tables xix
Nomenclature xx
List of Symbols xx
Acronyms and Abbreviations xxii
Chapter 1: INTRODUCTION 1
1.1 Background 1
1.2 Problem Statement 5
1.3 Specific Aims And Objectives Of The Research 6
1.4 Scope Of The Research 6
1.5 Thesis Outline 7
Chapter 2: LITERATURE REVIEW 8
2.1 Background 8
2.2 Advantages Of Steel-Concrete Composite Construction 8
2.3 Components Of Steel-Concrete Composite Construction 10
2.4 Mechanism Of Steel Concrete Composite Action 10
2.5 Advantages Of Shear Connector 13
2.6 Different Categories Of Shear Connectors 14
2.6.1 Headed Stud Shear Connectors 14
2.6.2 Perfobond Ribs Shear Connectors 15
2.6.3 Composite Dowel Shear Connector 16
2.6.4 C-Shaped Channel And Angle Shear Connectors 17
2.6.5 Combination Of Different Shear Connectors 19
2.7 Design Codes On Shear Connectors 19
2.7.1 Bangladesh National Building Code (BNBC)-2020 20
2.7.2 AISC 360-16 (2016) 21
2.7.3 CSA S16-09 (2009) 21
2.7.4 Eurocode 4 (2004) 22

2.7.5 JSCE (2005) 23
2.7.6 ACI 318-08 (2008) 23
2.7.7 Channel Connector as per AISC 360-16 (2016) and CSA S16-09 (2009) 24
2.7.8 Channel Shear Connector [Eurocode 4 (CEN 2001)] 25
2.7.9 Angle Shear Connector [Eurocode 4, CEN 2001] 26
2.8 Advantages Of Headed Stud Shear Connector Over Other Shear Connectors 27
2.9 Push Out Test 28
2.10 Previous Research 30
2.10.1 Tests By Slutter and Fisher (1966) 30
2.10.2 Tests By Menzies and Mainstone (1967) 31
2.10.3 Tests by Hallam (1976) 31
2.10.4 Tests by Foley and Oehlers (1985) 31
2.10.5 Tests by Amar Prakash et. el. 31
2.10.6 Numerical study by Md. Manik Mia 32
2.10.7 Numerical study by Huu Thanh Nguyen & Seung Eock Kim 32
2.11 Finite Element Analysis (FEA) Using Ansys 32
2.12 Research Gap 34
Chapter 3: METHODOLOGY 35
3.1 Introduction 35
3.2 Geometry Of Push Out Test 35
3.3 Material Properties 40
3.3.1 Concrete 40
3.3.1.1 Identifying Coupled Damage-Plasticity Microplane Model Parameters 41
3.3.2 Structural Steel 45
3.3.3 Reinforcement 46
3.3.4 Headed Shear Stud 47
3.4 Boundary Conditions 48
3.5 Contact And Interactions 50
3.5.1 Contact Between Concrete Slab and Steel Beam 50
3.5.2 Contact Between Steel Beam Flange and Headed Shear Stud 51
3.5.3 Contact Between Concrete Slab And Headed Shear Stud 52
3.5.4 Surface To Surface Contact & Target Modelling 54
3.6 Finite Element Meshing & Element Selection 55

3.6.1 Mesh Convergence Study 56
3.6.2 Meshing of Concrete Slab & Element selection 57
3.6.3 Meshing of Steel Beam & Element selection 58
3.6.4 Meshing of Headed Shear stud & Element selection 60
3.6.5 Meshing of Reinforcement & Element selection 61
3.6.6 Mesh Quality Check 63
3.7 Analysis Settings And Solution Strategy 67
Chapter 4: RESULTS AND DISCUSSIONS 69
4.1 General 69
4.2 Preliminary Validation Of The Finite Element Model 69
4.3 Comparison of FE Analysis Results with CSA S6-14, bnbc-2020, & AASHTO LRFD 71
4.3.1 Ultimate Shear Resistance According to CSA S6-14: 71
4.3.2 Ultimate Shear Resistance According to BNBC-2020: 72
4.3.3 Ultimate Shear Resistance According to AASHTO LRFD: 73
4.4 Fe Analysis Results For Perpendicular Headed Shear Stud 74
4.4.1 Load Slip Curve 74
4.4.2 Principal Stress Distribution at Concrete Slab 75
4.4.3 Von Mises Stress Distribution at Headed Shear Stud 77
4.4.4 Shear Stress (X-Y Plane) Distribution in Concrete Slab 79
4.4.5 Shear Stress Distribution In Headed Shear Stud 80
4.4.6 Damage Identification 80
4.4.7 Force and Displacement Convergence 83
4.5 Finite Element Analysis Results For 15 Degree Inclined Headed Shear Stud 84
4.5.1 Load slip curve 84
4.5.2 Principal stress distribution at concrete slab 85
4.5.3 Von Mises stress distribution at headed shear stud 87
4.5.4 Shear Stress (X-Y Plane) distribution in concrete slab 88
4.5.5 Shear Stress distribution in headed shear stud 88
4.5.6 Damage Identification 89
4.5.7 Force and Displacement Convergence 92
4.6 FE Analysis Results For 30 Degree Inclined Headed Shear Stud 93
4.6.1 Load Slip Curve 93

4.6.2 Principal Stress Distribution At Concrete Slab 94
4.6.3 Von Mises Stress Distribution At Headed Shear Stud 96
4.6.4 Shear Stress (X-Y Plane) Distribution In Concrete Slab 97
4.6.5 Shear Stress Distribution In Headed Shear Stud 98
4.6.6 Damage Identification 98
4.6.7 Force and Displacement Convergence 101
4.7 FE Analysis Results For 45 Degree Inclined Headed Shear Stud 102
4.7.1 Load Slip Curve 102
4.7.2 Principal Stress Distribution At Concrete Slab 103
4.7.3 Von Mises Stress Distribution At Headed Shear Stud 105
4.7.4 Shear Stress (X-Y Plane) Distribution In Concrete Slab 107
4.7.5 Shear Stress Distribution In Headed Shear Stud 108
4.7.6 Damage Identification 108
4.7.7 Force and Displacement Convergence 111
4.8 Comparison Of FE Analysis Results For Perpendicular & Inclined Headed Shear Stud (HSS) 111
4.8.1 Ultimate Shear Resistance & Maximum Displacement 112
4.8.2 Variation of Principal Stress in Concrete Slab 114
4.8.3 Variation of Compression Damage of Concrete Slab 117
Chapter 5: CONCLUSIONS & RECOMMENDATIONS 118
5.1 Conclusions 118
5.2 Recommendations For Future Study 120
REFERENCES 121
APPENDICES 130
A 1.1 Coupled Damage-Plasticity Microplane Model APDL Code Input in ANSYS 130

List of Figures

Fig. No.	Figure Caption	Page No.
Fig. 1.1	Large Span Steel Concrete Composite Floor System	4
Fig. 1.2	Components of Steel-Concrete Composite Floor	4
Fig. 2.1	Components of steel concrete composite structure	10
Fig. 2.2	Deflected Shape of Composite and non-composite Beams	12
Fig. 2.3	Strain Variation in Non composite and Composite Beams	12
Fig. 2.4	Headed Stud Shear Connectors	13
Fig. 2.5	Load transmission mechanism of headed stud shear connector in solid concrete slab	14
Fig. 2.6	Perfobond rib shear connectors	15
Fig. 2.7	Y-shaped perfobond rib shear connectors	16
Fig. 2.8	Composite dowel shear connector	17
Fig. 2.9	(a) Channel shear connector, (b) angle shear connector	18
Fig. 2.10	Different systems of shear connectors used for the West Coast region and Canterbury composite bridges	18
Fig. 2.11	Headed stud shear connectors with a single perfobond rib	19
Fig. 2.12	Rigid channel shear connector and the parameters of rigid shear connectors	26
Fig. 2.13	Representative L-shaped angle shear connector	27

Fig. 2.14	Push-out test arrangement as per Eurocode 4	29
Fig. 2.15	Slip capacity determination as per Eurocode 4	30
Fig. 3.1	Geometry of push-out test specimen	35
Fig. 3.2	Headed shear stud	36
Fig. 3.3	Push-out Test Specimen	37
Fig. 3.4	Smooth three-surface microplane cap yield function	38
Fig. 3.5	Stress-Strain Relationship for Structural Steel	44
Fig. 3.6	Stress-Strain Relationship for Reinforcement	45
Fig. 3.7	Stress-Strain Relationship for Headed Shear Stud	46
Fig. 3.8	Z-Axis symmetric Boundary Condition	46
Fig. 3.9	X-Axis Symmetric Boundary Condition	47
Fig. 3.10	Fixed Support at the Bottom Surface of the Concrete Slab	47
Fig. 3.11	Displacement Loading: (a) Downward (Push), (b) Upward (Pull)	48
Fig. 3.12	Frictionless Contact Between Steel Beam Flange & Concrete Slab	49
Fig. 3.13	Bonded Contact Between Steel Beam Flange & Headed Shear Stud	50
Fig. 3.14	Frictional Contact Between Concrete & Headed Shear Stud	51
Fig. 3.15	CONTA174 Geometry	52
Fig. 3.16	TARGE170 Geometry	53
Fig. 3.17	Mesh Convergence Study	54
Fig. 3.18	Linear Cartesian Mesh of Concrete Slab	55

Fig. 3.19	CPT215 Structural Solid Geometry	56
Fig. 3.20	Linear Cartesian Mesh of Steel Beam	56
Fig. 3.21	SOLID185 Structural Solid Geometry	57
Fig. 3.22	Linear Tetrahedral Meshing of Headed Shear Stud	58
Fig. 3.23	Solid285 Structural Solid Geometry	58
Fig. 3.24	Meshing of Reinforcement	59
Fig. 3.25	REINF264 used with 3-D 8-Node brick element CPT215	60
Fig. 3.26	Element Quality	61
Fig. 3.27	Aspect Ratio	61
Fig. 3.28	Jacobian Ratio	62
Fig. 3.29	Warping Factor	62
Fig. 3.30	Maximum Corner Angle	63
Fig. 3.31	Skewness	64
Fig. 3.32	Newton Raphson Iteration Method	65
Fig. 4.1	Validation of FE Push-Out Test Model with Experimental Test	67
Fig. 4.2	Comparison of Ultimate Shear Strength of Headed Shear Stud obtained from CSA S6-14, BNBC-2020, AASHTO LRFD & FE Analysis	71
Fig. 4.3	Load Slip Curve for Perpendicular Headed Shear Stud	72
Fig. 4.4	Principal Stress Distribution in Concrete Slab	73
Fig. 4.5	Factor of Safety of Concrete Slab	74
Fig. 4.6	Equivalent Von Mises Stress Distribution at Headed Shear Stud	75

Fig. 4.7	Factor of Safety of Headed Shear Stud	75
Fig. 4.8	Shear Stress (X-Y Plane) Distribution in Concrete Slab	76
Fig. 4.9	Shear Stress Distribution in Headed Shear Stud	77
Fig. 4.10	Compression Damage for Perpendicular Headed Shear Stud	78
Fig. 4.11	Tension Damage for Perpendicular Headed Shear Stud	79
Fig. 4.12	Force Convergence for Perpendicular Headed Shear Stud	80
Fig. 4.13	Displacement Convergence for Perpendicular Headed Shear Stud	80
Fig. 4.14	Comparison of Load Slip Curve for Perpendicular and 15 Degree Inclined Headed Shear Stud (HSS)	81
Fig. 4.15	Principal Stress Distribution in Concrete Slab for 15 Degree Inclined HSS	82
Fig. 4.16	Factor of Safety of Concrete Slab for 15-Degree Inclined Headed Shear Stud	83
Fig. 4.17	Von Mises stress distribution at 15-degree inclined headed shear stud	84
Fig. 4.18	Factor of Safety of 15-Degree Inclined Headed Shear Stud	84
Fig. 4.19	Shear Stress (X-Y Plane) distribution in concrete slab	85
Fig. 4.20	Shear Stress (X-Y Plane) distribution in 15-Degree Inclined Headed Shear Stud	86
Fig. 4.21	Compression Damage for 15-Degree Inclined Headed Shear Stud	87
Fig. 4.22	Tension Damage for 15-Degree Inclined Headed Shear Stud	88

Fig. 4.23	Force Convergence for 15-Degree Inclined Headed Shear Stud	89
Fig. 4.24	Displacement Convergence for 15-Degree Inclined Headed Shear Stud	89
Fig. 4.25	Comparison of Load Slip Curve for Perpendicular and 30 Degree Inclined Headed Shear Stud (HSS)	90
Fig. 4.26	Principal Stress Distribution in Concrete Slab for 30 Degree Inclined HSS	91
Fig. 4.27	Factor of Safety of Concrete Slab for 30-Degree Inclined Headed Shear Stud	92
Fig. 4.28	Von Mises stress distribution at 30-degree inclined headed shear stud	93
Fig. 4.29	Factor of Safety of 30-Degree Inclined Headed Shear Stud	93
Fig. 4.30	Shear Stress (X-Y Plane) distribution in concrete slab	94
Fig. 4.31	Shear Stress (X-Y Plane) distribution in 30-Degree Inclined Headed Shear Stud	95
Fig. 4.32	Compression Damage for 30-Degree Inclined Headed Shear Stud	96
Fig. 4.33	Tension Damage for 30-Degree Inclined Headed Shear Stud	97
Fig. 4.34	Force Convergence for 30-Degree Inclined Headed Shear Stud	98
Fig. 4.35	Displacement Convergence for 30-Degree Inclined Headed Shear Stud	98
Fig. 4.36	Comparison of Load Slip Curve for Perpendicular and 45 Degree Inclined Headed Shear Stud (HSS)	99

Fig. 4.37	Principal Stress Distribution in Concrete Slab for 45 Degree Inclined HSS	100
Fig. 4.38	Factor of Safety of Concrete Slab for 45-Degree Inclined Headed Shear Stud	101
Fig. 4.39	Von Mises stress distribution at 45-degree inclined headed shear stud	102
Fig. 4.40	Factor of Safety of 45-Degree Inclined Headed Shear Stud	103
Fig. 4.41	Shear Stress (X-Y Plane) distribution in concrete slab	104
Fig. 4.42	Shear Stress (X-Y Plane) distribution in 45-Degree Inclined Headed Shear Stud	105
Fig. 4.43	Compression Damage for 45-Degree Inclined Headed Shear Stud	106
Fig. 4.44	Tension Damage for 45-Degree Inclined Headed Shear Stud	107
Fig. 4.45	Force Convergence for 45-Degree Inclined Headed Shear Stud	108
Fig. 4.46	Displacement Convergence for 45-Degree Inclined Headed Shear Stud	108
Fig. 4.47	Comparison of Load Slip Curve for Perpendicular & 15,30,45 Degree Inclined Headed Shear Stud (HSS) Subjected to Downward (Push) Displacement Loading	110
Fig. 4.48	Comparison of Load Slip Curve for Perpendicular & 15,30,45 Degree Inclined Headed Shear Stud (HSS) Subjected to Upward (Pull) Displacement Loading	111
Fig. 4.49	Principal Stress Distribution in Concrete Slab for Perpendicular Headed Shear Stud (HSS)	112

Fig. 4.50 Principal Stress Distribution in Concrete Slab for 15 Degree Inclined Headed Shear Stud (HSS) 112
Fig. 4.51 Principal Stress Distribution in Concrete Slab for 30 Degree Inclined Headed Shear Stud (HSS) 113
Fig. 4.52 Principal Stress Distribution in Concrete Slab for 45 Degree Inclined Headed Shear Stud (HSS) 113
Fig. 4.53 Variation of Compression Damage of Concrete Slab 114

List of Tables

Table No.	Table Caption	Page No.
Table 3.1	Dimensions Of Headed Shear Stud Used in FE Analysis	38
Table 3.2	Coupled Damage-Plasticity Microplane Model Parameters	43
Table 3.3	Properties Of Structural Steel	45
Table 3.4	Properties Of Reinforcement	46
Table 3.5	Properties Of Headed Shear Stud	47
Table 3.6	Maximum Force Reaction for Different Element Size of Concrete Slab	56
Table 3.7	ANSYS Recommended Scale for Skewness	67
Table 4.1	Comparison Between Experimental and FE Analysis Results	70
Table 4.2	Comparison of Ultimate Shear Strength of Headed Shear Stud obtained from CSA S6-14, BNBC-2020, AASHTO LRFD & FE Analysis	74
Table 4.3	Ultimate Shear Resistance & Maximum Displacement	112

Nomenclature

List of Symbols

Symbol	Meaning	Unit	Section
M_{slab}	Moment Resisted by Concrete Slab	Nm	2.4
M_{beam}	Moment Resisted by Steel Beam	Nm	2.4
$\sum M$	Total Resisting Moment	Nm	2.4
Asc	Cross Sectional Area of Headed Shear Stud	mm^2	2.7.1
Ec	Modulus of Elasticity of concrete	MPa	2.7.1
f'_c	Compressive Strength of Concrete	MPa	2.7.1
w_c	Unit Weight of Concrete	kg/m^3	2.7.1
Fu	Tensile Strength of Headed Shear Stud	MPa	2.7.1
Rg	Group Effect Factor	--	2.7.1
Rp	Position Effect Factor	--	2.7.1
t_f	Flange Thickness	mm	2.7.1
t_w	Web Thickness	mm	2.7.1
L_c	Length	mm	2.7.1
q_r	Performance Factored resistance	N	2.7.3
φ_{sc}	Shear Connector's Resistance Factor	--	2.7.3
h	Shear Stud's Height	mm	2.7.3
d	Shear Stud's Diameter	mm	2.7.3

γ_v	$safety\ factor\ for\ shear\ resistance$	--	2.7.4
n	total number of anchors in the group	--	2.7.6
P_{Rd}	The Design Resistance	N	2.7.8
A_{f1}	Front surface area	mm^2	2.7.8
A_{f2}	Enlarged front surface area considering slope 1: 5	mm^2	2.7.8
γ_c	safety factor	--	2.7.8
F_{ck}	Compressive Strength of Concrete	MPa	2.7.8
ν	Poisson's Ratio	--	3.3.1
f_{uc}	Uniaxial Compressive Strength	MPa	3.3.1
f_{bc}	Biaxial Compressive Strength	MPa	3.3.1
f_{ut}	Uniaxial Tensile Strength	MPa	3.3.1
σ_v^c	Intersection point abscissa between compression cap and dracker-prager yield function	MPa	3.3.1
R	Ratio between the major and minor axis of the cap	--	3.3.1
D	Hardening material constant	MPa^2	3.3.1
R_T	Tension cap hardening constant	--	3.3.1
γ_{co}	Compression Damage Thresholds	--	3.3.1
γ_{to}	Tension Damage Thresholds	--	3.3.1
β_t	Tension Damage Evolution Constant	--	3.3.1
β_c	Compression Damage Evolution Constant	--	3.3.1
c	Nonlocal interaction range parameter	mm^2	3.3.1
m	Over-nonlocal averaging parameter	--	3.3.1

Acronyms and Abbreviations

EC	Eurocode
CSA	Canadian Standard Association
BNBC	Bangladesh National Building Code
AISC	American Institute of Steel Construction
ANSYS	Analysis System
FEA	Finite Element Analysis
RCC	Reinforced Cement Concrete
FEM	Finite Element Method
HSS	Headed Shear Stud
ASCE	American Society of Civil Engineers
JSCE	Japan Society of Civil Engineers
ACI	American Concrete Institute
CEN	Commission for European Normalization
AASHTO	American Association of State Highway and Transportation Officials
LRFD	Load and Resistance Factor Design
CDPM	Concrete Damage Plasticity Model
DOF	Degree of Freedom
CPT	Coupled Pore-pressure Thermal
APDL	Ansys Parametric Design Language

Chapter 1: INTRODUCTION

1.1 BACKGROUND

Composite structural members are composed of two or more distinct materials. The capability to combine the abilities of individual material to generate a single unit that functions better overall than its discrete basic parts is the primary advantage of composite elements. Steel-concrete composites are the most widely used composite component in construction, although there are other varieties as well, such as timber-steel, concrete-timber, concrete-plastic and so forth.

Concrete is a material that resists less in tension yet performs well in compression. On the other hand, steel has a very high tensile strength, even when used minimally. Concrete-steel composite elements, which are widely used for structures like bridges, warehouses, sheds, and multi-story buildings, combine the higher compression carrying capacity of concrete with the higher tension-resistance of steel to create a lightweight, highly effective unit.

Several advantages are associated with composite constructions that can assist individuals in coastal and earthquake-prone areas in developing sustainable housing. Composite structures and the sensational demand for accommodations can have a big impact on social, financial, and economic aspects of life. Bangladesh and other developing nations in Asia find it difficult to meet the housing needs of an expanding middle class. The shoring of labour costs and the charge of building constituents is the reason for the high rent in housing. Therefore, the majority of residents with lower to middle class incomes are now concerned about affordable, sustainable housing. The superior structural performance and durability of composite structures have led to an

increasing use of these structures in seaside and earthquake-prone areas. In contrast to conventional building materials like brick and concrete, they are lightweight. For having a high strength-to-weight ratio, which means they can support heavy loads without being bulky or heavy themselves, makes them an ideal choice for structures like buildings, bridges, and towers that must be strong and lightweight. They can be designed to be flexible, which allows them to bend and absorb the energy of these forces without breaking or collapsing [1].

Composite structures can be tailored to fulfill particular design specifications. This means that they can be used to create unique and innovative structures tailored to the needs of people in coastal and earthquake-prone locations. The slab thickness of the composite structure is small. After major earthquakes or tsunamis, the destroyed composite structural materials are less than conventional RCC structures. Therefore, the wasted materials can be easily moved to another place quickly, and the rescue program can start immediately. Composite structures are sustainable and eco-friendly. They can be recycled and reused. This makes them an ideal choice for people looking for sustainable accommodations with minimal environmental impact. Composite structures need a reduced amount of time to build than pure RCC structures, which reduces overall costs [1].

For full composite action, it is required to transfer the horizontal shear forces developed at the interface of steel beam and concrete slab. Shear connectors are welded to the steel beam flange and embedded in the concrete slab to transfer the horizontal shear forces. Shear connectors can boost a girder's load-carrying capacity by about 50% when compared to non-composite girders [2].

Fig. 1.1 Large Span Steel Concrete Composite Floor System [5]

In composite structures, headed stud shear connectors are frequently used to join concrete slabs to steel beams; however, if they fail, the structure may collapse. Longitudinal shear transmission between the steel and concrete components is the fundamental component of composite structures. The main mechanisms for longitudinal shear transfer are chemical bonding, friction, and mechanical interaction of interfacial media. In the design and analysis of composite structures, friction and mechanical actions are important, but chemical bonding is frequently disregarded [3]. Shear connectors embedded into composite structures' concrete can achieve mechanical interaction. The characteristics of the concrete determine the shear load transferring part when shear connectors are embedded into composite structures. The compression zone area is usually increased by the shear connector. Additionally, it turns on slab reinforcement in the compressive and tensile areas. The concrete layer receives the longitudinal shear load

transfer from it. It helps transport larger loads to the steel beam. Shear connectors are typically made of mild steel, but their strength is an important factor in increasing the system's overall efficiency [4]. The design strength of the shear connections is ascertained by means of numerical push-out tests and experiments. Only the equations and values are included in the present design codes like EC4, CSA-S16, BNBC and AISC 360-16 for perpendicularly placed headed shear stud with zero inclination. However, neither the literature nor the most recent design standards, such as BNBC (2020), provide information to determine the shear carrying capacity or performance of inclined headed stud shear connectors. In this numerical study, an effort has been made to determine the load-slip behaviour and shear strength of inclined headed shear studs in steel concrete composite construction by finite element analysis using ANSYS software.

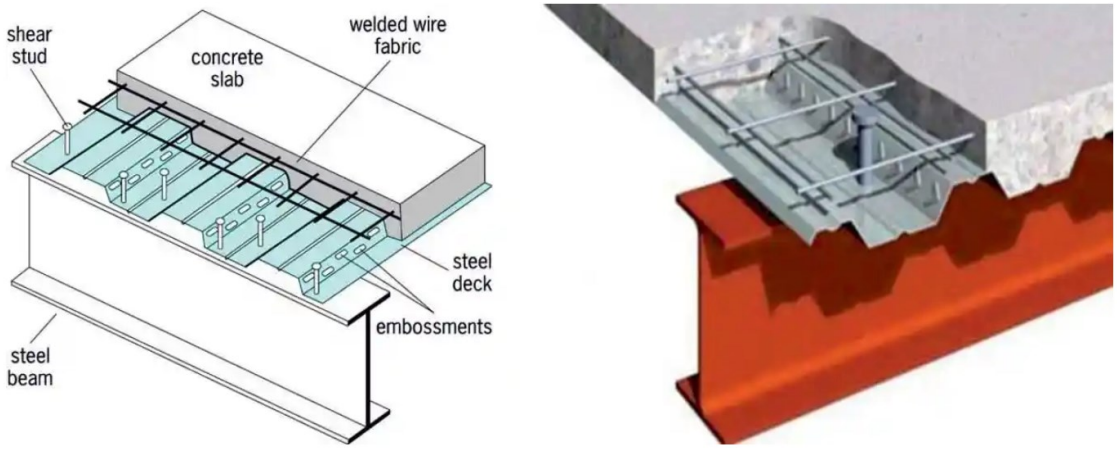

Fig. 1.2 Components of Concrete Steel Composite Floor [6]

This section includes an overview of the findings of this numerical study, along with its contributions and relevance. This research explores the structural performance of the inclined shear key in concrete steel composite structure by finite element analysis (FEA) using ANSYS software. The study's background is conferred in Segment 1.1, and Sector 1.2 covers the problem statement. The research aims & objectives are offered in Section

1.3, while the scope of the research is covered in Segment 1.4. An outline of the residual chapters in the thesis is provided in section 1.5.

1.2 PROBLEM STATEMENT

The steel-concrete composite framing system as presented in Fig. 1.2, consists of RCC/Steel/Composite column and steel concrete composite deck floor system. The best qualities of each material are combined in an incredibly effective way to maximize construction methods. A shaped steel deck and concrete slab are joined to a rolled or built-up steel beam, which is the most typical configuration seen in composite floor systems. By creating a stiff horizontal diaphragm, the composite floor system distributes seismic and wind shears to the lateral load-resisting systems and stabilizes the building system as a whole. By roughly two and three times, respectively, the load carrying capacity and stiffness (i.e., deflection reduction) are increased by composite action [7]. Shear connectors guarantee that the section behaves compositely, while steel supplies the tension element and concrete forms the compression flange. The effectiveness of the composite action depends on the shear transfer capacity, load-slip behaviour, stiffness, ductility and failure mode of the shear connector due to the application of load.

Usually widely used headed stud type shear connectors are welded perpendicularly to the surface of the flange of steel beam with zero inclination. Some of the shear connectors unconsciously get welded at an inclined angle during this process. The assumption of composite action may be invalidated if inclined shear studs are incapable to transfer adequate forces to the nearby concrete to develop full composite actions. Nevertheless, depending on the direction of the inclined angle with respect to the loading direction, inclined shear studs may also likely provide an increased ultimate load capacity. When shear connectors are inclined in the reverse way of the applied load, inclination helps the shear connector to claw the concrete effectively and resist more lateral movement. If shear carrying capacity and stiffness of shear connector can be improved by the inclination,

construction having greater span will be possible using smaller steel section, deflection will be within control and overall construction cost will be minimized.

1.3 SPECIFIC AIMS AND OBJECTIVES OF THE RESEARCH

- To develop the finite element model of the standard push-out test of steel concrete composite structure according to Eurocode 4 using FEM based ANSYS software.
- Validation of the standard push out test numerical model having perpendicularly placed headed shear stud with the previous experimental test results.
- To investigate the load-slip behaviour of inclined headed shear stud having inclination angle 15-degree, 30-degree & 45-degree subjected to downward and upward displacement along the longitudinal axis of the steel beam in steel concrete composite structure.
- To investigate the ductility characteristics of different inclined shear key which is an important parameter for lateral load resistance in concrete steel composite structure.
- Analysing the overall structural performance like ultimate shear load resistance & maximum slip of the inclined shear key, to suggest an optimization of inclination of the headed shear stud for the best performance in concrete steel composite construction.

1.4 SCOPE OF THE RESEARCH

The scope of the study includes developing of finite element model of standard push out test using finite element-based software ANSYS to investigate the behaviour of steel concrete composite structure. The study emphases on the investigation of load-slip behaviour, failure pattern, stress distribution and other relevant properties of steel-concrete composite structures. The developed finite element model will consider

nonlinear material behaviour, interface conditions and complex geometries to realistically capture the structural response. For ideal condition headed shear stud will be considered as placed perpendicularly with the flange surface of steel section. To validate the numerical model, the load-slip curve achieved from numerical finite element analysis will be compared with the previous experimental results. In further study, the FE model will be developed for inclined headed shear studs. Inclined headed shear studs will be considered as placed at inclination angle 15-degree, 30-degree and 45-degree with the flange surface. The load-slip curve and ultimate shear resistance of the inclined headed shear studs will be compared with the perpendicularly placed headed shear studs (HSS). Considering the overall structural performance, the best orientation angle of the inclined headed shear studs will be determined.

1.5 THESIS OUTLINE

This report is arranged into 05 chapters. In the present chapter contextual of the study, problem statement, scope, aims & objectives of the research are introduced.

Chapter 2 presents an overall literature study on different categories of shear keys and their performance in composite beam construction for buildings and bridges, different codes, Finite element modelling, push out test of steel concrete composite structure etc.

In Chapter 3, Methodology describes the development procedure of finite element model of push out test.

In Chapter 4, data analysis, load-slip curve validation with the experimental results, load-slip curve for different inclined headed shear stud, overall results and discussions are covered.

In Chapter 5, the project work's conclusions, and future recommendations are presented.

Chapter 2: LITERATURE REVIEW

2.1 BACKGROUND

In order to prevent longitudinal slippage and separation between the two materials, shear connectors are used to join the concrete and steel components of the steel-concrete composite structure. [8]. For many years, composite structural systems have been utilized in a range of applications, such as bridge construction, to optimize material efficiency. Globally, the use of steel-concrete composite construction is growing in popularity as a substitute to only steel and only concrete construction. However, for Bangladesh's construction industry, this steel-concrete composite construction system is a relatively new idea [7]. It is going popular day by day due to its several special features.

2.2 ADVANTAGES OF STEEL-CONCRETE COMPOSITE CONSTRUCTION

A clear and concise explanation of the effectiveness and adaptability of composite construction is that steel and concrete behave identically in compression & tension respectively. By linking the two materials as a structure, these advantages can be combined to create a lightweight, extremely competent design that is capable of withstanding both axial and flexural forces.

Since this is the most practical and cost-effective approach for low storied buildings, reinforced concrete (RC) members are employed in the framing arrangement for the majority of constructions. However, because of the higher dead load, decreased stiffness, limited span, and dangerous formwork, this sort of structure is no longer profitable for medium-to high-rise buildings. For medium-to high-rise buildings, steel-concrete composite frame systems can offer an efficient and cost-effective solution to the majority

of these issues [7]. A cost versus story curve demonstrates that the RCC frame method is less expensive than the composite system for low-rise structures. However, composite construction becomes economical than RCC construction for buildings with more than 15 stories [7]. ASCE research indicates that the extreme shear strength of a floor slab can be improved by 85% through the use of steel-concrete composite. [9]. The following are additional advantages and benefits:

- The building sector needs improved inventions to overcome the threat of natural calamities like earthquakes, cyclones, etc. The mass of the structure is crucial to its functional performance in the case of such natural disasters. Because of this, it is necessary to lessen the structure's load or mass. Steel-concrete composite structural system is 25 percent lighter than conventional reinforced concrete construction. Owing to the light weightiness of steel-concrete composite system site erection and installation are relatively easy and labour cost minimization is possible [9]
- Using comparatively small cross sectional area higher strength than the conventional RC construction can be achieved.
- Due to the light weight of concrete steel composite system forces in the supporting structural components can be reduced and foundation cost can also be minimized.
- The expensive steps involved in old-style concrete forming, such as supporting, stripping, and other temporary works, are eliminated with composite systems.
- Steel concrete composite system allows to span longer distance without providing intermediate columns.
- Subsequent floors can be casted without waiting for the formerly cast floors to solidify. The composite floor is positively moment-reinforced by the steel decking system, which requires minimal temperature bars to prevent cracking.

- easy handling, quick construction work, convenient transportation are possible in steel concrete composite construction.

2.3 COMPONENTS OF STEEL-CONCRETE COMPOSITE CONSTRUCTION

A solid cast-in-place concrete slab is either positioned on top and connected to a steel I-shaped girder in a steel concrete composite structure. The most common method for casting concrete slabs is onto a cold-formed steel deck, which is supported by an I-shaped section of steel. Shear connectors keep the concrete slab and steel beam joined. Shear connectors prevent slippage between the steel beam and concrete slab by transferring the horizontal shear forces. Different components of steel-concrete composite structure are revealed in Fig. 2.1.

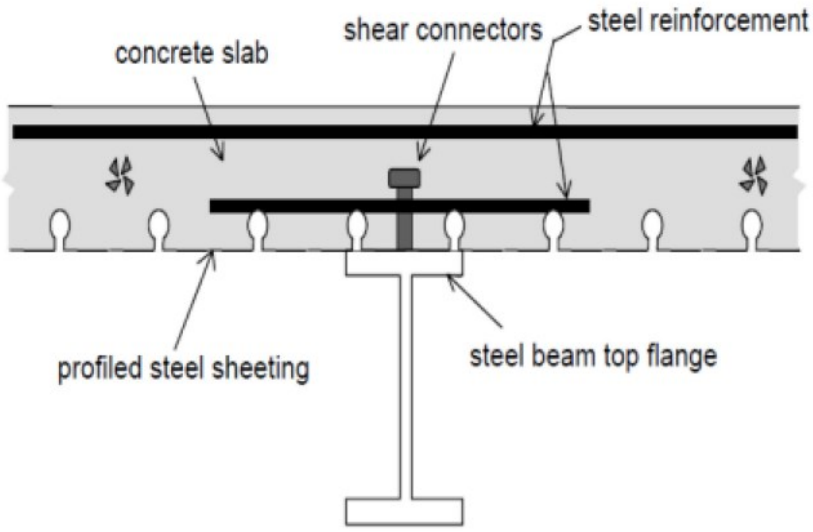

Fig. 2.1 Components of steel concrete composite structure [2]

2.4 MECHANISM OF STEEL CONCRETE COMPOSITE ACTION

When the reinforced concrete slab and supporting steel beam (Fig. 2.2.a) are innately connected and bend as a single unit, as illustrated in Fig. 2.2.b, composite action is developed. The measures taken to guarantee the development of a single linear strain between the top of the concrete slab and the bottom of the steel beam will determine how

much composite action develops. If the friction between the concrete slab and steel beam is disregarded, the concrete slab and steel beam individually bear a portion of the load in the non-composite beam (Fig. 2.2.a). When a non-composite beam bends under the force of gravity, its top surface is compressed and its bottom surface is in tension due to the deformation of the concrete slab. As a result, the plane of contact will experience a discontinuity. Only the vertical internal force will operate between the steel beam and the concrete slab because friction is ignored. Between the concrete slab and steel beam, there is no relative slip when complete composite action develops (Fig. 2.3.c). The concrete slab is compressed, shortened, and the steel beam is extended by horizontal shear forces acting at their interface. When there is no interaction between the concrete slab and steel beam in a non-composite, the total resisting moment equals

$$\sum M = M_{slab} + M_{beam} \tag{2.1}$$

Here,

M_{slab} = Moment Resisted by Concrete Slab

M_{beam}= Moment Resisted by Steel Beam

$\sum M$ = Total Resisting Moment

The neutral axes of the slab and the beam are closer to each other when there is partial interaction between the concrete slab and the steel beam, as seen in Fig. 2.3.b. The limited interaction will cause the straight slip to lessen. The result of the partial interaction is the partial development of the maximum tension and compression forces, C and T, in the steel beam and concrete slab, respectively. The counterattacking moment of the section then augmented by Te or Ce. When full interaction, also called a full composite action, is developed between the slab and the beam, no slippage occurs; the strain diagram that emerges is shown in Fig. 2.3.c. There is only one neutral axis in this situation, and it is situated beneath the slab and above the beam. Moreover, the tensile and compressive

forces, C_1 and T_1, respectively, are larger than the partial interaction forces. The fully developed composite section's resisting moment then becomes [10].

$$\sum M = T_1 e_1 \quad \text{or} \quad C_1 e_1 \tag{2.2}$$

Here,

T_1= Tensile Force & C_1= Compressive Force

e_1= Distance Between the Line of Action of Compressive and Tensile Force

$\sum M$= Total Moment Resisted by the Fully Developed Composite Section

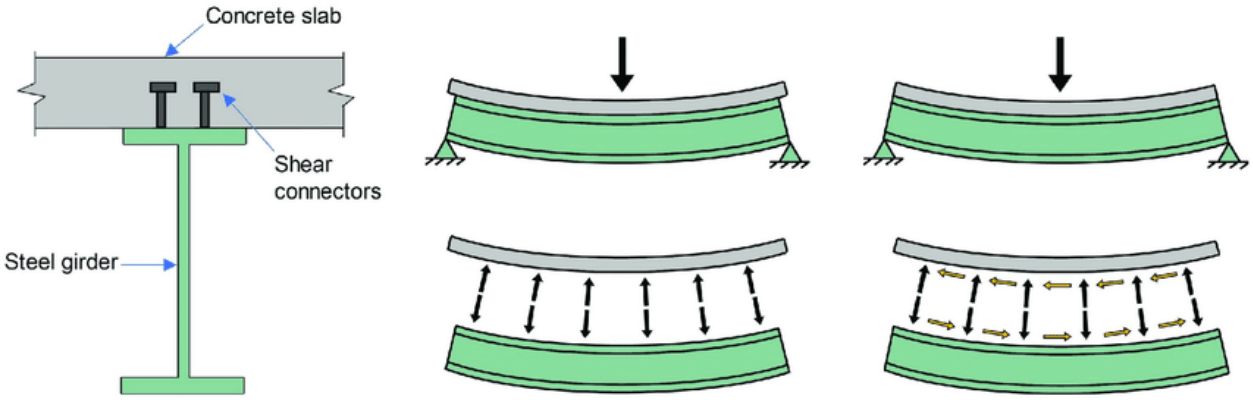

(a) (b) (c)

Fig. 2.2 Deflected shape of composite and non-composite beams [2]

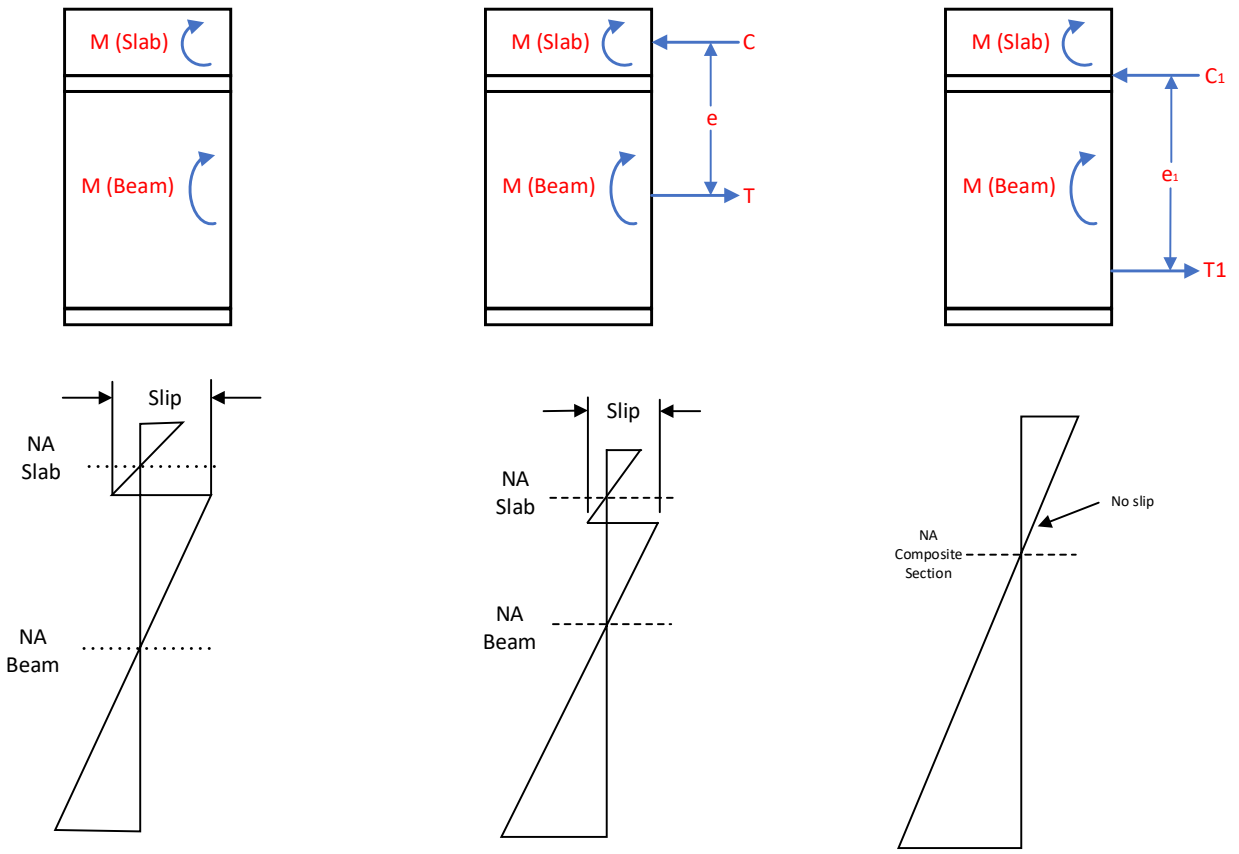

(a) No Interaction (b) Partial Interaction (c) Full Composite Action

Fig. 2.3 Strain Variation in Non composite and Composite Beams

2.5 ADVANTAGES OF SHEAR CONNECTOR

- Shear connectors provide strong resistance against shearing failure in composite structures and have a high load bearing capacity.
- During construction, a very high rate of production is possible.
- Operating ease while construction is underway. For welding, there is no specific skill needed.
- Adaptability in building design.
- To create a concrete slab, Shear Connectors can be welded through Deck Sheets.
- Sturdy, long-lasting, steady, and earthquake-resistant

2.6 DIFFERENT CATEGORIES OF SHEAR CONNECTORS

2.6.1 Headed Stud Shear Connectors

The headed studs seen in Fig. 2.4 are the shear connectors that are most frequently utilized in industries. They provide steel shanks with an anchorage head to prevent slabs in composite structures from shifting vertically and that can withstand longitudinal shear forces (Ollgaard et al. [11]). Typically, specialized welding equipment is needed to connect a headed stud in a steel girder beam. Ideally, the strength of welding will be higher than the stud strength. But when these joints are repeatedly loaded, fatigue issues typically arise [12] [13] [14]. Numerous studies on stud connectors have been conducted since Viest invented the headed stud shear connector seven decades ago [15].

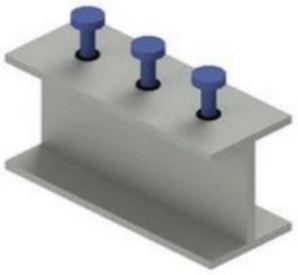

Fig. 2.4 Headed Stud Shear Connectors [11]

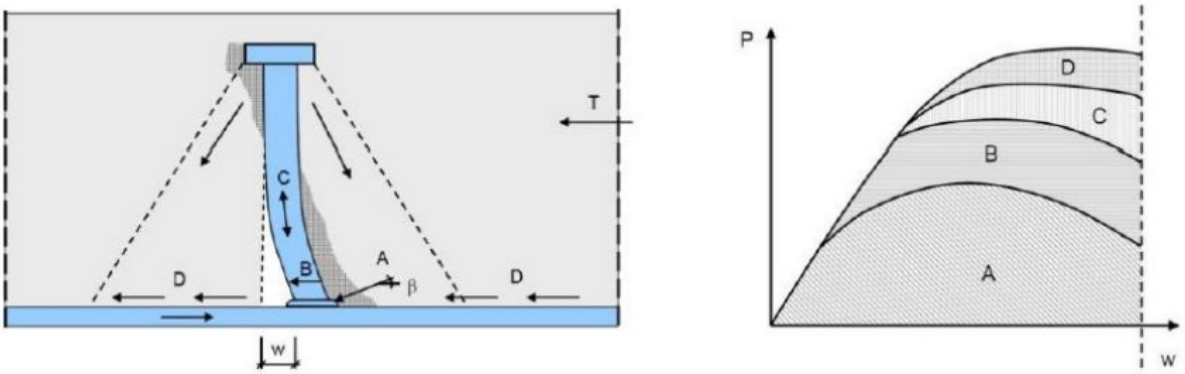

Fig. 2.5 Load transfer mechanism of headed shear stud connector in concrete slab [4])

Langershausen [4] created a model to show how stud connectors transfer load in solid slab applications. In Fig. 2.5, the capacity of the connector is composed of four distinct parts. First, a sizable portion of the shear force along the longitudinal axis from the bottom of the stud (A) reacts with the weld collar as soon as it contacts the nearby concrete. At the foot of the stud, the concrete crushes due to multiaxial high bearing loads. The shear stresses are then distributed higher up by the stud's shank (B). The stud's shank (C) is subject to bending and tensile stresses because the connector's base can move sideways while the stud's top is submerged in unaltered concrete and cannot deform. Because compressive pressures in the concrete beneath the stud head balance tensile stresses, additional forces (D) are created. The shear connection breakdowns when the shank of the stud merges with the failure due to shear tension above the weld collar.

2.6.2 Perfobond Ribs Shear Connectors

Perfobond-ribs shear connectors are easier to install and have a higher fatigue strength than conventional headed studs (Leonhardt et al. [16], Oguejiofor and Hosain [17-19]). The T-rib perfobond shear connectors were designed by Vellasco et al. [20] to transfer forces (Fig. 2.6.a). Vianna et al. [21] designed the T-rib perfobond shear connector's web plate, which had one or two rows of two (Fig. 2.6.b) or four (Fig. 2.6.c) holes. A PBL shear connector that works well with mixed girder arrangements made up of steel and prestressed reinforced cement concrete (RCC) was introduced by Ahn et al. [22]. Vianna et al.'s study [23] evaluated the slip capacity, shear resistance, and failure mechanism of T-rib connectors by examining a number of variables, including strength of concrete, hole position of connector, reinforcement and slab's thickness. The geometry of the shear connector was emphasized by Costa-Neves et al. [24], who also introduced double T-perfobond (Fig. 2.6. d) and I-perfobond (Fig. 2.6.e) connectors for composite girders. The

performance of TPBL, T shear connectors, and T-block in fire was experimentally investigated by Rodrigues and Lam [25].

(a) (b) (c) (d) (e)

Fig. 2.6: Perfobond rib shear connectors [20] [21] [22] [23] [24]: (a) T-ribs, (b) two holes in Trib, (c) four holes in two rows T-rib, (d) 2T Perfobond T-rib, and (e) I-Perfobond T-rib

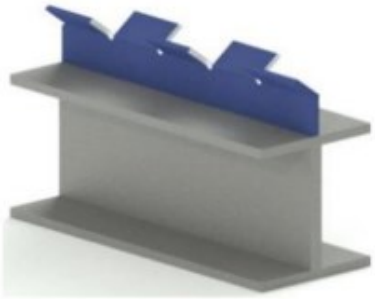

Fig. 2.7: Y-shaped perfobond rib shear connectors [26]

Kim et al. [26] created the "Y"-shaped PBL shear connector, which is depicted in Fig. 2.7 Continued investigational and analytical research under static type of loading [27–29] and cyclic type of loading [30–32] has proven the connector's superiority in fatigue and shear resistance.

2.6.3 Composite Dowel Shear Connector

Kopp et al. [33] supplied the circumstantial information of puzzle-shaped (PZ) and clothoidal (CL) composite dowels (Fig. 2.8) for use as shear connectors in composite

beams. Technical rules for ultimate limit states, manufacturing, construction, and structural design principles have been developed using the data. By utilizing the symmetric shape of CL and PZ composite dowels, shear stress in composite structures can be distributed uniformly and, in both directions, (Seidlet al. [34]). These dowels have good fatigue resistance and radius connectors that are robust enough to withstand fatigue cracks. Hechleret al. [35] presented a fatigue design strategy in their paper for PZ continuous shear connections used in prefabricated composite beam construction.

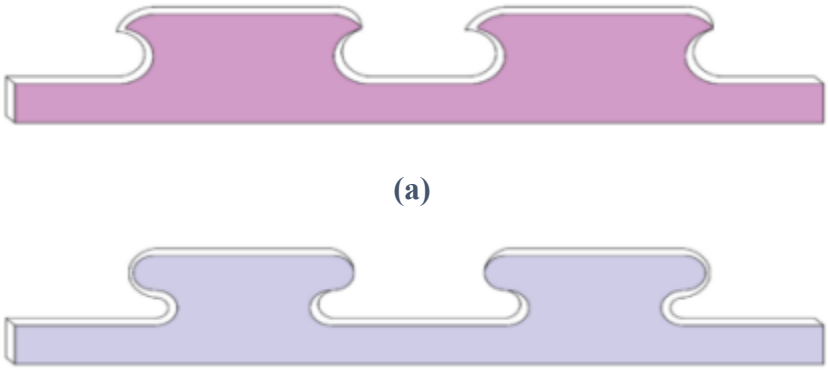

(a)

(b)

Fig. 2.8 Composite dowel shear connector

(a) Clothoidal shape and (b) puzzle shape [33]

2.6.4 C-shaped channel and angle shear connectors

The primary reasons for the possible development of C-type shear connectors are the low strength of headed studs and the difficulties in supplying transverse rebar in PBL holes [Fig. 2.9]. The established constructability benefits of channel connectors were attributed to their superior reinforcing environment and twice the shear strength of headed studs (Shariati et al. [38]). There are two types of C-shaped connectors: angle and channel profile. The results of push-out static loading experiments on composite structures with angle shear connectors were published by Rajaram [39].

According to the test results, the channel connector had an acceptable energy dissipation capability and a maximum bearing capacity that was roughly 47.5% and 92.1% higher than that of the angle and T-PBL connectors, respectively.

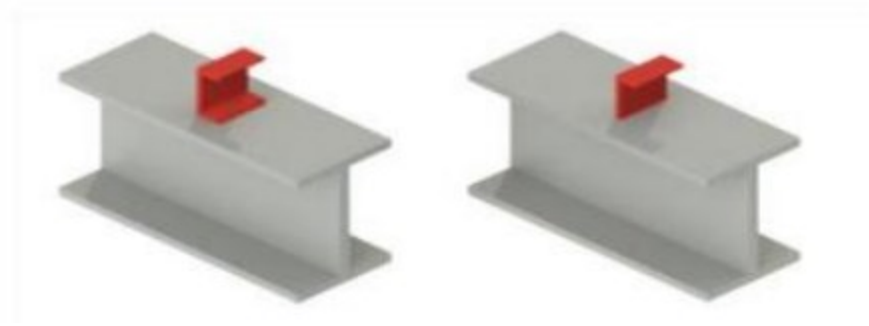

(a) (b)

Fig. 2.9: (a) Channel shear connector, (b) angle shear connector [38]

Hicks et al. [40] assessed the shear connectors in bridges from the Gisborne and Hawke's Bay regions, as well as the Canterbury and West Coast areas. It was noted that 72% and 63% of the bridges in the Gisborne, Hawke's Bay, Canterbury, and West Coast regions (Fig. 2.10) used welded channels, and 18% and 30% used V-angles as a shear connection. Conversely, the percentage of bridges with shear studs or other connectors installed is between 3% and 7%.

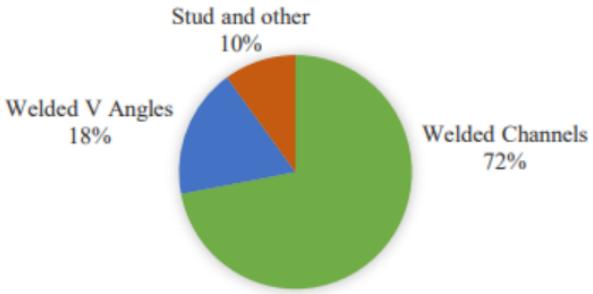

Fig. 2.10: Different systems of shear connectors used for the West Coast region and Canterbury composite bridges [40]

2.6.5 Combination of different shear connectors

Researchers have been able to enhance the shear behavior of composite structures by combining headed stud and PBL shear connectors. Deng et al. [41] created and verified a grouping of headed shear connectors with a solo perfobond rib (Fig. 2.11) in order to evaluate the mode of fracture, shear carrying capacity, load-slip behaviour, and ductility using ten test specimens for push-out.

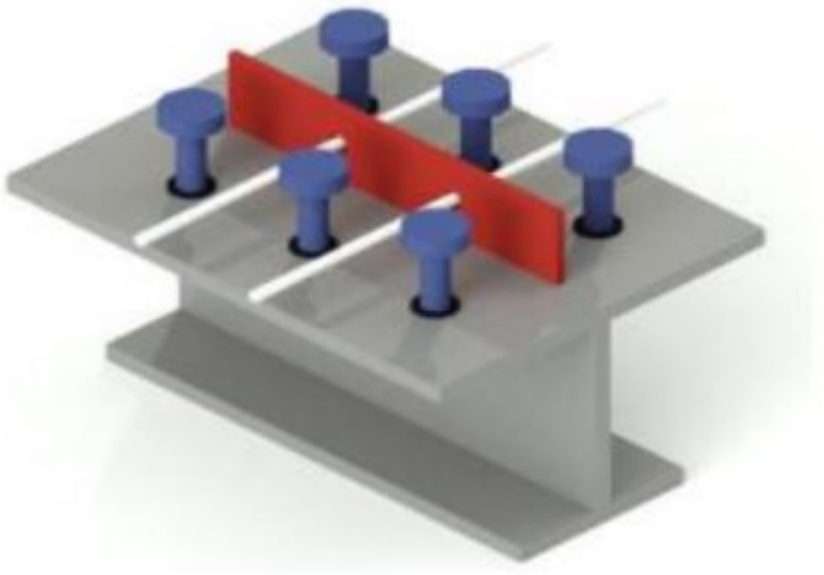

Fig. 2.11: Headed stud shear connectors with a single perfobond rib [41]

2.7 DESIGN CODES ON SHEAR CONNECTORS

The design strength of the shear connector is a crucial component in the creation of a composite part. The design values and equations are provided by professional standard codes. The equation and provisions of the design code currently cover only headed stud type shear connectors and a limited other kinds of shear connectors. The following section discusses available codes of practice for headed stud shear connector & channel shear connector.

2.7.1 Bangladesh National Building Code (BNBC)-2020

Headed stud shear (HSS) connector's shear strength:

As per the Bangladesh National Building Code (BNBC)-2020 [43] the shear strength of one headed stud shear connector implanted in solid concrete slab in composite construction can be expressed as

$$Qn = 0.5\ A_{sc}\sqrt{(f'cEc)} < RgRpAscFu \quad (2.3)$$

Where, A_{sc} = Headed stud shear connector's cross-sectional area (mm^2)

E_c = Modulus of Elasticity of concrete (MPa)

$= 0.043{w_c}^{1.5}\sqrt{f'_c}$, w_c =concrete's unit weight ($1500 \le w_c \le 2500\ kg/m^3$)

Fu = Tensile strength of a headed stud shear connector (MPa)

Rg= group effect factor

Rp= position effect factor

Strength of channel shear connectors:

Strength of one channel shear connector can be calculated using following formula

$$Q_n = 0.3(t_f + 0.5t_w)L_C\sqrt{f'_c E_C} \quad (2.4)$$

here,

t_f = Flange thickness (mm)

t_w = Web thickness (mm)

L_c = Length (mm)

E_c = Modulus of Elasticity of concrete (MPa)

$= 0.043{w_c}^{1.5}\sqrt{f'_c}$, w_c =concrete's unit weight ($1500 \le w_c \le 2500\ kg/m^3$)

2.7.2 AISC 360-16 (2016)

48 push-out specimens were tested with 16 mm and 19 mm studs embedded in both ordinary and lightweight concrete. The concrete's strength, cross-sectional area, and modulus of elasticity all affect how strong a shear connection is in a solid slab. The upper limit of the test data was determined by following Eq. 2.5 regarding the connector's tensile strength. The nominal shear capacity (Qn) was also determined in AISC 360-16 by accounting for the group variables and the location of the shear connector

$$Qn = 0.5\ Asc\sqrt{(f'cEc)} < RgRpAscF \qquad (2.5)$$

In this expression;

Rg= Factor of group effect

Rp= Factor of position effect

Asc= The cross-sectional area (mm^2)

Fu= Tensile strength of a shear connector (N/mm^2)

$f'c$= The compressive strength of concrete (N/mm^2)

Ec= The modulus of elasticity of concrete (N/mm^2)

2.7.3 CSA S16-09 (2009)

The shear capacity of an end-welded stud in a solid slab that is headed or hooked and has a h/d ratio of at least 4.0 is

$$q_r = 0.5\ \varphi_{sc}A_{sc}\sqrt{(f'_cE_c)} \le \varphi_{sc}A_{sc}\ F_u \qquad (2.6)$$

here,

q_r = Performance Factored resistance (N)

φ_{sc} = Shear connector's Resistance Factor [0.8]

A_{sc}= Shear connector's cross-sectional area (mm^2)

$f'c$= The compressive cylinder strength of concrete (N/mm^2)

Ec= The elasticity modulus of concrete (N/mm2)

Fu = Shear connector's tensile strength (MPa)

h = Shear stud's height (mm)

d = Shear stud's diameter (mm)

2.7.4 Eurocode 4 (2004)

Two equations (Eqs. 2.7 and 2.8) for the shear resistance of welded headed shear connectors in solid slabs are provided by Eurocode 4 clause 6.6.3.1. The minimum value obtained from these two equations was used to calculate the design resistance (P_{Rd}). Shear connector failure and concrete failure are the two primary failure modes that are addressed by these two equations.

$$P_{Rd} = \frac{(0.29\alpha d^2\sqrt{f_{ck}E_c})}{\gamma_v} \tag{2.7}$$

$$P_{Rd} = \frac{0.8f_u\pi d^2}{4\gamma_v} \tag{2.8}$$

here,

$\alpha = 0.2\left(\frac{h_{sc}}{d}+1\right) \leq 1.0, \qquad for\ 3 \leq \frac{h_{sc}}{d} \leq 4$

$\alpha = 1.0, \qquad for\ \frac{h_{sc}}{d} > 4$

$d = shank\ diameter\ of\ the\ stud\ shear\ connector(mm)\ (16\ mm \leq d \leq 25\ mm)$

$h_{sc} = height\ of\ the\ stud\ shear\ connector\ (mm)$

$f_u = \ ultimate\ tensile\ strength\ (N/mm^2)$

$f_{ck} = characteristic\ compressive\ strength\ of\ concrete\ cylinder\ (N/mm^2)$

$E_c = Modulus\ of\ elasticily\ of\ concrete\ (N/mm^2)$

$\gamma_v = safety\ factor\ for\ shear\ resistance\ (\gamma_v = 1.25)$

2.7.5 JSCE (2005)

For two distinct failure modes (stud and concrete), the Japanese Standard Specifications for Steel and Composite Structures specify the minimum value for the shear resistance of the welded headed studs. These can be found in Equations 2.9 and 2.10. This case is limited to height to diameter ratio as $h_{ss}/d_{ss} \geq 4$

$$V_{sud} = (31A_{ss}\sqrt{(\frac{h_{ss}}{d_{ss}})} * f'_{cd} + 1000)/\gamma_b \quad (2.9)$$

$$V_{sud} = A_{ss}f_{sud}/\gamma_b \quad (2.10)$$

here,

$A_{ss} = stud\ shank\ cross\ sectional\ area\ (mm^2)$

$d_{ss} = shear\ stud\ connector\ diameter\ (mm)$

$h_{ss} = shear\ connector\ height\ above\ the\ flange\ (mm)$

$f_{sud} = design\ tensile\ strength\ of\ stud\ (N/mm^2)\ (=\frac{f'_{suk}}{1})$

$f_{suk} = characteristic\ tensile\ strength\ of\ stud\ (N/mm^2)$

$f'_{cd} = design\ compressive\ strength\ of\ concrete\ (N/mm^2)\ (=\frac{f'_{ck}}{1.3})$

$f'_{ck} = characteristic\ compressive\ strength\ of\ concrete\ (N/mm^2)$

$\gamma_v = is\ the\ partial\ safety\ factor\ for\ shear\ resistance\ (\gamma_v = 1.3)$

2.7.6 ACI 318-08 (2008)

The steel strength of the anchor in shear, which can be found in Equations 2.11 and 2.12, respectively, determines the nominal strength of an anchorage, V_{sa}, for a cast-in headed bolt or post installed anchor and a cast-in headed stud anchor.

$$V_{sa} = nA_{se}f_{uta} \quad (2.11)$$

$$V_{sa} = n\ 0.6\ A_{se} f_{uta} \quad (2.12)$$

Here,

n = total number of anchors in the group

A_{se}= single anchor's effective cross-sectional area (in^2)

f_{uta}= smaller of 1.90fya and 125 ksi.

f_{ya}= the specified yield strength of the anchor

f_{uta}= the specified tensile strength of the anchor steel

2.7.7 Channel Connector as per AISC 360-16 (2016) and CSA S16-09 (2009)

The most recent American Standard (AISC 360-16) states the following formula to calculate the strength of a channel shear connector embedded in a slab of solid concrete:

$$Q_n = 0.3(t_f + 0.5t_w)L_c\sqrt{(f'_c E_C)} \quad (2.13)$$

here,

$Q_n = Strength\ of\ one\ channel\ shear\ connector\ (N)$

$t_f = Flange\ thickness\ of\ (mm)$

$t_w = Web\ thickness\ (mm)$

$L_c = Length\ (mm)$

$f'_c = Compressive\ strength\ of\ concrete\ (MPa)$

$E_c = The\ elasticity\ modulus\ of\ concrete\ (MPa)$

This formula is a slightly altered version of the formula created by Slutter and Driscoll [44].

CSA S16-09 (2009):

The current Canadian Standard states that the factored resistance q_{rs} of a channel shear connector embedded in a solid concrete slab is to be determined using Eq. 2.14:

$$Q_{rs} = 36.5\varphi_{sc}(t_f + 0.5t_w)L_c\sqrt{f'_c} \quad (2.14)$$

here,

$\varphi_{sc} = Resistance\ factor$

$t_f = Flange\ thickness\ (mm)$

$t_w = Web\ thickness\ (mm)$

$L_c = Length\ (mm)$

$f'_c = Compressive\ strength\ of\ concrete\ (MPa)$

The results of 41 push-out specimen tests conducted at Lehigh University are also the basis for this equation [44].

2.7.8 Channel shear connector [Eurocode 4 (CEN 2001)]

This connector's usual orientation is depicted in Fig. 2.12. We call this type of connector a block connector. A steel tie is used to avoid uplift due to the channel's arrangement.

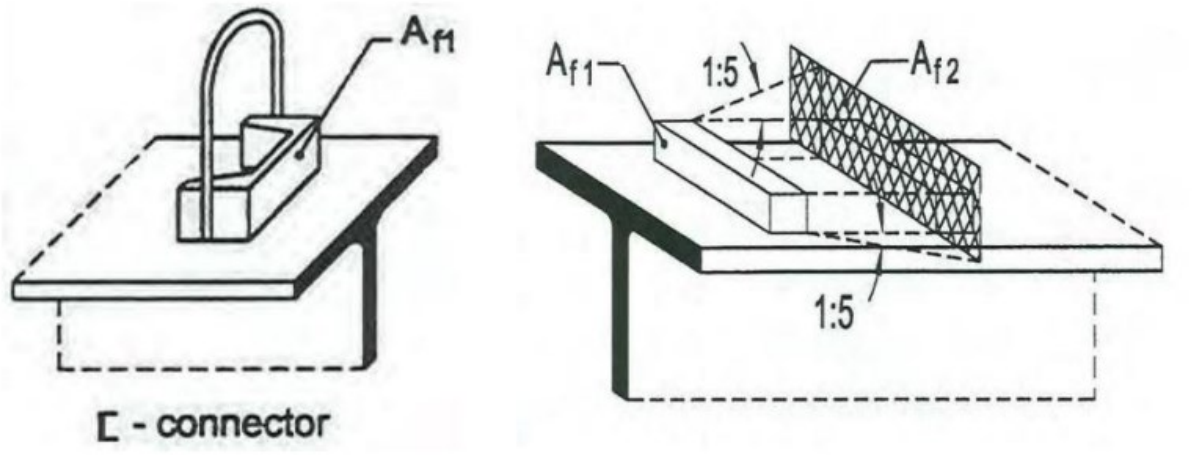

Fig. 2.12 Rigid channel shear connector and the parameters of rigid shear connectors (Eurocode 4)

The design resistance (P_{Rd}) of this type of block shear connector can be determined using following formula

$$P_{Rd} = \eta A_{f1} F_{ck} / \gamma_c \quad (2.15)$$

here,

A_{f1} = Front surface area

A_{f2} = Enlarged front surface area considering slope 1: 5

$\eta = \sqrt{\frac{A_{f2}}{A_{f1}}}$ (smaller than 2.5 for normal concrete and 2 for light weight concrete

γ_c = safety factor

Block shear connectors are not popular in North America because these are rigid in nature and require extra tie.

2.7.9 Angle Shear Connector [Eurocode 4, CEN 2001]

The strength (P_{Rd}) of an angle shear connector embedded in a concrete slab as shown in Fig. 2.13 is as follows:

$$P_{Rd} = 10bh^{3/4} {f_{ck}}^{2/3} / \gamma_v \quad (2.16)$$

In this expression,

b = Length (mm)

h = Width (mm)

f_{ck} = Characteristic compressive strength of concrete (N/mm^2)

γ_v = safety factor for concrete, for the ultimate limit state, it is taken as 1.25

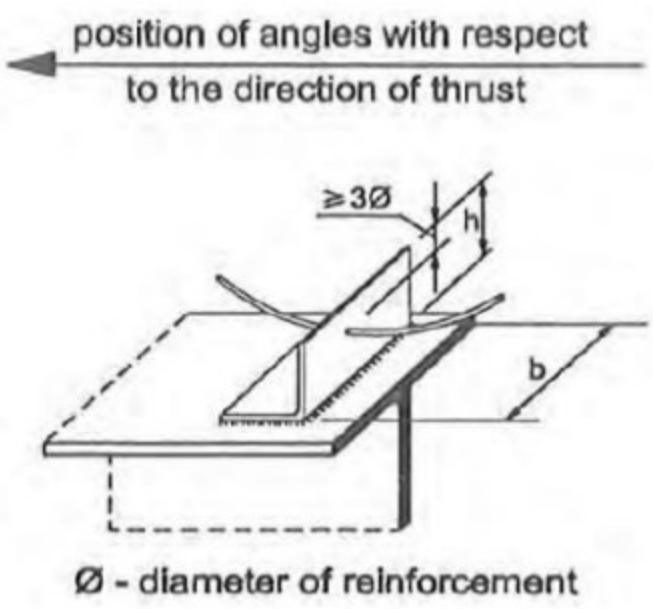

Fig. 2.13 Representative angle shear connector (L-shaped) [Eurocode 4]

2.8 ADVANTAGES OF HEADED STUD SHEAR CONNECTOR OVER OTHER SHEAR CONNECTORS

Headed stud shear connectors are superior to other types of connectors because:

1. They have good concrete anchoring, quick welding, and are ideal for use in steel deck slabs.

2. They don't obstruct the slab reinforcement.3. Concrete located near the connectors can be compacted satisfactorily.

4. In every direction, it provides the same shear strength.

5. Easy production of large-scale sizes.

6. Contains standard dimensional head that acts as a resistance factor for slab uplift

2.9 PUSH OUT TEST

Push-out tests are a popular technique for analysing shear connection capacity and failure mechanisms. A steel section with shear connectors inserted into concrete slabs on both flanges is a typical push-out specimen. Vertical downward load or displacement is applied on the web of the steel section. It is considered that the load is distributed equally among the slabs and that only the connectors transmit the load from the steel section (Viest [15]). However, the information about push-out test is found in Eurocode 4 and is depicted in Fig. 2.14 and pertains to welded shear connectors in solid concrete slabs. To cut down on the expense and duration of a full-scale test, this test is utilized in place of the composite beam test. The calculation of slip capacity using Eurocode 4 is shown in Fig. 2.15.

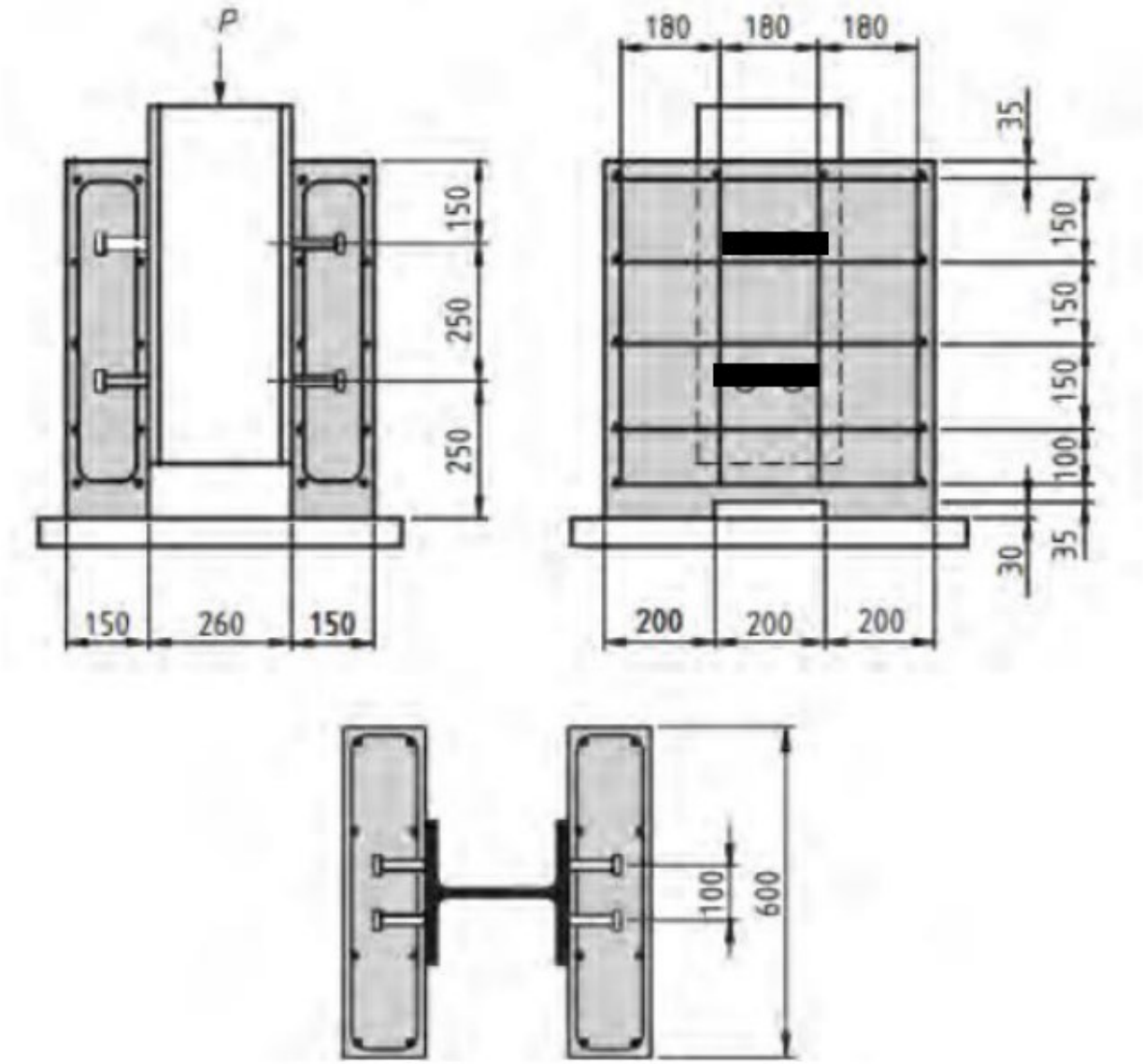

Fig. 2.14 Push-out test arrangement as per Eurocode 4

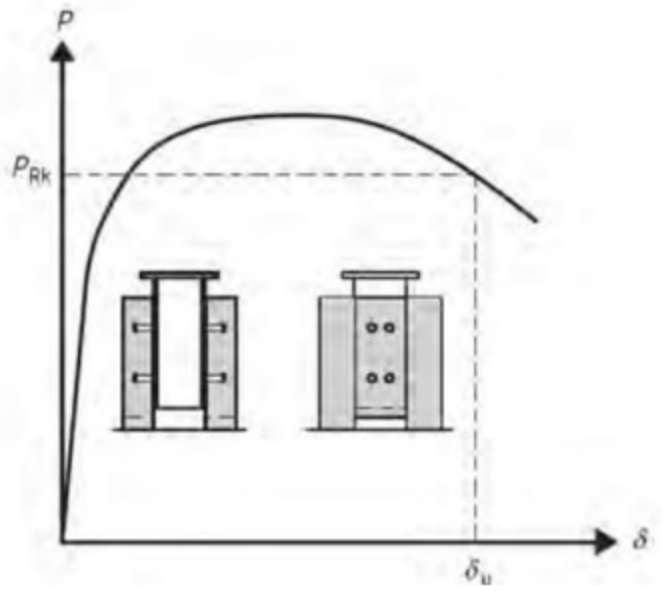

Fig. 2.15 Slip capacity determination as per Eurocode 4

A shear connector's ductility can be ascertained through push-out tests. The slip capacity at the interface between the composite concrete slab and the steel beam determines this. Shear connectors are deemed ductile if their capacity for deformation is sufficiently high. Eurocode 4 states that the shear connector is ductile if the slip becomes greater than 6 mm. A notable plastic deformation characterizes the headed shear connector's good ductile behaviour. On the other hand, brittle behaviour with little plastic deformation is identified in a shear connector that does not cross the 6 mm threshold [52].

2.10 PREVIOUS RESEARCH

Many push-out tests were carried out by multiple researchers. This section will provide a thorough review of the research conducted by earlier researchers.

2.10.1 Tests By Slutter and Fisher (1966)

One of the primary sources for the study of headed shear stud is the test conducted at Leigh University by Slutter and Fisher in 1966. Slutter and Fisher's (1966) research, which tested push-out specimens (35 nos.) with a concrete slab connected to a steel beam and

came to the conclusion that fatigue life is an index of stress range and peak value of the load is not significant [44].

2.10.2 Tests By Menzies and Mainstone (1967)

They conductedtest on different types (HSS, Channel and bar) of shear connectors. 19 mm diameter and 100 mm height headed shear studs were considered for 11 static type and 23 fatigue type tests. It is reasonable to anticipate some variations in strength if the strength of the concrete varies. Their research revealed that stud shear connectors experienced greater variations in strength than bar and channel shear connectors [45].

2.10.3 Tests by Hallam (1976)

They conducted 17 nos. push out test and 13 nos. fatigue test with fixed amplitude value and adjustable range of the stress. According to their research, the most crucial factor in predicting the static strength, load slip behaviour, and life of fatigue of a shear connector is the concrete's compressive strength [46].

2.10.4 Tests by Foley and Oehlers (1985)

The strength of HSS was investigated through 129 push-out tests. The findings demonstrated that the application of cyclic loads causes stud shear connectors' static strength to decrease. In line with the findings of Mainstone and Menzies (1967) [47], there was a 50% reduction in static strength according to two tests, and a 73% reduction in another test.

2.10.5 Tests by Amar Prakash et. el.

Their research took into account the confinement of reinforced concrete. According to experimental results, concrete confinement near the headed shear stud greatly increased the concrete's compressive strength and splitting resistance; as a result, push out specimens should take this into consideration [48].

2.10.6 Numerical study by Md. Manik Mia

Using a finite element model, a comprehensive parametric study was conducted with varying stud diameters and concrete strength to examine the behaviour of both small and large headed shear studs. A numerical analysis revealed that while slip decreases as concrete strength increases, shear capacity increases. The small and large shear connectors both showed signs of a shank failure mode. Research revealed that the EC4, typically provides a less estimate of the shear carrying capacity of a headed shear stud, but the CSA S6-14, gives overestimation by approximately 22.3% [49].

2.10.7 Numerical study by Huu Thanh Nguyen & Seung Eock Kim

Parametric study of the 32-specimen considering different diameter of the stud and strength of concrete was conducted by FE analysis. Study showed that AASHTO LRFD specification gives overestimation of the shear carrying capacity by about 27 percent. EC4 gives conservative estimation for 22 to 25 mm diameter stud and overestimation for 30 mm diameter stud by up to 8.7 percent [50].

2.11 FINITE ELEMENT ANALYSIS (FEA) USING ANSYS

Engineers and designers now depend heavily on Finite Element Analysis (FEA) to simulate and examine the behaviour of various components and structures. It helps them to guarantee structural integrity, optimize performance, and forecast how a design will behave under different loading scenarios. Finite Element Analysis is a numerical technique that breaks down large, challenging engineering problems into smaller, easier-to-manage components. The behaviour of the entire structure or component is represented by these elements, also referred to as finite elements, which are interconnected. Based on the system's material characteristics, applied loads, and boundary conditions, FEA models the system's physical behaviour. FEA offers important insights into critical parameters such as heat transfer, vibration, deformation, stress

distribution, and others by solving a set of equations derived from the governing principles of physics.

A popular software package for FEA and other engineering simulations is called ANSYS. It provides an extensive set of tools and functionalities for the analysis of problems in structural, thermal, fluid, electromagnetic, and Multiphysics fields. Engineers in a variety of industries choose ANSYS because of its robust solvers, user-friendly interface, and strong post-processing capabilities. To better understand their designs, users can use ANSYS to solve equations, define material properties, apply loads and constraints, create complex finite element models, analyse simulation results, and more.

Advantages FEA using ANSYS:

Design Optimization: Engineers can improve designs through iteration and optimization with ANSYS in order to maximize performance, reduce weight, increase efficiency, and boost reliability.

Virtual Prototyping: FEA enables engineers to test their designs virtually in a variety of operating environments, saving money on expensive physical prototypes and speeding up the design process.

Structural Analysis: ANSYS offers comprehensive structural analysis capabilities, such as fatigue, buckling, composite materials, and linear and nonlinear analyses.

Thermal Analysis: By using ANSYS, users can examine temperature distribution, heat stress, and heat transfer in systems and components to maximize cooling options and guarantee secure operating environments.

Fluid Dynamics: Engineers can simulate and analyse fluid flow, heat transfer, and aerodynamics for optimized designs with the help of ANSYS's robust computational fluid dynamics (CFD) capabilities.

2.12 RESEARCH GAP

It is found from the literature review that in BNBC, AISC 360-16, AASHTO LRFD, Eurocode 4, JSCE, ACI 318-08, no designs equations are available for the determination of shear strength of inclined headed shear stud. Several researchers conducted their experimental and numerical investigation on headed shear stud considering perpendicular orientation. But during the construction of steel-concrete composite structure some headed shear stud may be get welded having some inclination due to oblivion or lack of proper skill. In that case if the inclined headed shear stud becomes fail to transfer the transverse shear, the assumptions of steel-composite action may be invalidated. Here the numerical study is conducted using ANSYS software for perpendicular and inclined headed shear stud to determine the load slip behaviour, ultimate shear strength, failure pattern by standard push out test.

Chapter 3: METHODOLOGY

3.1 INTRODUCTION

The initial step of this study is to develop an accurate and efficient non-linear three-dimensional finite element push out test model to investigate the behaviour of headed stud shear connector in steel concrete composite construction. The finite element-based software ANSYS was used in the analysis. Several criteria, such as the model's ability to capture the nonlinear response, plasticity and damage behaviour of concrete were considered during finite element modelling. The results of the developed finite element push out model were confirmed against the test results carried out by Gattesco and Giuriani [51]. The finite element analysis result was also compared with the design strength calculated using the equations suggested by Bangladesh National Building Code (BNBC)-2020 [43], European Code (EC4) [52] and AASHTO LRFD [53] for headed stud shear connectors in steel-concrete composite structures. Further studies were conducted considering the same material properties, contact settings, meshing, boundary conditions, analysis settings and other parameters of the validated finite element push out model to investigate the behaviour of inclined headed shear stud connectors in push out test considering 15-degree, 30-degree and 45-degree angle of inclination. This systematic approach allowed for a comprehensive investigation of the push out test and provided valuable insights into the behaviour of the tested system under different conditions.

3.2 GEOMETRY OF PUSH OUT TEST

The push-out test specimen in the experiment study of Gattesco and Giuriani [51] is investigated in this study. This specimen is in accordance with the standard push-out test

specimen in European Code (EC4) [52]. The overall geometry of the specimen is shown in Fig. 3.1. The geometry of push out test specimen is prepared in solid modelling CAD software ANSYS SpaceClaim.

The width, height and thickness of the concrete slab is 600 mm, 650 mm & 200 mm respectively. Total 8 nos longitudinal bar and total 5 nos tie bar was used as reinforcement in concrete slab. The diameter of both horizontal and vertical reinforcement is 16 mm. The length of the web is 255 mm, the width of the flange is 255 mm. The thickness of the both web and flange is 14 mm. The overall length of the Headed shear stud is 125 mm, the height of head is 9 mm, the diameter of the shank is 19 mm and the diameter of the head of shear stud is 31 mm.

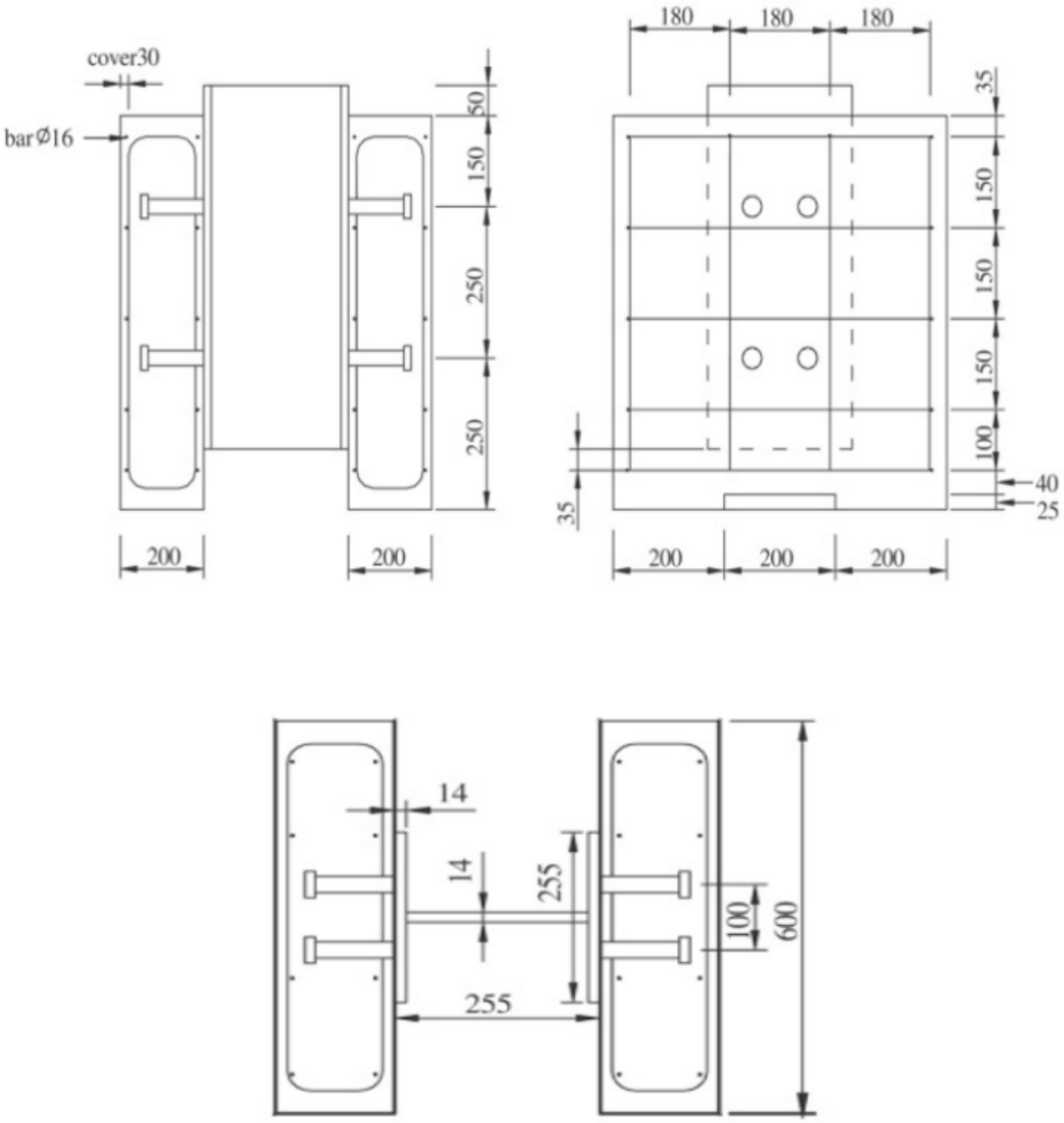

Fig. 3.1 push-out test specimen (Gattesco and Giuriani [51])

It should be mentioned that in order to account for the complex contact interactions and fracture mechanisms, HSS has modelled with the precise geometry.

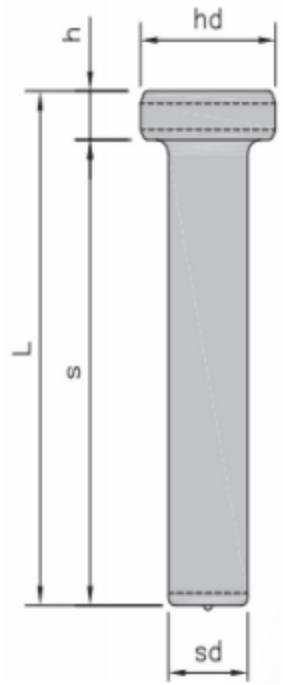

Fig. 3.2 Headed shear stud (Gattesco and Giuriani [51])

Table 3.1. Dimensions of headed shear stud

Diameter (sd) mm	Shank Height (s) mm	Head Height (h) mm	Overall, Height (L) mm	Head Diameter (hd) mm
19	116	9	125	31

Owing to the push-out specimen's symmetry, only 25% of the entire model is used, and suitable boundary conditions have been applied to reproduce the entire model.

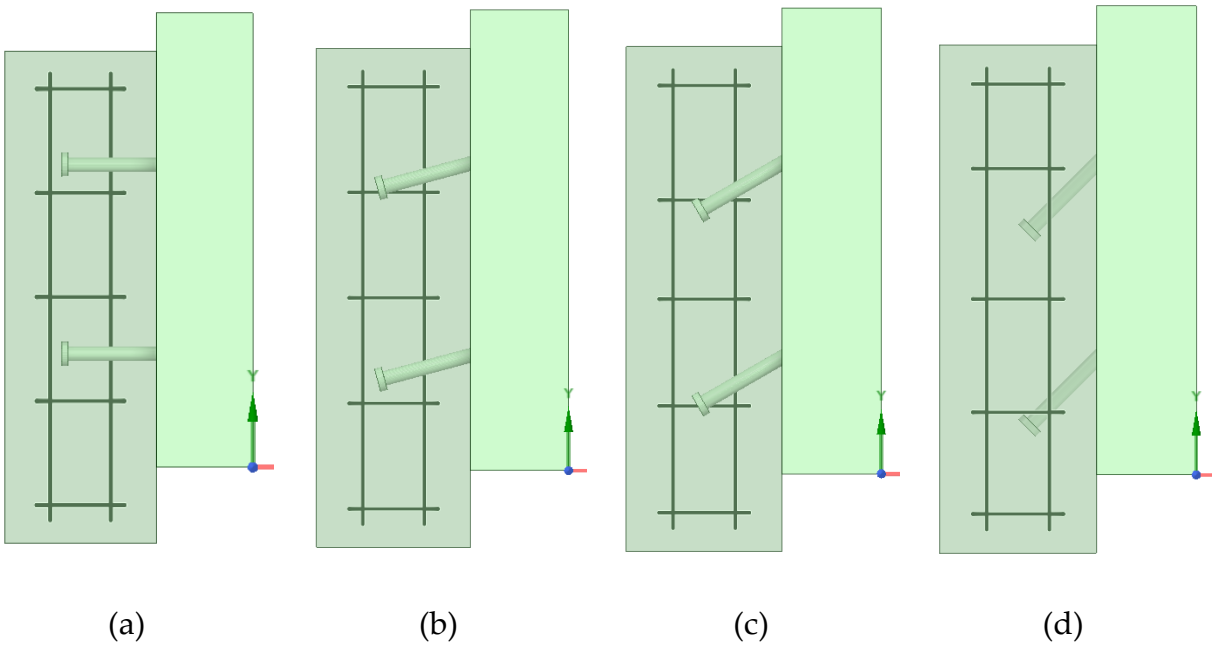

(a) (b) (c) (d)

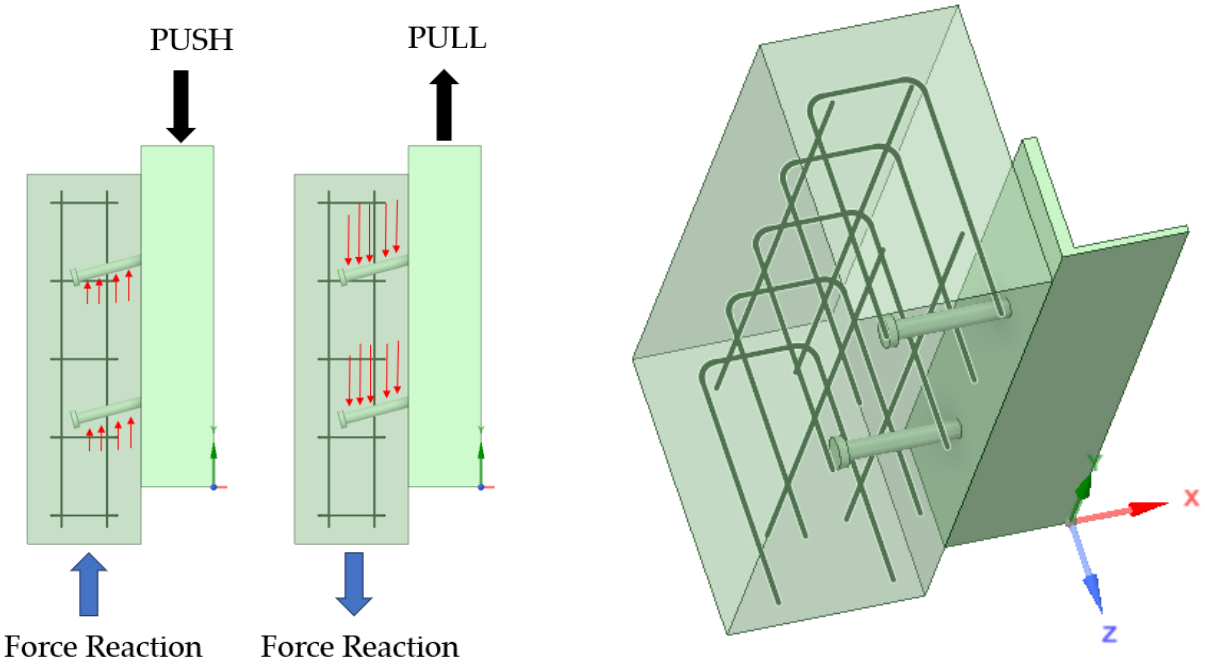

(e) (f) (g)

Fig. 3.3 Push-out Test Specimen: (a) Perpendicular HSS, (b) 15-Degree Inclined HSS, (c) 30- Degree Inclined HSS, (d) 45-Degree Inclined HSS, (e) Downward Loading (Push), (f) Upward Loading (Pull), (g) Isometric view (Quarter Part)

3.3 MATERIAL PROPERTIES

Concrete, Structural Steel & MS Deformed reinforcing bar are used in the test specimen. Using the relevant material models found in the ANSYS finite element reference section, the nonlinear behaviour of these materials is integrated into the model. In the sections that follow, the material models and their mechanical characteristics that were utilized in the finite element modelling are explained.

3.3.1 Concrete

The coupled concrete damage plasticity microplane (CDPM) concrete model, which can be found in the ANSYS material reference section, was used to model concrete. The research of Zreid and Kaliske [54] [55] [56] served as the foundation for the creation of this CDPM model. In the CDPM model of concrete, Fig. 3.4 depicts a smooth three surface Drucker-Prager cap yield function.

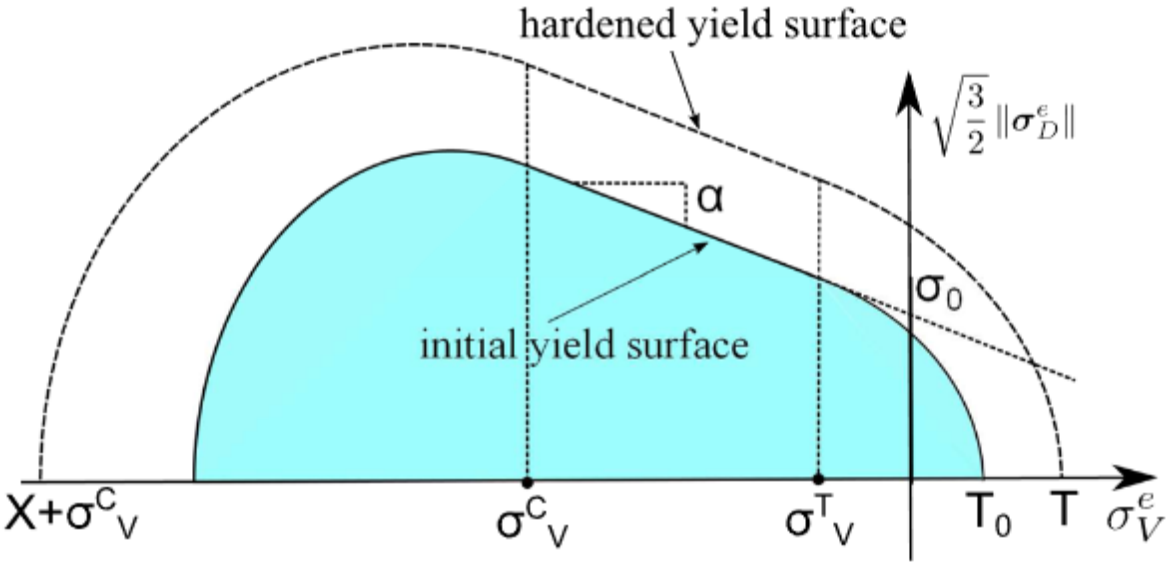

Fig. 3.4 Smooth three-surface microplane cap yield function [54] [55] [56]

The following factors are considered when assessing concrete damage:

- There are differences in the way damage begins and progresses in compression and tension.
- In tension, concrete is more brittle, and softening sets in almost instantly after the elastic limit.
- After the elastic limit in compression, some hardening is seen prior to softening.
- As a result of crack closure, the stiffness lost during tensile cracking is regained during the transition from tension to compression states. But the damage that was incurred during compression is still present when tension is applied.

3.3.1.1 Identifying Coupled Damage-Plasticity Microplane Model Parameters

For the purpose of assessing concrete's tension and compression damage, the CDPM model needs fifteen parameters. Following are some hints and tips for microplane model parameter identification [57].

• **Elasticity**

The elastic region of the material stress-strain curve can be used to determine the modulus of elasticity and Poisson's ratio, or empirical formulas that are published in the literature can be used.

• **Plasticity**

For materials like concrete, the strength parameters f_{uc}, f_{bc} and f_{ut} are typical material properties. If f_{uc} is known, empirical relations can be used in the absence of complete testing data.

$$f_{bc} = 1.15 f_{uc} \tag{3.1}$$

$$f_{ut} = 1.4 \left(\frac{f_{uc}}{10}\right)^{2/3} \tag{3.2}$$

Experimental data from triaxial experiments are required to determine the compression cap parameters. Applying a hydrostatic load until the yielding starts allows one to find the intersection point between the hydrostatic axis and the initial compression cap. It is more difficult to locate the intersection point between the Drucker-Prager function and the compression cap. If this data is unavailable, an empirical estimate can be made as follows:

$$\sigma_V^C = -\frac{2}{3} f_{bc} \tag{3.3}$$

The parameter R can therefore be calculated as:

$$R = X_0 / f_1(\sigma_V^C) \tag{3.4}$$

• Damage and Hardening

Cyclic tests are required to determine the hardening and damage parameters. These parameters are connected because the softening and the unloading slope are determined by their interaction. Through a uniaxial cyclic compression test, the values of D, β_c and γ_{c0} are determined.

In a similar manner, R_T, β_t and γ_{to} are determined by a uniaxial cyclic tension test. If uniaxial cyclic tension tests are not conducted, $R_T = 1$, $\beta_t = 1.5\,\beta_C$ can be utilized as initial values. Since tension softening begins almost immediately after the elastic limit, the tension damage threshold γ_{to} is frequently set to zero.

• Nonlocal Parameters

The nonlocal interaction range (c) and the over-nonlocal interaction range (m) were the two parameters that were defined in this method. The over-nonlocal parameter (m) is a numerical parameter that provides mesh-independent convergence behaviour and regularizes the solution for any value greater than 1. The typical value of the parameter

(m) is 2.5. On the other hand, the interaction range parameter (c), which can be computed using the equation, determines the nonlocal interaction damage parameters [58] [59].

$$c \geq 4L2$$

where, L is the maximum length of the element

Table 3.2 describes the CDPM model parameters [54], [55], [56]

Table 3.2 Coupled Damage-Plasticity Microplane Model Parameters

Parameter Type	Parameter Sub type	Parameter	Description	Unit	Selected Value
Elasticity	--	E	Modulus of Elasticity	MPa	24000
	--	ν	Poisson's Ratio	--	0.2
Plasticity	Drucker-Prager yield function	f_{uc}	Uniaxial Compressive Strength	MPa	26.00
		f_{bc}	Biaxial Compressive Strength	MPa	29.90
		f_{ut}	Uniaxial Tensile Strength	MPa	2.60
	Compression cap	σ_v^c	Intersection point abscissa between compression cap and dracker-prager yield function	MPa	-19.93

		R	Ratio between the major and minor axis of the cap	--	2.0
	Hardening	D	Hardening material constant	MPa^2	40000
		R_T	Tension cap hardening constant	--	1.0
Damage	--	$\gamma_{co}, \gamma_{to},$	Tension and compression damage thresholds	--	$2e^{-5}$ 0
	--	β_t, β_c	Tension and compression damage evolution constants	--	9000 6000
Nonlocal Parameters	--	c	Nonlocal interaction range parameter	mm^2	1500
	--	m	Over-nonlocal averaging parameter	--	2.5

3.3.2 Structural Steel

For structural steel, stress-strain relationship (bi-linear) is considered as shown in Fig. 3.5. Table 3.3 describes the different properties of structural steel.

Table 3.3 Properties of structural steel

Parameter Type	Parameter Sub type	Unit	Selected Value
Isotropic Elasticity	Young's Modulus	MPa	210000
	Poisson's Ratio	--	0.3
	Bulk Modulus	MPa	175000
	Shear Modulus	MPa	80769
Bi-linear isotropic hardening	Yield Strength	MPa	320
	Tangent Modulus	MPa	0

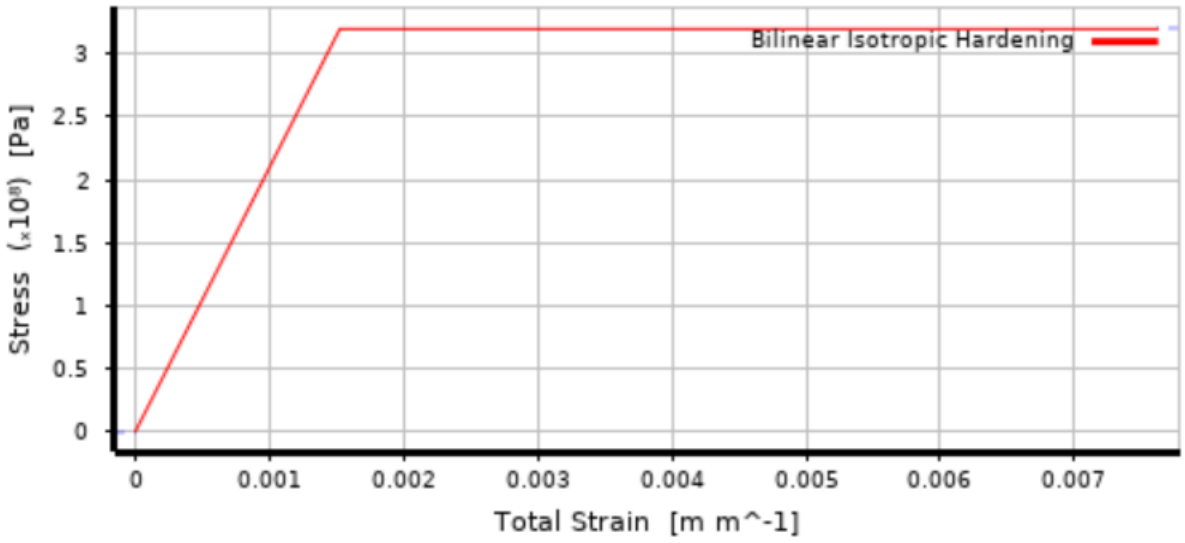

Fig. 3.5 Stress-Strain Relationship for Structural Steel

3.3.3 Reinforcement

For Reinforcement, stress-strain relationship (bi-linear) have been assumed as shown in Fig. 3.6. Table 3.4 describes the different properties of structural steel.

Table 3.4 Properties of Reinforcement

Parameter Type	Parameter Sub type	Unit	Selected Value
Isotropic Elasticity	Young's Modulus	MPa	208000
	Poisson's Ratio	--	0.3
	Bulk Modulus	MPa	173330
	Shear Modulus	MPa	80000
Bi-linear isotropic hardening	Yield Strength	MPa	400
	Tangent Modulus	MPa	0

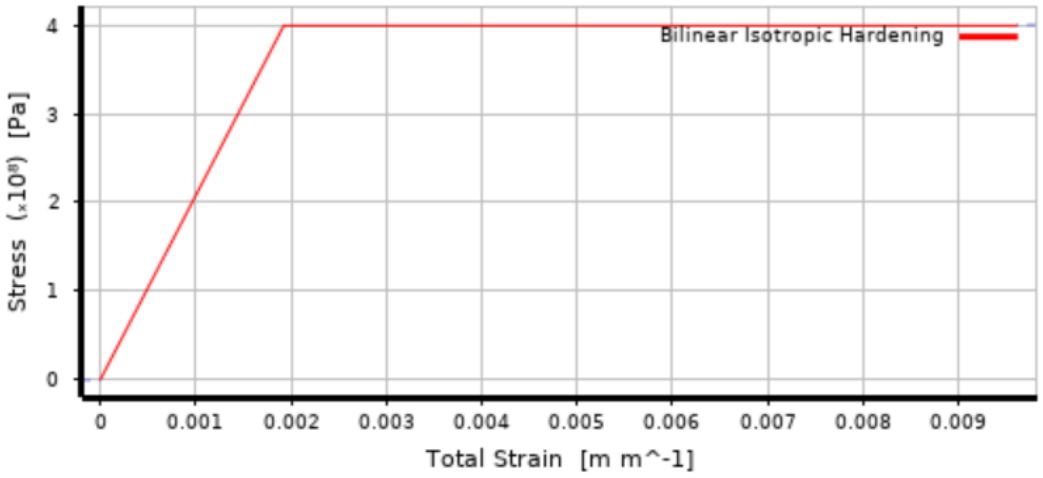

Fig. 3.6 Stress-Strain Relationship for Reinforcement

3.3.4 Headed Shear Stud

For HSS stress-strain relationship is considered as shown in Fig. 3.7. Table 3.5 describes the different properties of headed shear stud.

Table 3.5 Properties of Headed Shear Stud

Parameter Type	Parameter Sub type	Unit	Selected Value
Isotropic Elasticity	Young's Modulus	MPa	208000
	Poisson's Ratio	--	0.3
	Bulk Modulus	MPa	173330
	Shear Modulus	MPa	80000
Bi-linear isotropic hardening	Yield Strength	MPa	350
	Ultimate Strength	MPa	480
	Tangent Modulus	MPa	40000
Damage Initiation Criteria	Tensile fiber failure mode	--	Maximum Strain
	Failure mode (Compressive fiber)	--	Maximum Strain
	Failure mode (Tensile matrix)	--	Maximum Strain
	Failure mode (Compressive matrix)	--	Maximum Strain

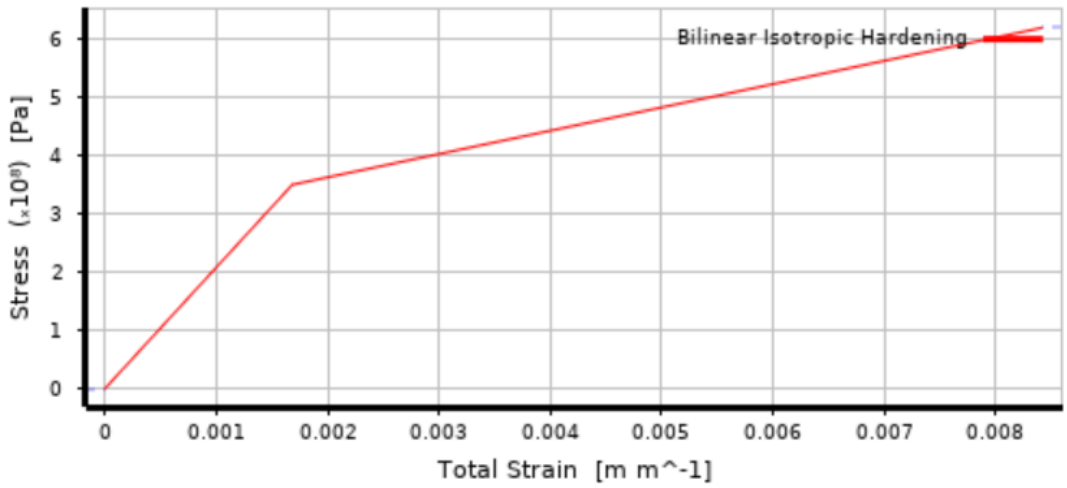

Fig. 3.7 Stress-Strain Relationship for Headed Shear Stud

3.4 BOUNDARY CONDITIONS

For the experimental program to be simulated correctly, boundary conditions are crucial, and any inappropriate boundary conditions could lead to entirely different and incorrect results. Choosing the appropriate boundary condition becomes crucial in this thesis in order to replicate the experimental test results. Symmetry Region 2 is subjected to the Z-axis symmetric boundary condition (BC), which prevents any nodes on the surface from shifting in the Z direction and restricts rotation about the X and Y axes, as seen in Fig. 3.8.

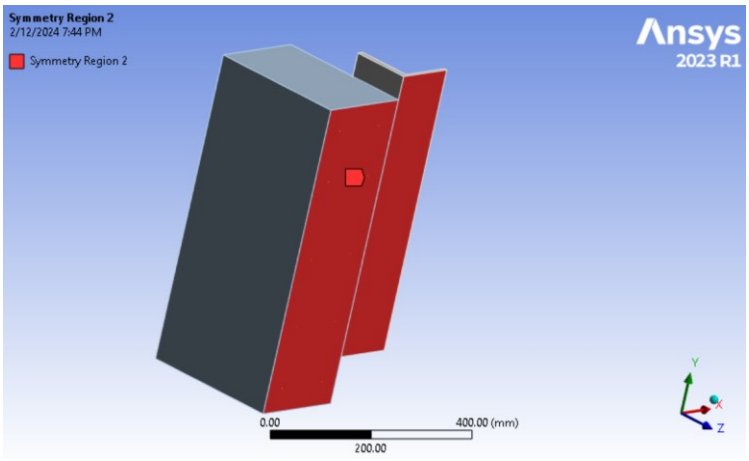

Fig. 3.8 Z-Axis symmetric Boundary Condition

Symmetry region 1, which is the centre of the web of the steel beam, is subjected to the X-axis symmetrical BC in order to constrain all the nodes of the steel beam web in the X-direction as well as revolution about the Y and Z axes as exposed in Fig. 3.9.

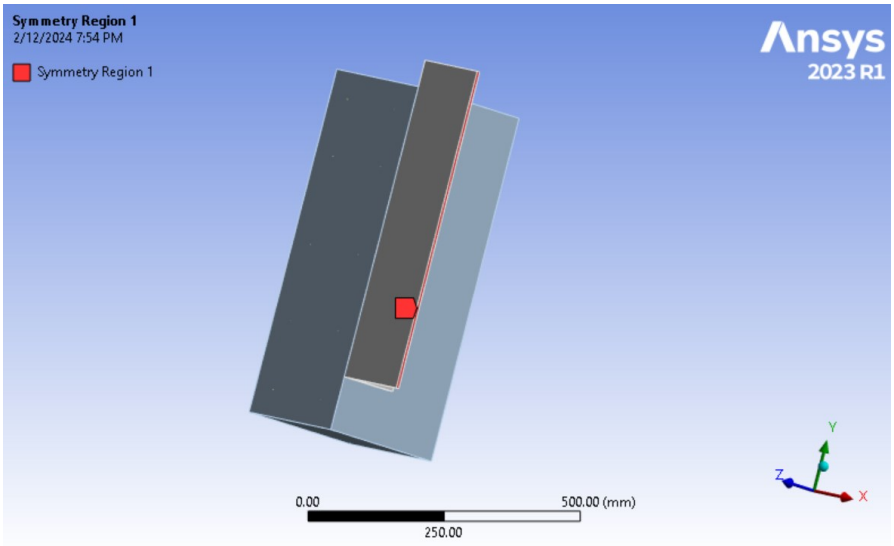

Fig. 3.9 X-Axis Symmetric Boundary Condition

All rotational and translational movements are restricted at the concrete slab bottom surface, applying fixed support which is represented by Fig. 3.10

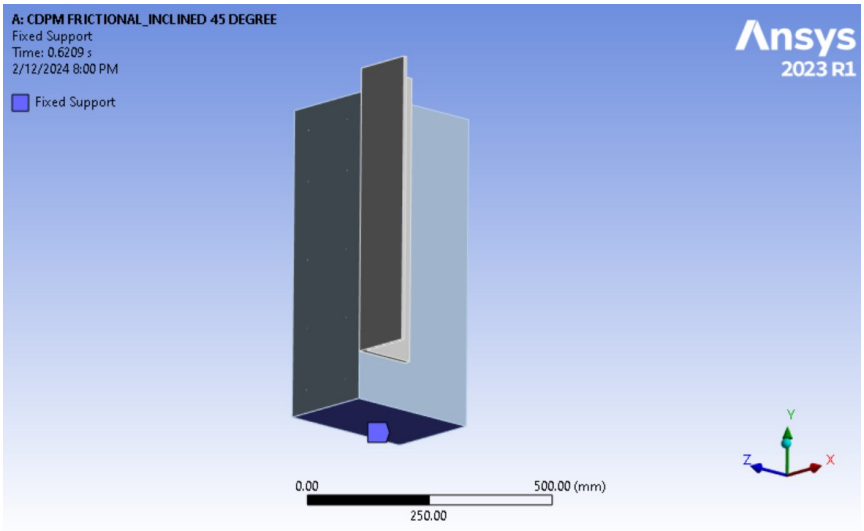

Fig. 3.10 Fixed Support at the Bottom Surface of the Concrete Slab

Displacement loading along the direction of positive & negative Y-axis was applied at the top surface of the steel section as shown in Fig. 3.11

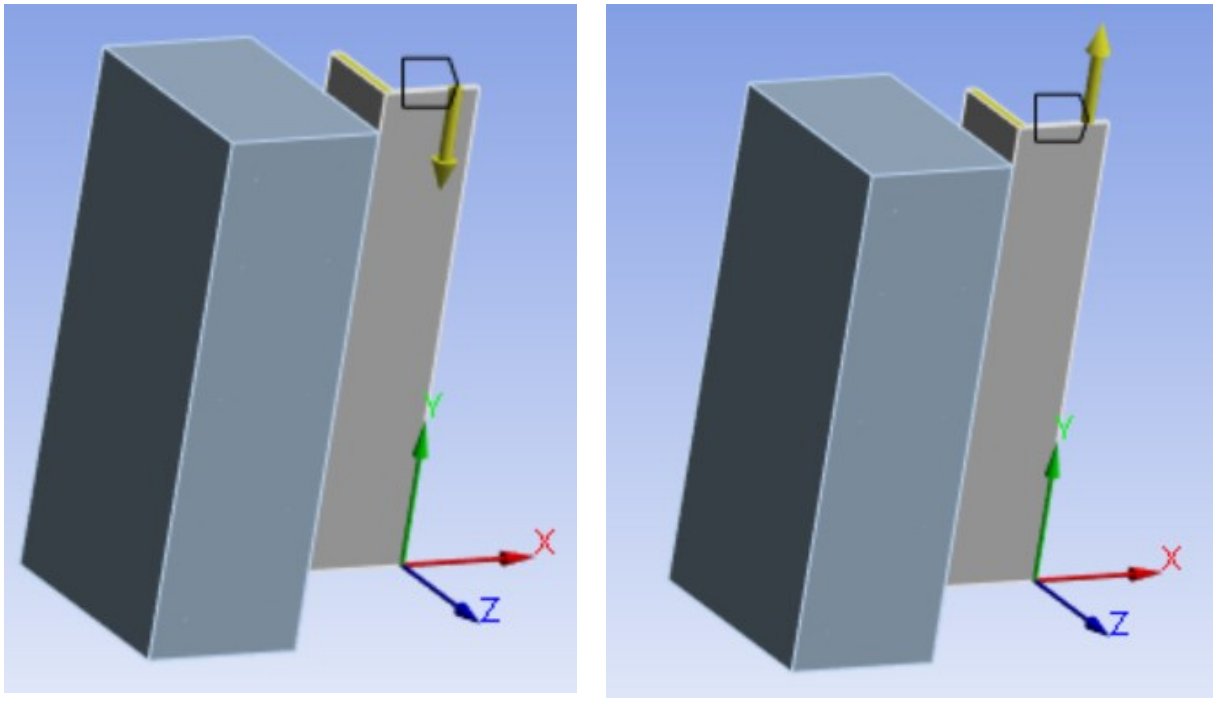

(a) (b)

Fig. 3.11 Displacement Loading: (a) Downward (Push), (b) Upward (Pull)

3.5 CONTACT AND INTERACTIONS

For contact between different fragments of the model in ANSYS, the surface-to-surface contact technique was applied. Contact and interactions between different parts of the push out test geometry is described below.

3.5.1 Contact Between Concrete Slab and Steel Beam

As seen in Fig. 3.12, a frictionless interaction is used between the steel beam and the concrete slab. Frictionless interaction is used in order to represent the appropriate test condition, because lubricating the flange prevented attachment at the boundary between the steel beam flange and the concrete slab in tests conducted by Gattesco and Giuriani

[51]. The load is supposed to be shifted from the steel I beam to the headed shear studs (HSS) and then to the concrete slab in this interaction. In contact settings, steel beam was selected as target body and concrete slab was selected as contact body. Augmented Lagrange based contact formulation and nodal projected normal from contact-based detection method was used. Normal stiffness factor was considered as 0.1 considering bending dominated problem and stiffness was updated at each iteration. Time step was controlled using automatic bisection and to ensure no gap between the parts, interface treatment is considered as adjust to touch.

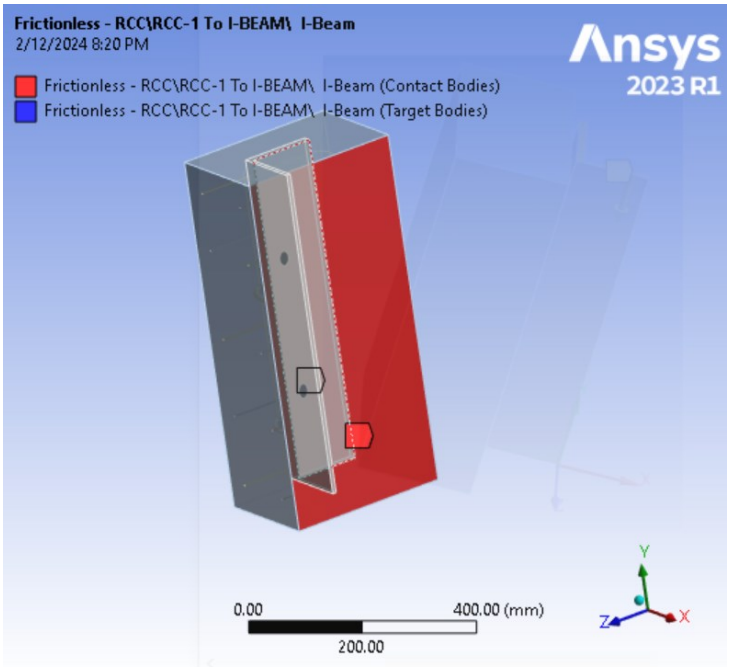

Fig. 3.12 Frictionless Contact Between Steel Beam Flange & Concrete Slab

3.5.2 Contact Between Steel Beam Flange and Headed Shear Stud

Bonded Contact was considered between steel beam flange and Headed shear stud as shown in Fig. 3.13. In contact settings, steel beam was selected as target body and headed shear stud was selected as contact body. Multi-point constraints (MPC) based contact formulation and nodal projected normal from contact-based detection method was used. When compared to alternative settings, the nodal projected normal from the contact

detection method yields more precise interaction tractions and stresses of the underneath elements. The target and contact surface designations have less of an impact on the results. The nodal projected normal from the contact detection method exhibits smoother variation in the determined force of contact distribution across multiple target components. Creating a set of MPC equations that expresses the connection between the DOFs of the two surrounded nodes—that is, how the DOFs of one node are dependent on the other's and vice versa, is the fundamental idea behind using MPC. Pinball region was considered as program controlled.

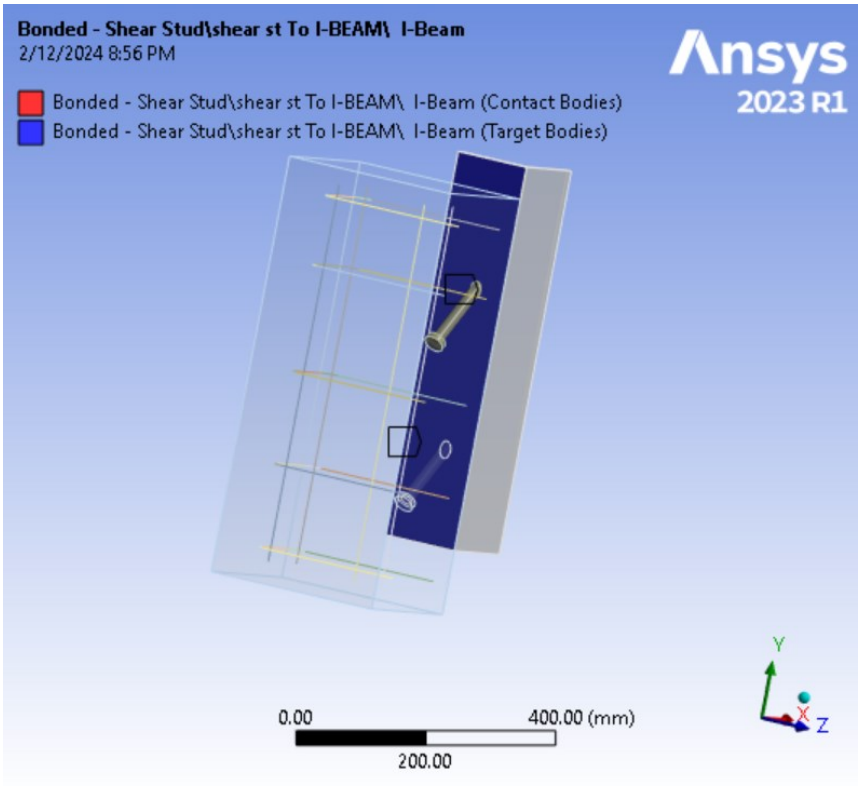

Fig. 3.13 Bonded Contact Between Steel Beam Flange & Headed Shear Stud

3.5.3 Contact between concrete slab and headed shear stud

Frictional contact with frictional coefficient 0.5 was considered between concrete and embedded headed shear stud as shown in Fig. 3.14. From literature it was found that the static friction coefficient between steel and concrete may vary from 0.57 to 0.70 under

compressive stress [60]. Average friction coefficient may be taken as 0.50 under 1-68000 psi stress level [61]. In contact settings, headed shear stud was selected as target body and concrete slab was selected as contact body. Augmented Lagrange based contact formulation was used due to its acceptable accuracy and minimal computational time. The robustness of the Augmented Lagrange Method is achieved with minimal penetration. For contact detection nodal projected normal from contact-based detection method was used. Normal stiffness factor was considered as 0.1 considering bending dominated problem and stiffness was updated at each iteration. Time step was controlled using automatic bisection and to ensure no gap between the headed shear stud and concrete slab interface between them was treated as adjust to touch.

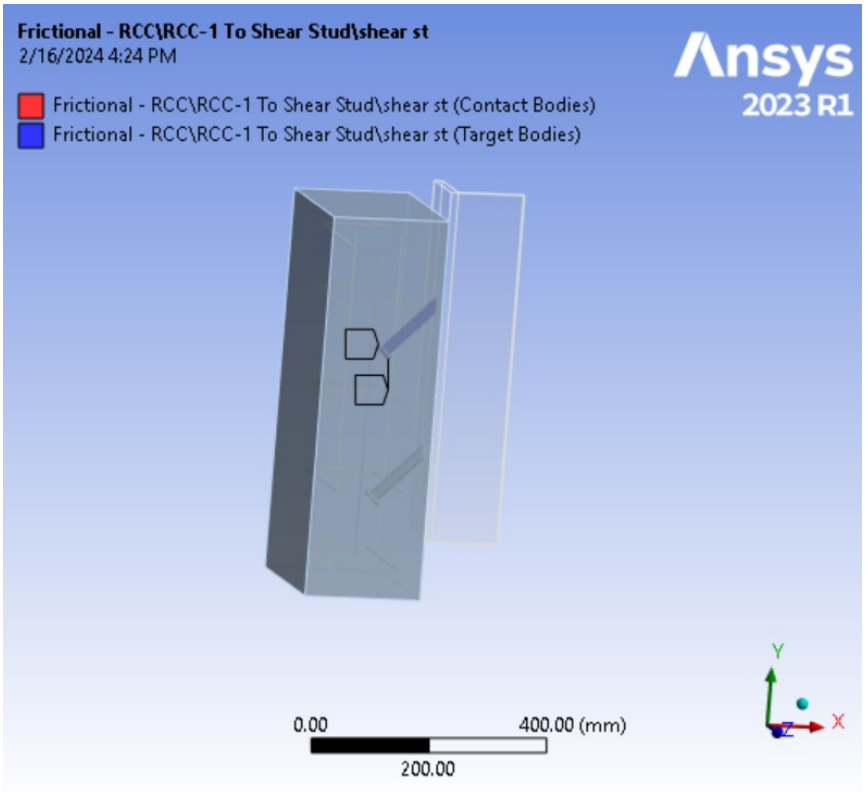

Fig. 3.14 Frictional Contact Between Concrete & Headed Shear Stud

3.5.4 Surface to Surface Contact & Target Modelling

For surface-to-surface contact modelling CONTA174 and for Surface-to-surface target modelling TARGE170 was selected by ANSYS. Both elements are described below.

CONTA174 Element Description

CONTA174 is used to represent contact and sliding between target faces. Coupled field contact, general interactions, pair-based interactions, shear & coulomb friction and three-dimensional structural analysis is possible using this contact model. The element has the indistinguishable geometric topographies as the solid or shell element face with which it is associated. When the surface of the element penetrates a corresponding target surface, contact is established. In order to mimic interface delamination, the element additionally permits the separation of bonded contact [57].

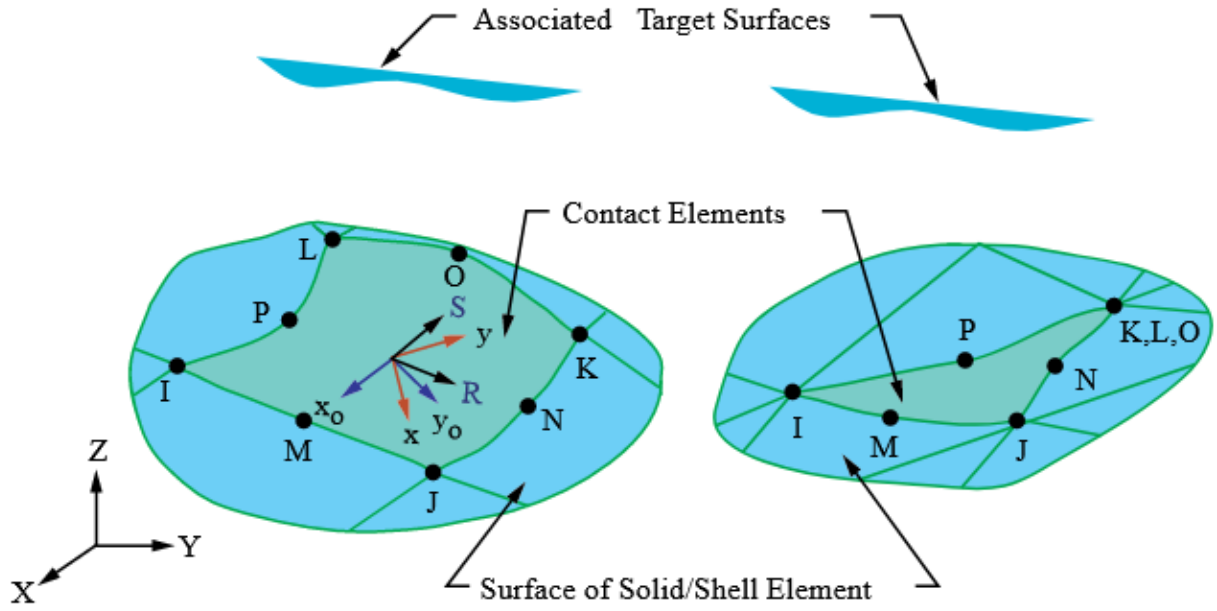

Fig. 3.15 CONTA174 Geometry [57]

TARGE170 Element Description

TARGE170 can be used for target modelling of the deformable solid, shell and line elements. It can be used to impose various parameters on the target segment element, such as translational or rotational displacement, temperature, forces, moments, voltage, magnetic potential, pore pressure, and concentration.

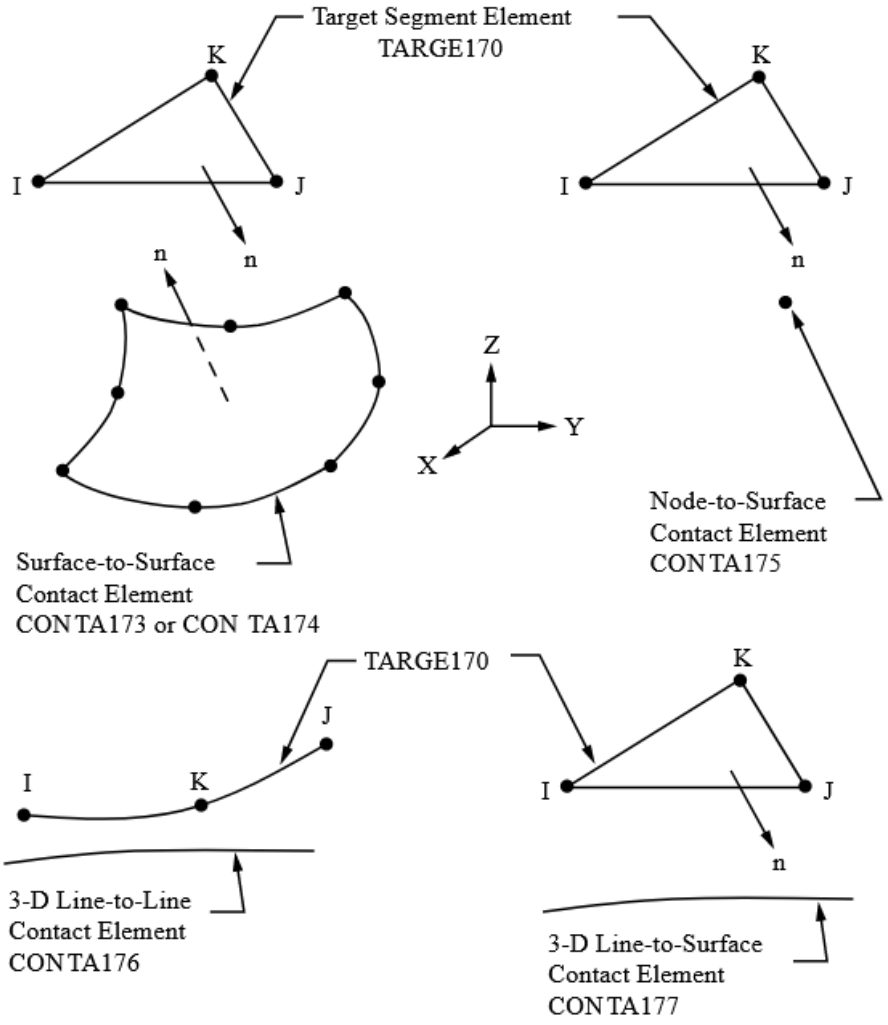

Fig. 3.16 TARGE170 Geometry [57]

3.6 FINITE ELEMENT MESHING & ELEMENT SELECTION

A good quality mesh is very important to obtain accurate results. Although a coarse mesh greatly shortens the required time for analysis, the results' precision is unacceptable. Too

much fine mesh increases the computational time but the accuracy of results is high. Considerable efforts have been made in this work for the selection of proper mesh size to obtain acceptable accuracy of results and minimal computational time.

3.6.1 Mesh Convergence Study

In push out test of steel concrete composite structure maximum part of the simulation time requires for the analysis of concrete slab. To get accurate stress distribution in concrete slab within minimal computational time selection of proper mesh size is very important. To ensure that element sizes are adequate for reaching the required level of accuracy in the solution obtained through finite element analysis, a mesh convergence study was conducted. Unit downward displacement was applied on steel beam and corresponding force reaction was determined for different mesh size of concrete slab from 10 mm to 25 mm. From mesh convergence study it is seen that force reaction is not being changed significantly for mesh size less than 20 mm. Table 3.6 shows the maximum force reaction for different element size of concrete slab

Table 3.6 Maximum force reaction for different element size of concrete slab

Element Size (mm)	Number of Elements	Maximum Force Reaction (kN)
25	10884	5.87
20	14560	44.82
18	18948	41.15
15	23216	41.58
12	36418	41.87
10	53424	41.98

Fig. 3.17 shows the force-displacement relationship for different mesh size of concrete slab. It is seen from the Fig. 3.17 that the force-displacement relationship is mostly identical for mesh size less than 20 mm.

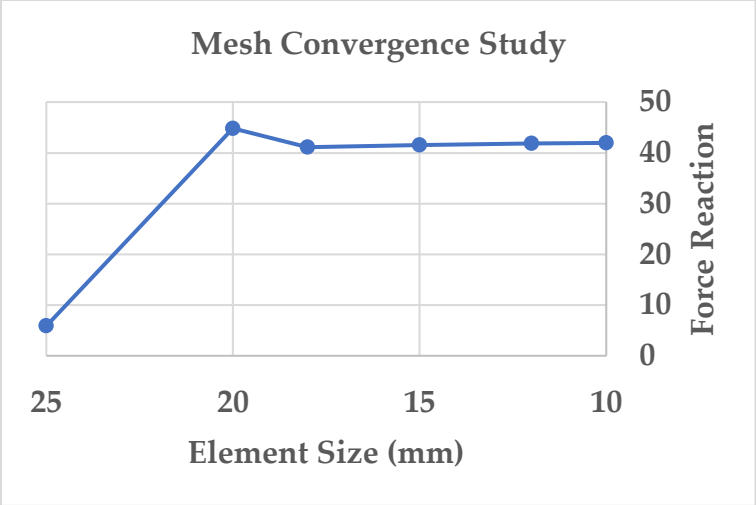

Fig. 3.17 Mesh Convergence Study

3.6.2 Meshing of Concrete Slab & Element selection

The concrete slab part was meshed with 3D eight node brick element CPT 215 using body fitted cartesian method as shown in Fig. 3.18. The Cartesian method fits the geometry with an unstructured, mostly uniformly sized hexa mesh that is aligned to the given coordinate system. Maximum element size was considered as 15 mm with finer mesh at the region of concrete where the shear studs are embedded. Element order was considered as linear.

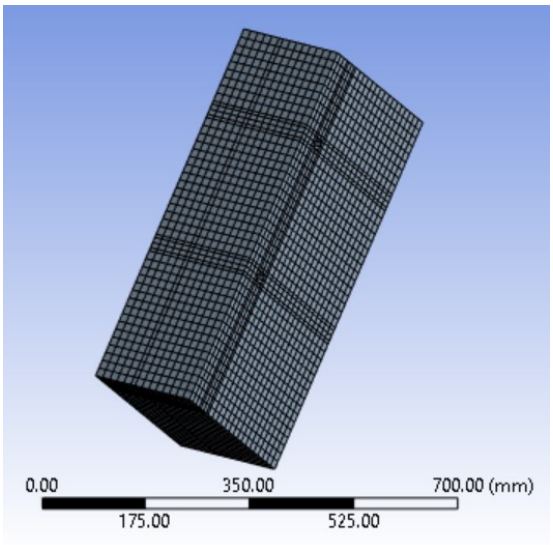

Fig. 3.18 Linear Cartesian Mesh of Concrete Slab

CPT215 Element Description

Fig. 3.19 illustrates the three-dimensional, eight-node coupled pore-pressure-thermal mechanical solid element, CPT215. The element is composed of eight nodes, each corner node of which has four (or possibly five) degrees of freedom:

- Translations along the x, y, and z directions
- Degree of freedom considering pore-pressure
- degree of freedom considering temperature

Large rebound, large strain competences, stress solidifying, and elasticity are included in CPT215.

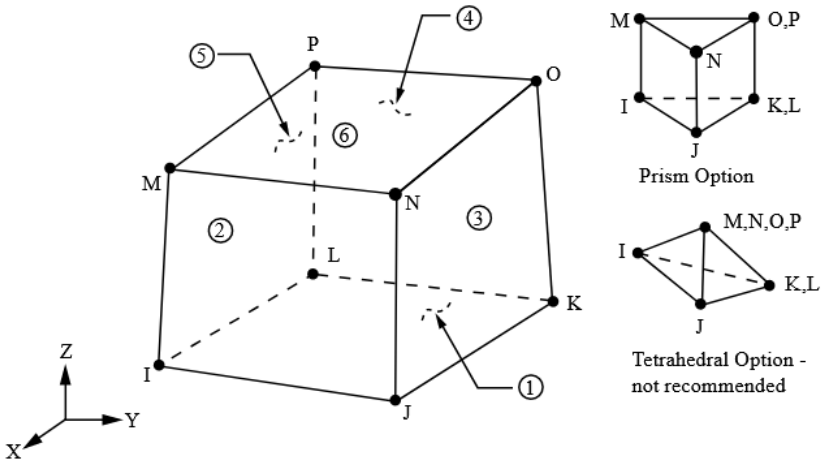

Fig. 3.19 CPT215 Structural Solid Geometry [59]

3.6.3 Meshing of Steel Beam & Element selection

The steel beam part was meshed with 3D eight node brick element SOLID185 using body fitted cartesian method as shown in Fig. 3.20. Maximum element size was considered as 10 mm. Element order was considered as linear.

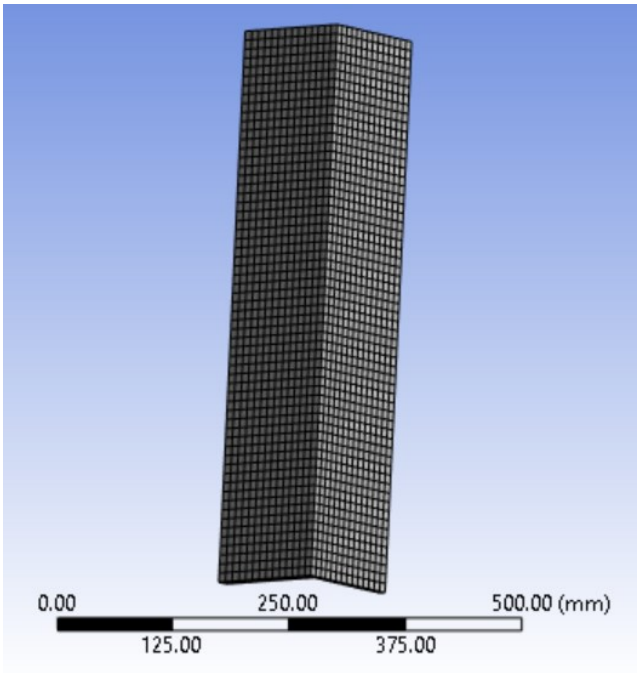

Fig. 3.20 Linear Cartesian Mesh of Steel Beam

SOLID185 Element Description

SOLID185 is a 3-D eight node brick element having three degrees of freedom (translations along the local x, y and z directions). It can consider large deformation, large strain abilities, creep, stress setting, hyper elasticity. Furthermore, it can simulate the deformations of fully incompressible hyper elastic materials and nearly incompressible elastoplastic materials using mixed formulation capabilities. When applied in irregular regions, prism, tetrahedral, and pyramid degenerations are permitted.

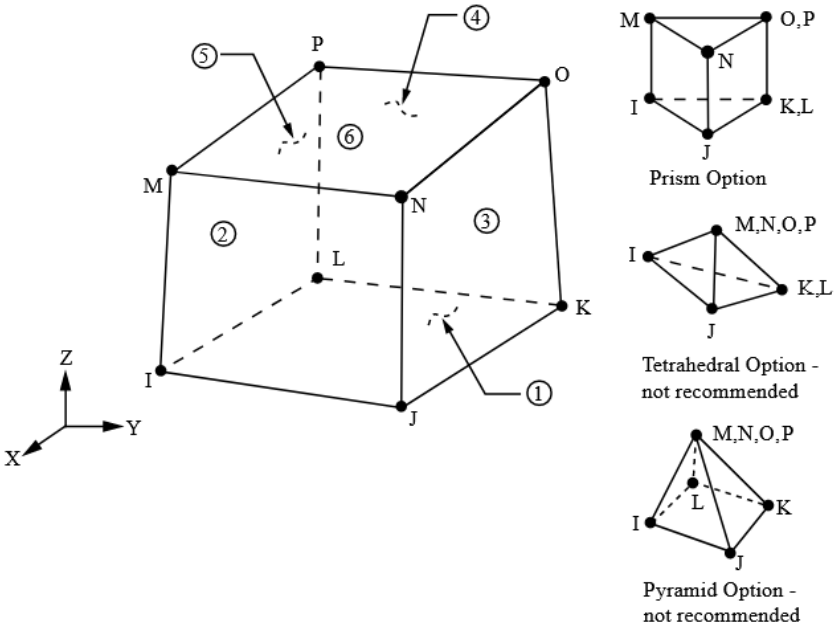

Fig. 3.21 SOLID185 Structural Solid Geometry [59]

3.6.4 Meshing of Headed Shear stud & Element selection

The headed shear stud part was meshed with 3-D 4-node tetrahedral element SOLID285 using patch conforming method as shown in Fig. 3.22. The method used in Patch Conforming Method is bottom-up. Beginning with the edges and faces, the meshing process proceeds into the volume. Every face and its boundaries are accepted, complied with, and blended together. This produces a clean, high-quality mesh. Maximum element size was considered as 6 mm. Element order was considered as linear.

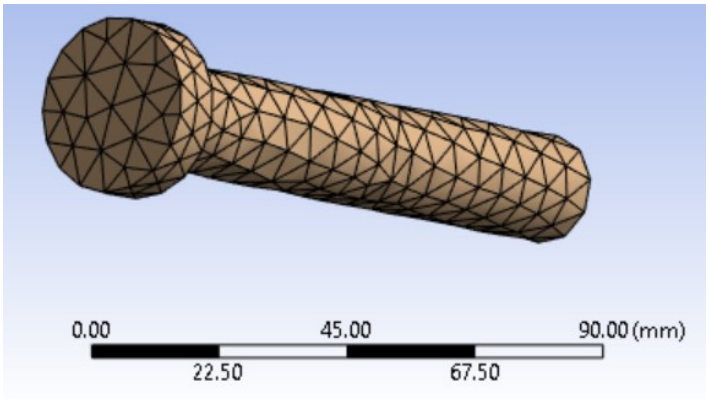

Fig. 3.22 Linear Tetrahedral Meshing of Headed Shear Stud

SOLID285 Element Description

As seen in Fig. 3.23, the SOLID285 element is a lower-order 3-D, 4-noded element. The element is composed of four nodes, each of which has four degrees of freedom: one hydrostatic pressure (HDSP) for all materials other than nearly incompressible hyperplastic materials, and three translations in the nodal x, y, and z directions. For nearly incompressible materials, the three translation degrees of freedom and the volume change rate are used at each node in place of hydrostatic pressure. The element's properties include large deflection, large strain capabilities, creep, hyper elasticity, and stress stiffening. It can simulate the deformations of elastoplastic materials that are almost incompressible, hyperplastic materials that are almost incompressible, and completely incompressible hyperplastic materials.

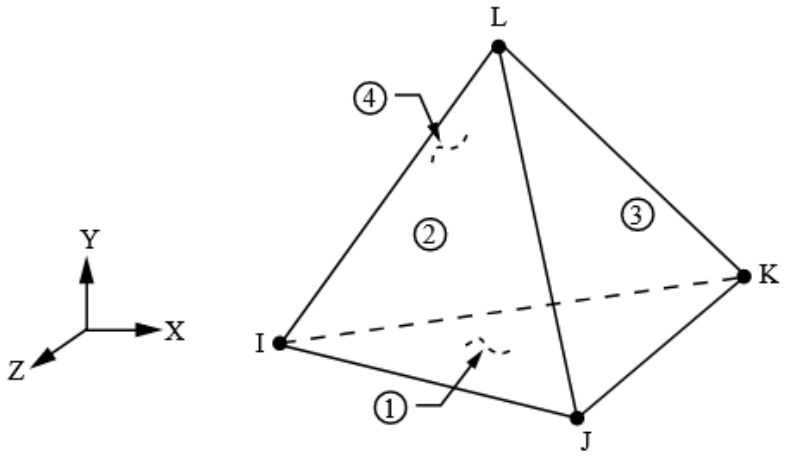

Fig. 3.23 Solid285 Structural Solid Geometry

3.6.5 Meshing of Reinforcement & Element selection

Reinforcement embedded in concrete slab was meshed using 3-D discrete reinforcing element REINF264 as shown in Fig. 3.24. This element works well with complex geometry and is mesh-independent, allowing for quick solution generation with a high rate of convergence. Element size was considered as 15 mm.

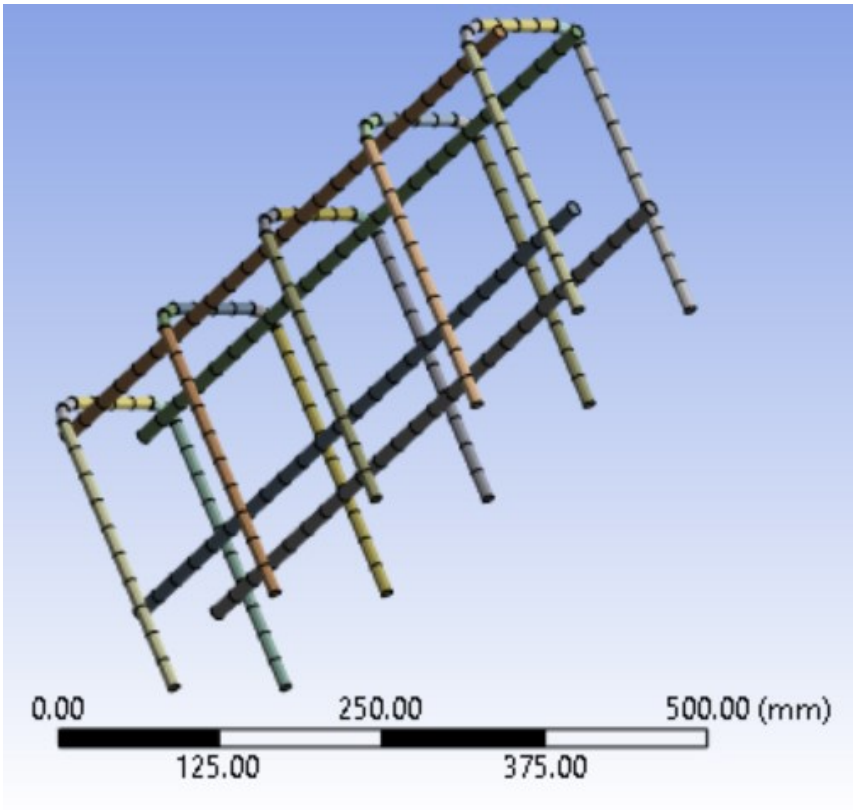

Fig. 3.24 Meshing of Reinforcement

REINF264 Element Description

To give additional reinforcing to standard 3-D link, beam, shell, and solid elements—also known as the base elements, REINF264 is applied. The component can be used to simulate reinforcing fibres in any orientation. As a spar with only uniaxial stiffness, each fibre is modelled independently. The REINF264 element has the same degrees of freedom, nodal locations, and connectivity as the base element. The properties of REINF264 include plasticity, creep, stress rigidifying, large rebound, and large strain competences.

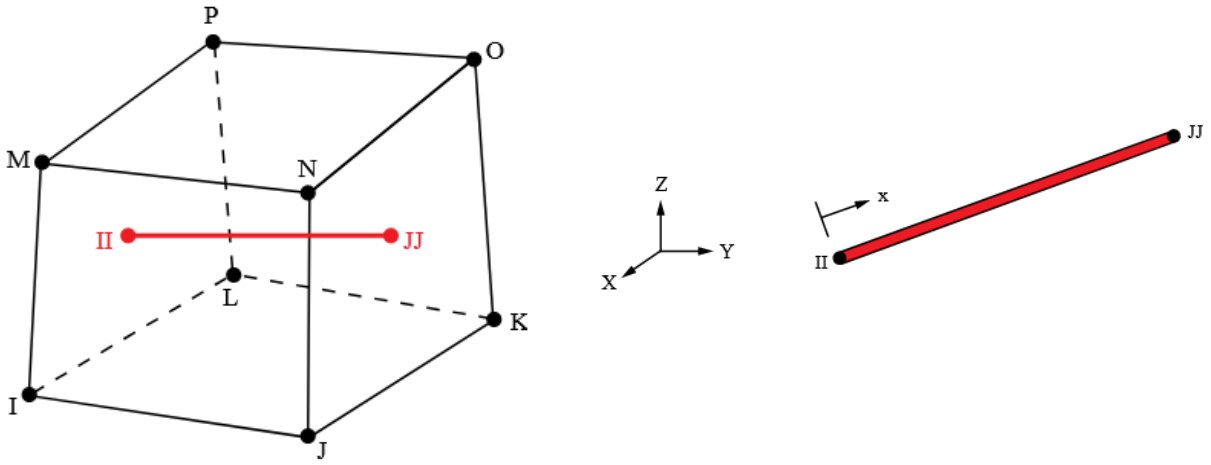

Fig. 3.25 REINF264 used with 3-D 8-Node brick element CPT215

3.6.6 Mesh Quality Check

A finite element simulation's outcome is greatly influenced by the mesh's quality. A mesh cell's quality can be measured in a number of ways. To assess the quality of mesh elements, ANSYS runs multiple geometrical checks on them. These measurements, or checks, are:

- Element Quality
- Aspect Ratio
- Jacobian Ratio
- Warping Factor
- Maximum Corner Angle
- Skewness

Different parameters of the mesh quality of the finite element push out test model is described below

Element quality:

The square root of the cube of the summation of the squares of the edge lengths for 3D elements, or the volume to the sum of the squares of the edge lengths for 2D quad/tri elements, determines the element quality. A composite quality metric with a range of 0 to 1 is called the element quality. A perfect cube or square is represented by a value of 1, and an element with a zero or negative volume is represented by a value of 0 [62] [63]. The results of the finite element model, as displayed in Fig. 3.26, indicate that the average element quality is 0.91 and the minimum element quality is 0.45.

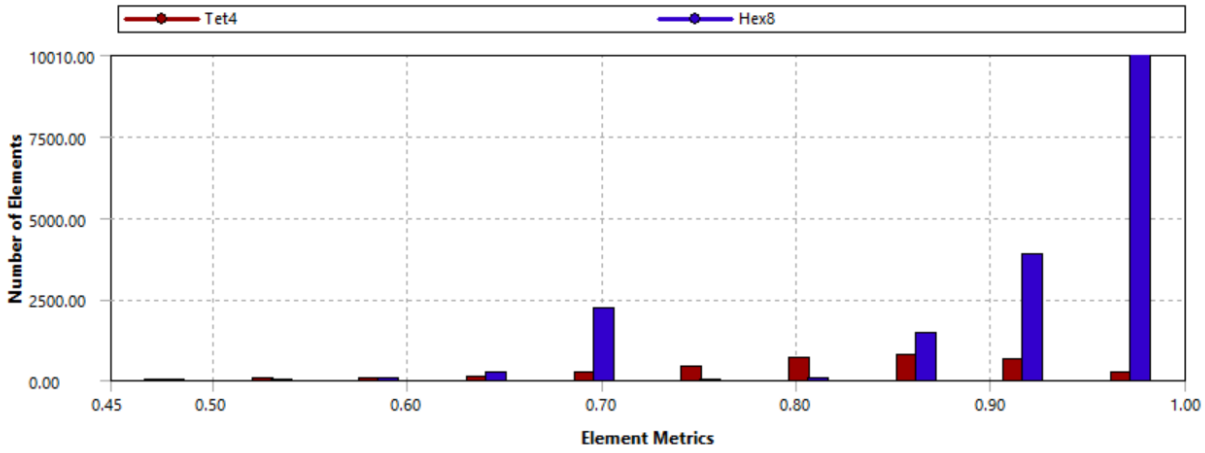

Fig. 3.26 Element Quality

Aspect Ratio:

The aspect ratio indicates the ratio of height to width for triangle and long sideways to short sideways for quadrilaterals. It ranges from 1 to infinite. A square is indicated by a value of 1.0 [62] [63]. Here as shown in Fig. 3.27 minimum aspect ratio is found as 1, maximum aspect ratio 4.54 and average aspect ratio is 1.46.

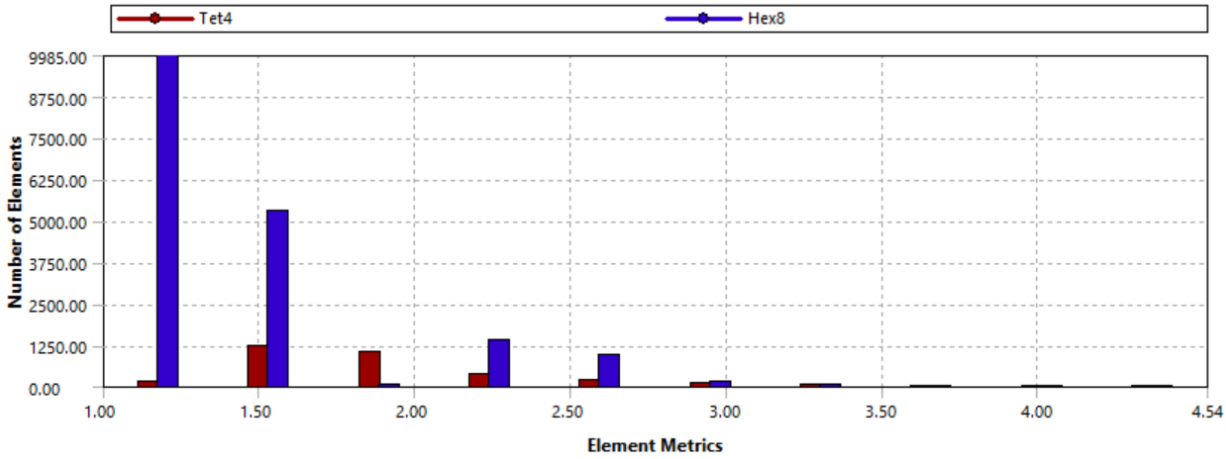

Fig. 3.27 Aspect Ratio

Jacobian Ratio:

A measurement of an element's shape in relation to an ideal element is called the Jacobian ratio. The type of element determines the ideal shape for it. The majority of the elements in a high-quality mesh have a Jacobian ratio between 1 and 10 (90% and above), with 1.0 being the ideal value [62] [63]. The average Jacobian ratio in this instance is 0.99, as seen in Fig. 3.28.

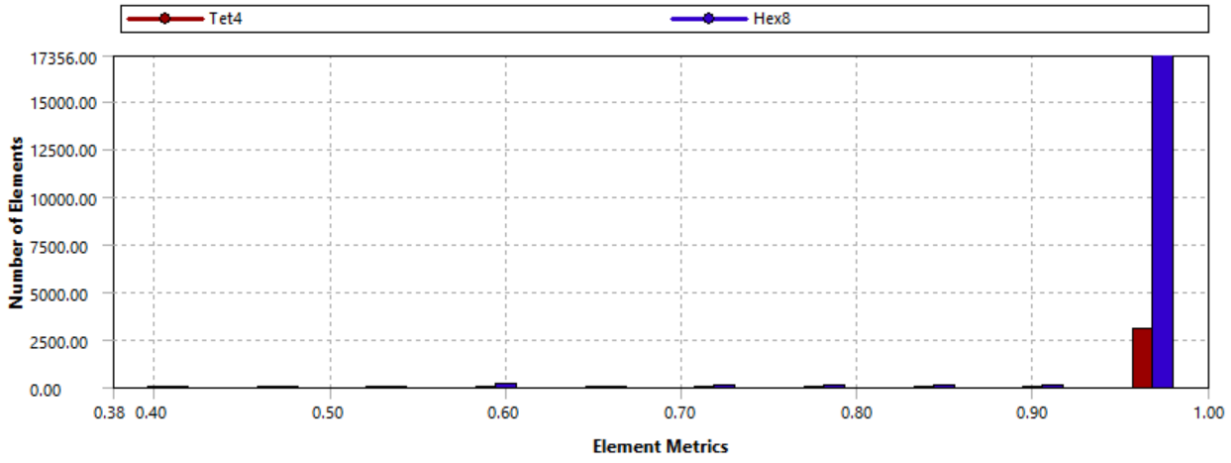

Fig. 3.28 Jacobian Ratio

Warping Factor:

A measurement of twisting and distortion is called warping. Zero is the ideal warping factor. The maximum warping factor in this case is zero, as Fig. 3.29 illustrates.

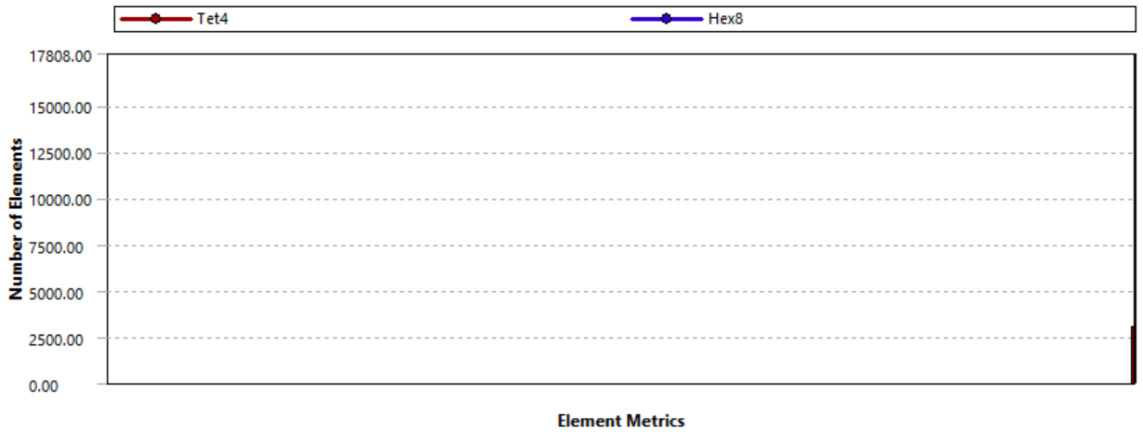

Fig. 3.29 Warping Factor

Maximum Corner Angle:

This is an element's extreme angle formed by two adjacent edges. The ideal maximum angle for a triangle is sixty degrees. It is 90 degrees for a quadrilateral. Here, 91.81 degrees is found to be the maximum corner angle.

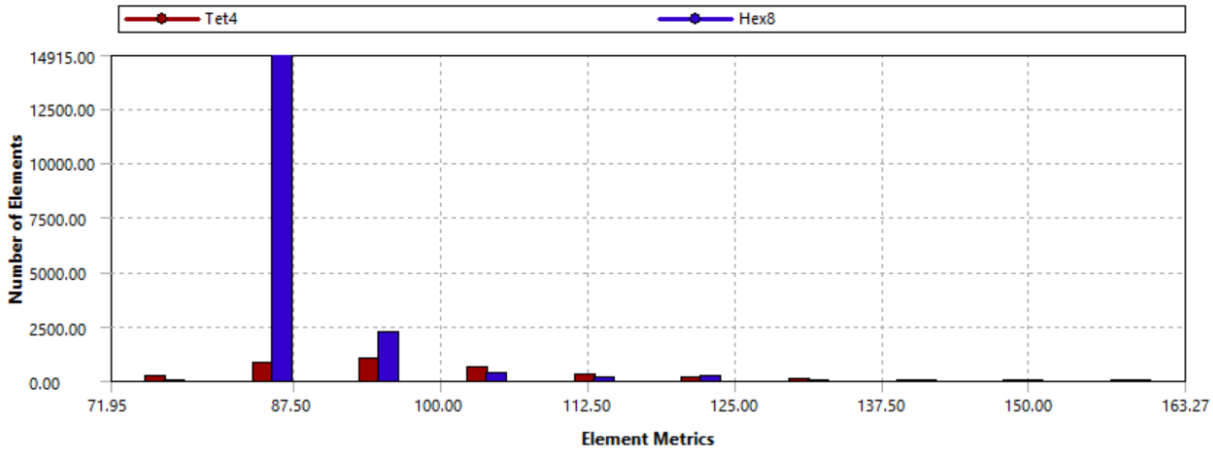

Fig. 3.30 Maximum Corner Angle

Skewness:

One of the main criteria for evaluating a mesh's quality is its skewness. How close a face or cell is to being ideal (equilateral or equiangular) is determined by its skewness. Here, $4.58e^{-2}$ is the average skewness.

Table 3.7 ANSYS Recommended Scale for Skewness [63]

Value of Skewness	Cell Quality
0.5 to 0.75	Reasonable
0.25 to 0.5	Decent
0 to 0.25	Outstanding
0	Square

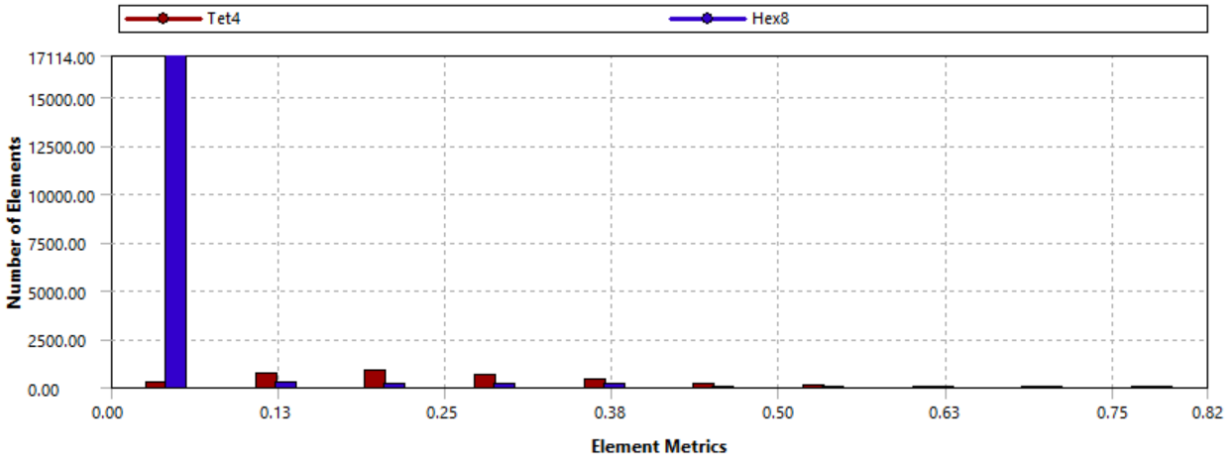

Fig. 3.31 Skewness

3.7 ANALYSIS SETTINGS AND SOLUTION STRATEGY

In this numerical study displacement control technique was used for load application by time step control in ANSYS. Number of steps was selected as 1 considering initial sub step 200, minimum sub step 200 and maximum sub step 100000. The auto time step feature was activated. By varying the load increment, auto time stepping, also referred to as time step optimization, seeks to shorten the solution time, particularly for nonlinear

and/or transient dynamic problems. The added benefit of automatic time stepping, if nonlinearities exist, is that it can appropriately increase loads and, in the event that convergence is not achieved, fall back to the previously converged solution (bisection). The degree of nonlinearities in the analysis and the structure's response frequency are two factors that determine how much load is increased. Newton Raphson Iteration method has been implemented here to find the solution of the problem.

Newton Raphson Iteration Method:

The Newton-Raphson Iteration technique is employed by ANSYS to address nonlinear problems. The displacement can be applied in multiple steps by breaking it down into a series of increments. The Newton-Raphson equilibrium iterations in a nonlinear analysis with one degree of freedom are shown in Fig. 3.32. The out-of-balance load vector, or the difference between the applied loads and the reestablishing forces, is evaluated by the Newton-Raphson method prior to each solution. After that, the program uses the out-of-balance loads to perform a linear solution and verifies convergence. Until the program converges, this iterative process is carried out.

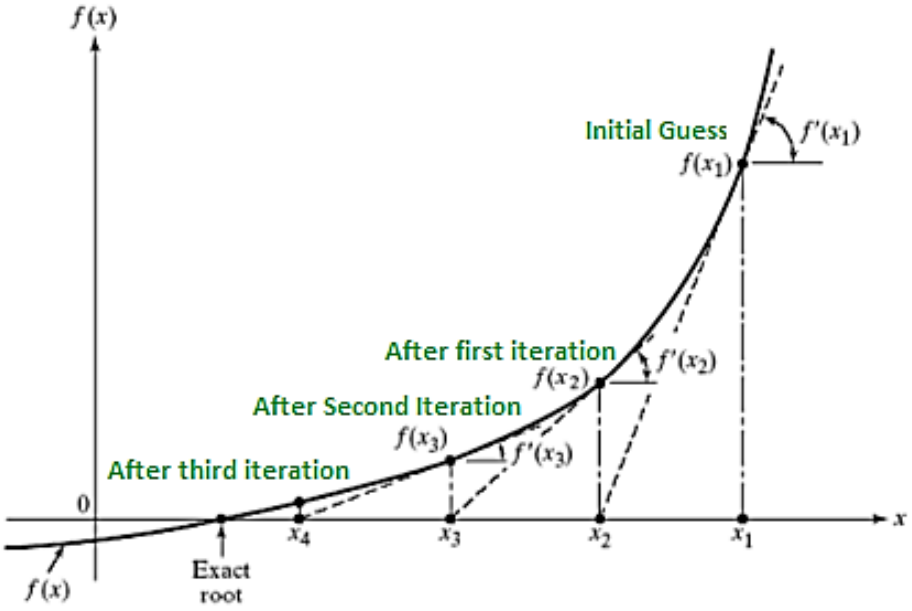

Fig. 3.32 Newton Raphson Iteration Method

Chapter 4: RESULTS AND DISCUSSIONS

4.1 GENERAL

In this numerical study the structural performance of inclined shear key in steel-concrete composite structure was evaluated using finite element model developed in ANSYS software. In this chapter Preliminary Validation of FE Model with the results of previous experimental test, load-slip curve of headed shear stud, ultimate shear resistance, principal stress and strain distribution, failure mode and other parameters are described.

4.2 PRELIMINARY VALIDATION OF THE FINITE ELEMENT MODEL

To increase the FE model's reliability, its results must be compared to those of the experiment. This validation process ensured that the numerical model accurately represented the behaviour of the push out test. The FE model for a 19 mm perpendicularly placed HSS is validated in Fig. 4.1, and its results are compared with those of the tests conducted by Gattesco and Giuriani (1996) [51]. Since the compressive cube strength of concrete (fcu) in their tests was set at 32.5 MPa, the compressive cylinder strength of concrete in FE analyses is assumed to be 26 MPa (0.8 fcu). As can be seen from Fig. 4.1, the ultimate strength of a single headed shear stud found from experimental test is 109.645 and the ultimate strength determined by the FE analysis is 113.175 kN, which is almost close to the test result. In the Gattesco and Giuriani (1996) test, the ultimate slip value was reported to be 9.70 mm; however, from FE analysis it is found to be 9.81 mm. The mean value of the P_{Test}/P_{FEA} ratio is 0.97. Table 4.1 displays a good comparison between the results of the experiment and the maximum slip at failure as determined by finite element analysis. Consequently, the shear connection capacity and load-slip behaviour of the headed shear stud with common and large diameter were successfully predicted by the finite element models.

Table 4.1 Comparison between experimental and FE Analysis results

Experimental Result		FE Analysis Result		
Ultimate Strength of Headed Shear Stud (kN)	Maximum Slip (mm)	Ultimate Strength of Headed Shear Stud (kN)	Maximum Slip (mm)	P_{Test}/P_{FEA}
109.645	9.70	113.175	9.81	0.97

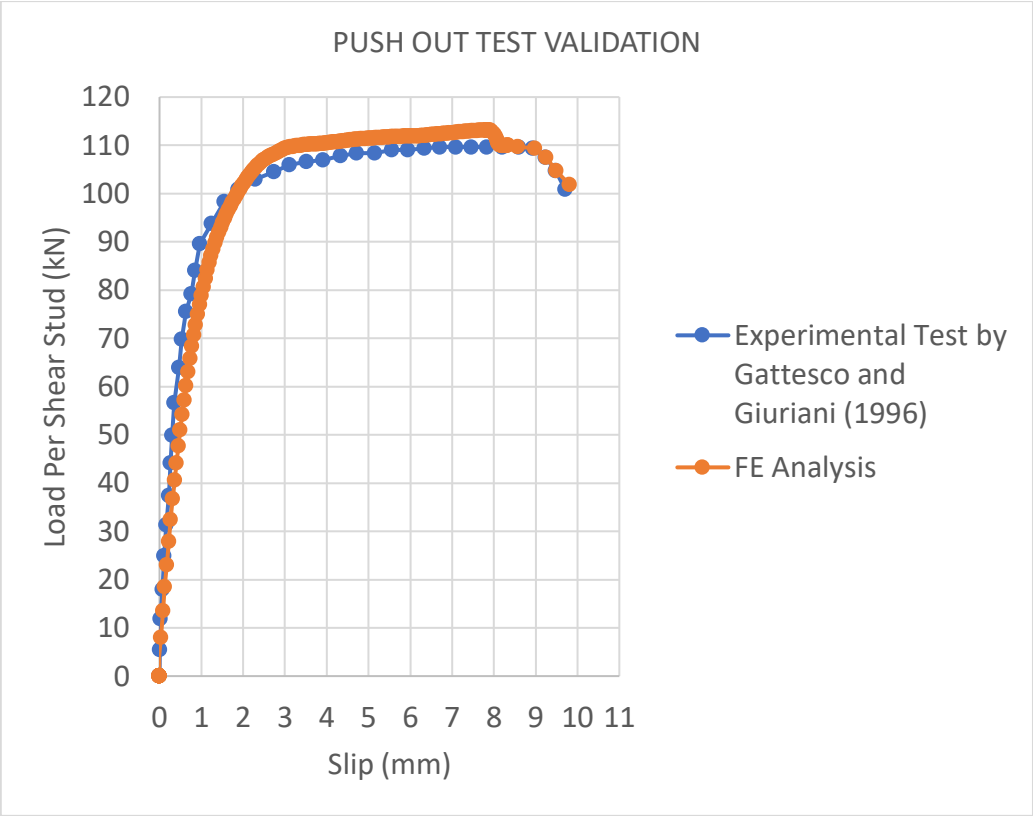

Fig. 4.1 Validation of FE Push-Out Test Model with Experimental Test [51]

4.3 COMPARISON OF FE ANALYSIS RESULTS WITH CSA S6-14, BNBC-2020, & AASHTO LRFD

4.3.1 Ultimate Shear Resistance According to CSA S6-14:

According to CSA S6-14 the ultimate shear resistance of a HSS shall be taken as lesser of the following equations 4.1 & 4.2

$$q_r = 0.5\ \varphi_{sc} A_{sc} \sqrt{(f'_c E_c)} \leq \varphi_{sc} A_{sc}\ F_u \quad (4.1)$$

$$q_r = \varphi_{sc} A_{sc}\ F_u \quad (4.2)$$

Ultimate shear strength calculation:

$q_r = 0.5\ \varphi_{sc} A_{sc} \sqrt{(f'_c E_c)}$

$= 0.5*0.8*\frac{3.1416*19*19}{4}*\sqrt{26 * 24000}$ N

= 89589 N

=89.589 kN

Again,

$q_r = \varphi_{sc} A_{sc}\ F_u$

$= 0.8*\frac{3.1416*19*19}{4} *480$ N

= 108875 N

= 108.875 kN

Hence, according to CSA S6-14 the ultimate shear resistance of a HSS is 89.589 KN

4.3.2 Ultimate Shear Resistance According to BNBC-2020:

According to Bangladesh National Building Code (BNBC)-2020 [43] the nominal shear strength of one headed stud shear connector embedded in solid slab in composite construction can be expressed as the lesser of the following equations 4.3 & 4.4.

Qn =0.5 $A_{sc}\sqrt{(f'cEc)}$ (4.3)

Qn =$RgRpAscF$u (4.4)

Ultimate shear strength calculation:

Qn = 0.5 $A_{sc}\sqrt{(f'cEc)}$

$= 0.5 * \frac{3.1416*19*19}{4} * \sqrt{26 * 24000}$

= 111985 N

= 111.985 KN

Qn = $RgRpAscF$u

= 1.0*0.85*$\frac{3.1416*19*19}{4}$*480 N

= 115679 N

= 115.679 kN

Hence, according to BNBC-2020 the ultimate shear resistance of a headed shear stud is 111.98 KN

4.3.3 Ultimate Shear Resistance According to AASHTO LRFD:

According to AASHTO LRFD the nominal shear strength of one headed stud shear connector embedded in solid concrete slab in composite construction can be expressed as the lesser of the following equations 4.5 & 4.6.

$$P = 0.5A_{sc}\sqrt{f_{ck}E_{cm}} \quad (4.5)$$

$$P = A_{sc}f_u \quad (4.6)$$

Ultimate shear strength calculation:

$$P = 0.5A_{sc}\sqrt{f_{ck}E_{cm}}$$

$$= 0.5 * \frac{3.1416*19*19}{4} * \sqrt{26 * 24000}\ \text{N}$$

$$= 111985\ \text{N}$$

$$= 111.985\ \text{KN}$$

$$P = A_{sc}f_u$$

$$= \frac{3.1416*19*19}{4} * 480\ \text{N}$$

$$= 136094\ \text{N}$$

$$= 136\ \text{KN}$$

Hence, according to AASHTO LRFD the ultimate shear resistance of a headed shear stud is 111.985 KN.

Fig. 4.2 & Table 4.2 represents the comparison between ultimate shear strength calculated according to CSA S6-14, BNBC-2020, AASHTO LRFD and FE Analysis. It is seen that the Ultimate shear strength found from FE analysis is closely matching with the calculated ultimate shear strength according to BNBC-2020 & AASHTO LRFD.

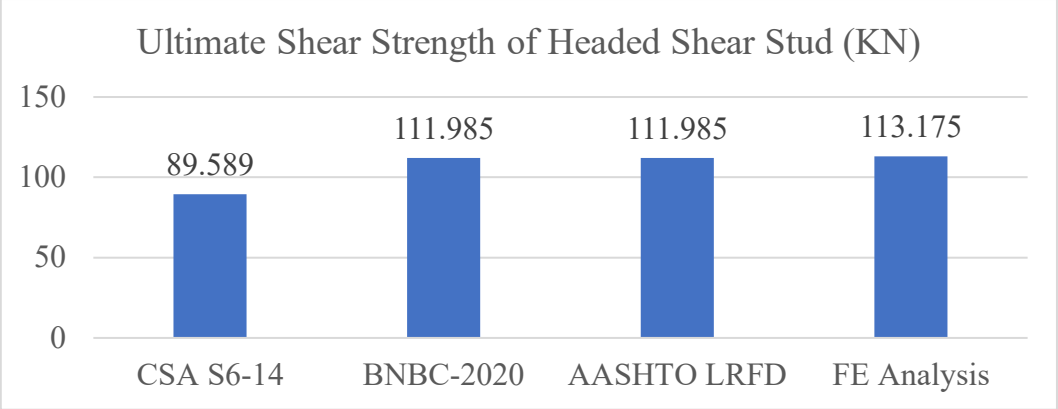

Fig. 4.2 Comparison of Ultimate Shear Strength of Headed Shear Stud

Table 4.2 Comparison of Ultimate Shear Strength of Headed Shear Stud obtained from CSA S6-14, BNBC-2020, AASHTO LRFD & FE Analysis

Parameter	CSA S6-14	BNBC-2020	AASHTO LRFD	FE Analysis	$\frac{P_{FEA}}{P_{CSA\,S6-14}}$	$\frac{P_{FEA}}{P_{BNBC-2020}}$	$\frac{P_{FEA}}{P_{AASHTO\,LRFD}}$
Ultimate Shear Strength of a Headed Shear Stud (KN)	89.589	111.985	111.985	113.175	1.26	1.01	1.01

4.4 FE ANALYSIS RESULTS FOR PERPENDICULAR HEADED SHEAR STUD

Finite element analysis results such as load slip curve, stress, strain, damage for perpendicular (0 degree inclined) headed shear stud are shown in this section.

4.4.1 Load Slip Curve

Fig. 4.3 represents the load slip curve for perpendicular (0 degree inclined) headed shear stud. It seen from the curve that the ultimate shear resistance of a headed shear stud embedded in concrete and welded to the flange of steel beam is 113.175 KN and maximum slip of steel beam at failure of concrete is 9.81 mm.

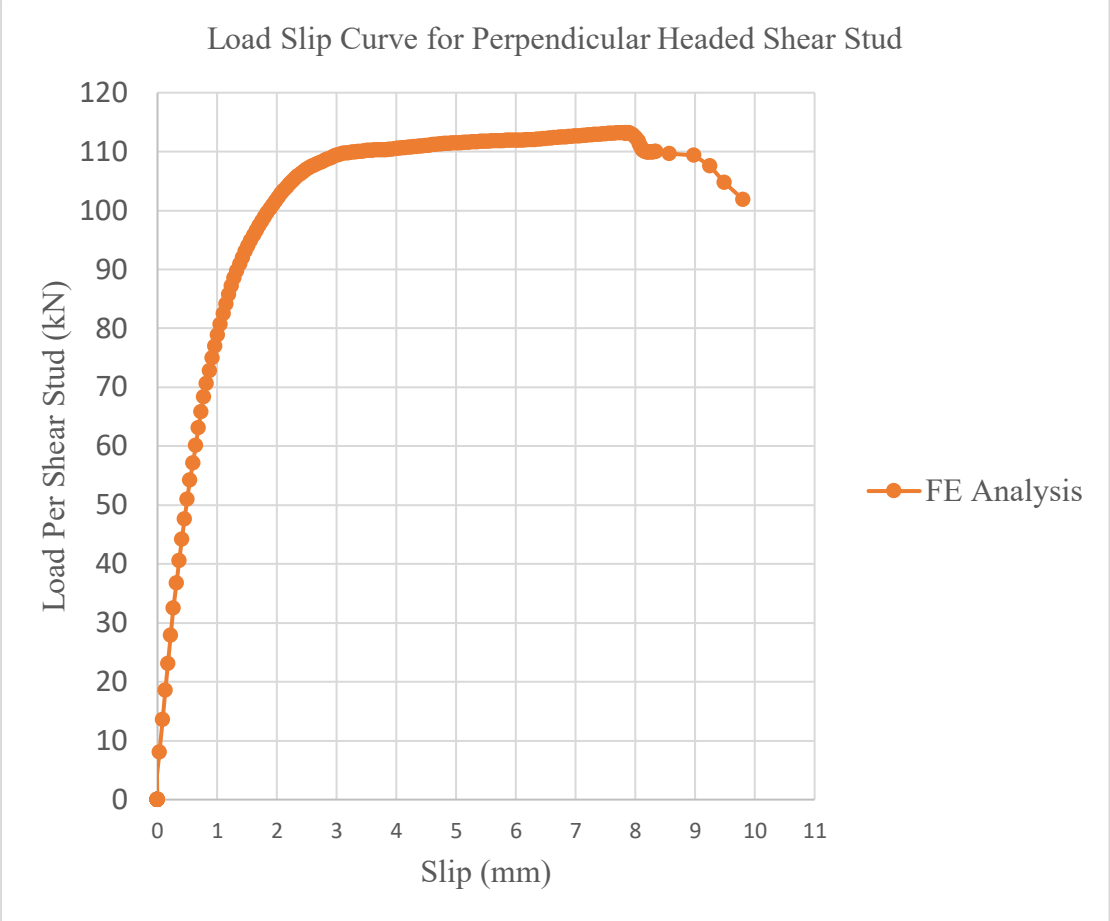

Fig. 4.3 Load Slip Curve for Perpendicular Headed Shear Stud

4.4.2 Principal stress distribution at concrete slab

Principal stress is generally used to determine failure of brittle type material. Positive value of principal stress designates tension and the negative value of principal stress indicates compression. Negative principal stress is compared with the ultimate compressive strength of a brittle material to determine the failure. It is seen from the Fig. 4.4 that the concrete located just below the bottom half of the headed shear stud is in compression. Maximum compressive stress is developed at the concrete slab part located at the bottom of the welded collar of headed shear stud.

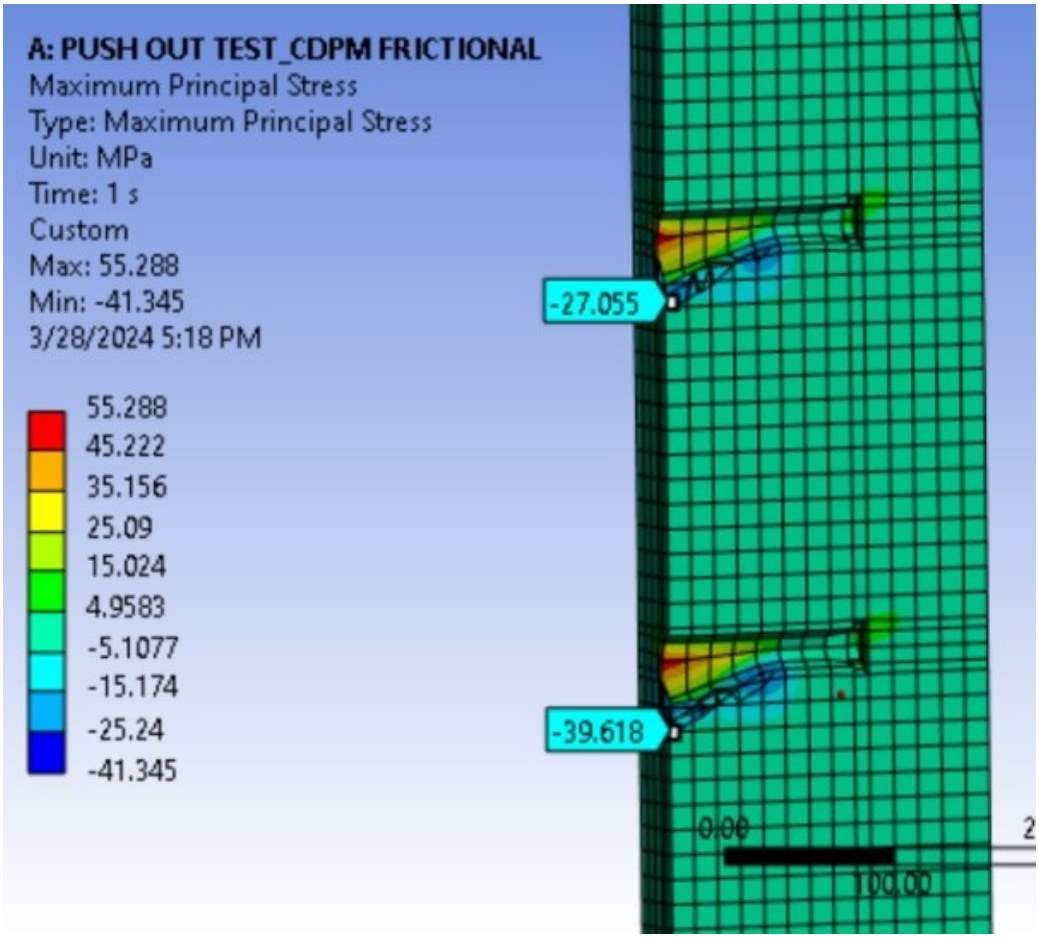

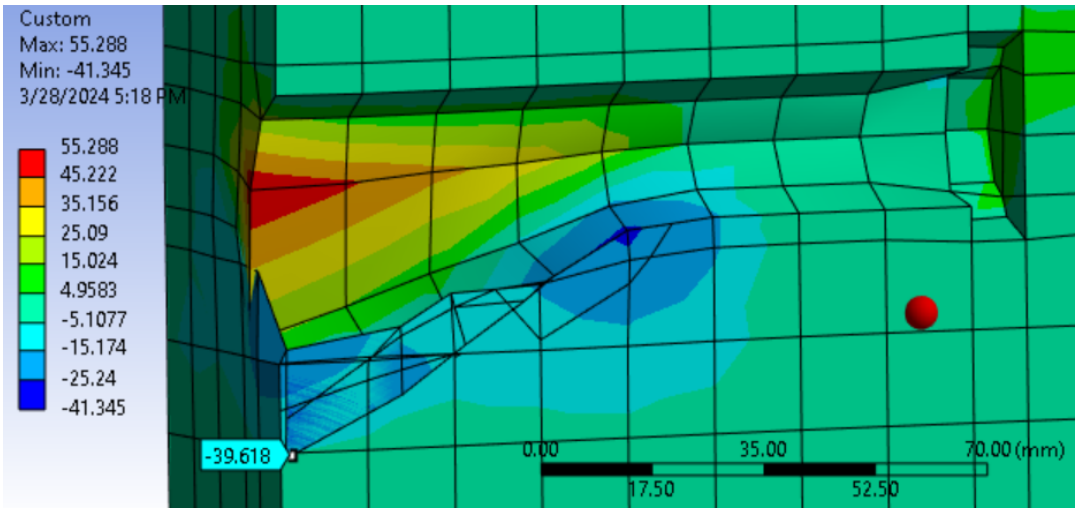

Fig. 4.4 Principal Stress Distribution in Concrete Slab

Fig. 4.5 indicates the factor of safety of concrete slab. It is seen that the factor of safety of concrete slab part located just below the bottom half of the headed shear stud is less than 1.0, which represents the failure of concrete at that region. Factor of safety greater than 1.0 indicates that the material is safe from failure due to the application of load.

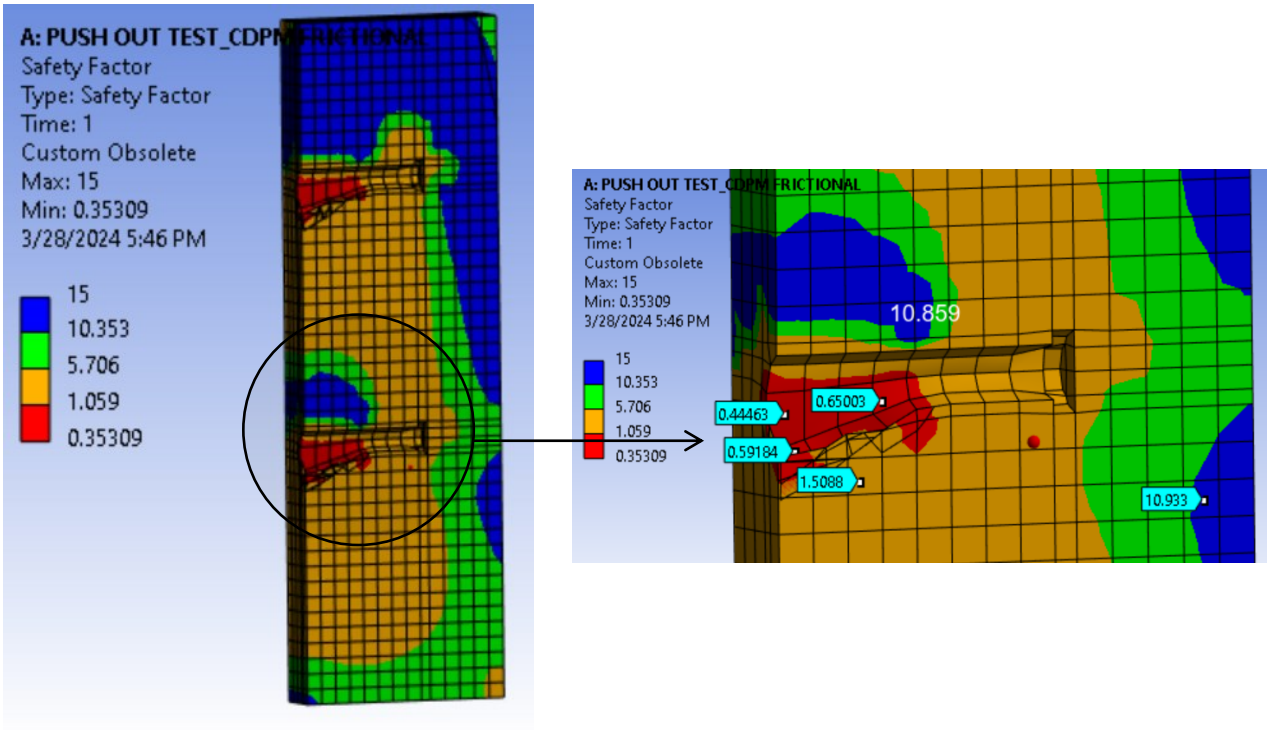

Fig. 4.5 Factor of Safety of Concrete Slab

4.4.3 Von Mises stress distribution at headed shear stud

Fig. 4.6 represents the distribution of equivalent von mises stress at different portion of the headed shear stud, it is seen from the Fig. that the maximum equivalent von mises stress developed at the region of contact between steel beam and headed shear stud. Maximum value of equivalent von mises stress is found to be 2806.8 MPa which is much greater than ultimate tensile strength of headed shear stud. If a cross section is considered at the region of the headed shear where the maximum equivalent von mises stress is generated it is seen that the overall section is not overstressed due to the application of load. As the overall section is not overstressed, yielding of the complete headed shear stud is not being occurred.

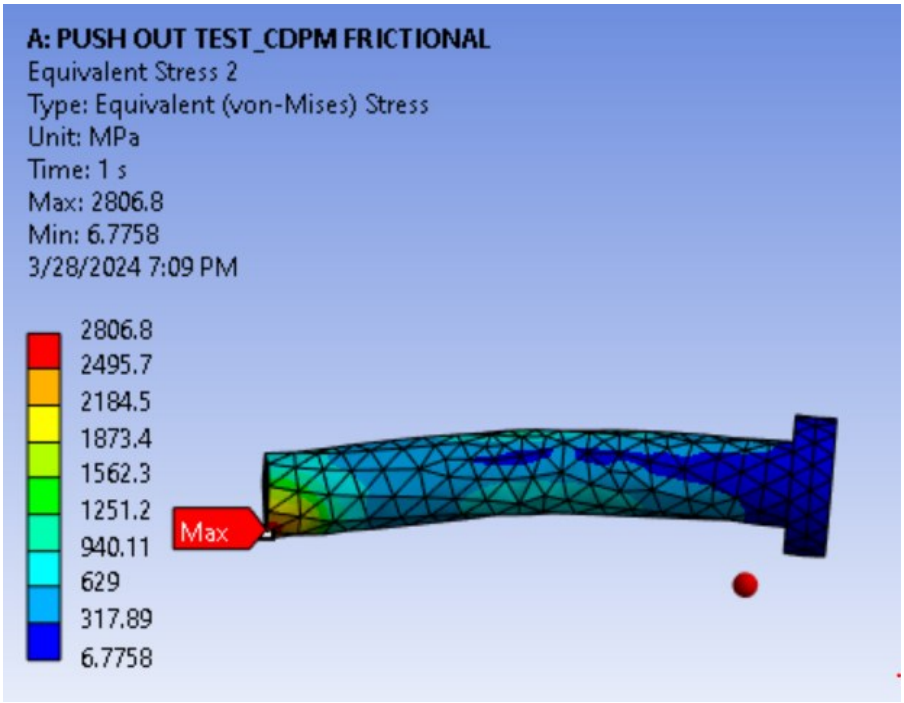

Fig. 4.6 Equivalent Von Mises Stress Distribution at Headed Shear Stud

Fig. 4.7 indicates the factor of safety of headed shear stud with respect to equivalent von mises stress. It is seen that the factor of safety of headed shear stud part located at the region of contact point between steel beam and headed shear stud is less than 1.0, which represents the yielding of headed shear stud at that region. Factor of safety greater than 1.0 indicates that the material is safe from failure due to the application of load.

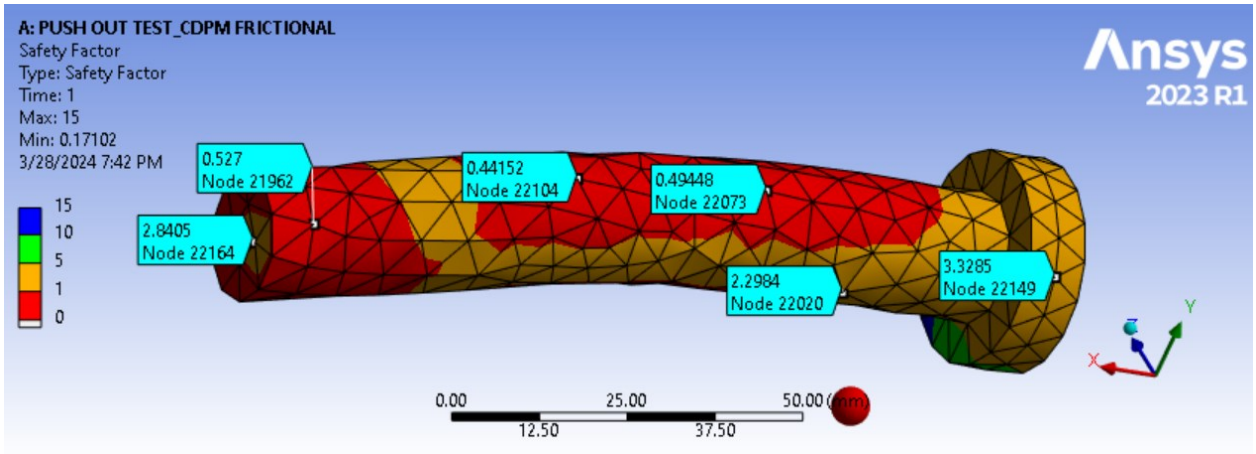

Fig. 4.7 Factor of Safety of Headed Shear Stud

4.4.4 Shear Stress (X-Y Plane) distribution in concrete slab

Fig. 4.8 shows the dispersal of shear stress in concrete slab along X-Y plane. Negative shear stress indicates downward and positive shear stress indicates upward movement.

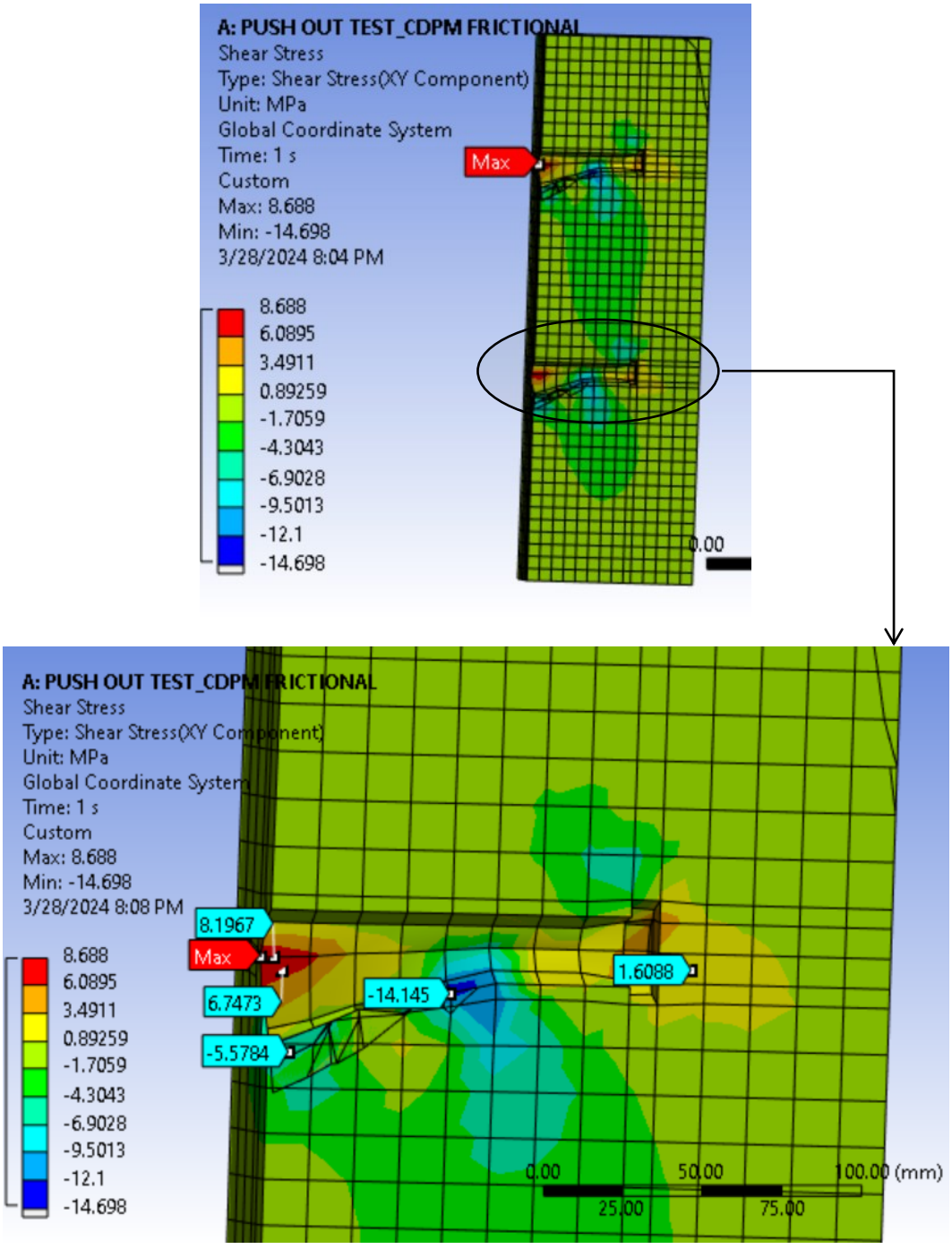

Fig. 4.8 Shear Stress (X-Y Plane) Distribution in Concrete Slab

4.4.5 Shear Stress distribution in headed shear stud

Fig. 4.9 shows the distribution of shear stress in headed shear stud. It is seen from the Fig. 4.9 that the shear stress is maximum at the point where the headed shear stud is connected with the steel beam while the shear stress is minimum at the head of the headed shear stud.

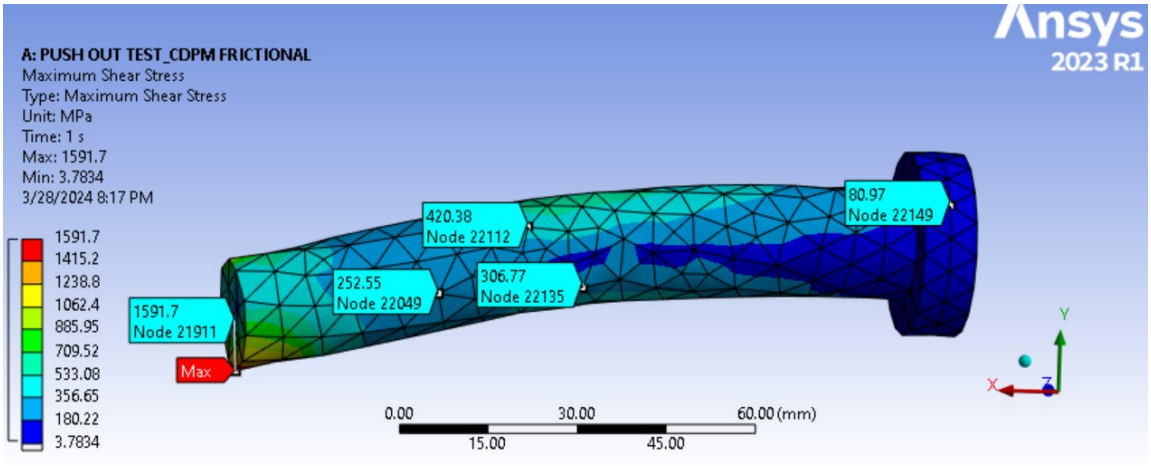

Fig. 4.9 Shear Stress Distribution in Headed Shear Stud

4.4.6 Damage Identification

In this study compression damage & tension damage is identified using following APDL command.

```
/SHOW,png
/ANG,1,
/VIEW,3,3,3,3 !Use these values to change the view
/gfile,600
SET,last !SET,Last = Outputs final result set
esel,s,ename,215
PLNSOL,MPDP,COMP
PLNSOL,MPDP,TENS
```

From the Fig. 4.10 and 4.11 it is seen that both the compression and tension damage occurred in the concrete slab near the location of headed shear stud due to maximum stress concentration.

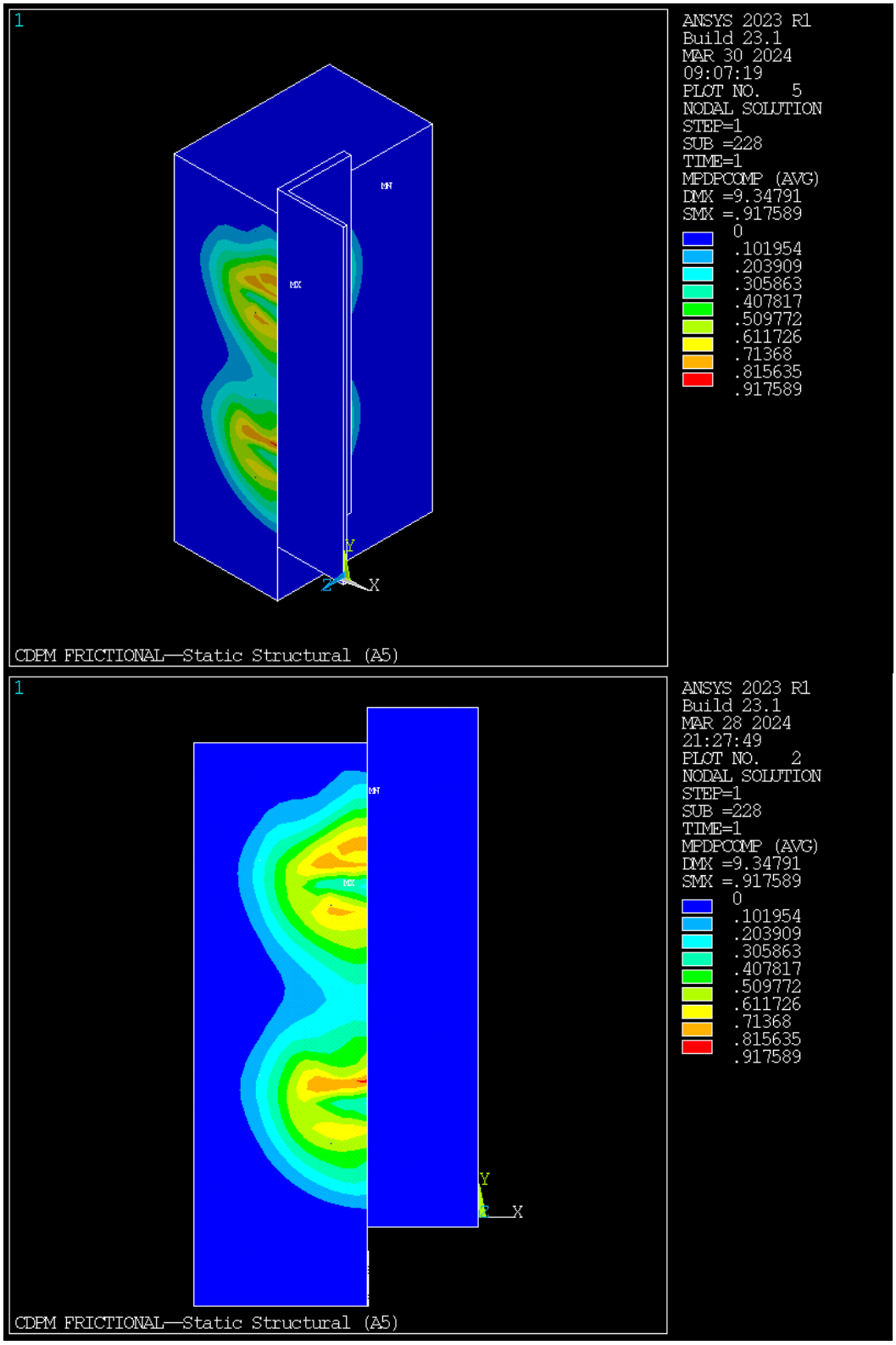

Fig. 4.10 Compression Damage for Perpendicular Headed Shear Stud

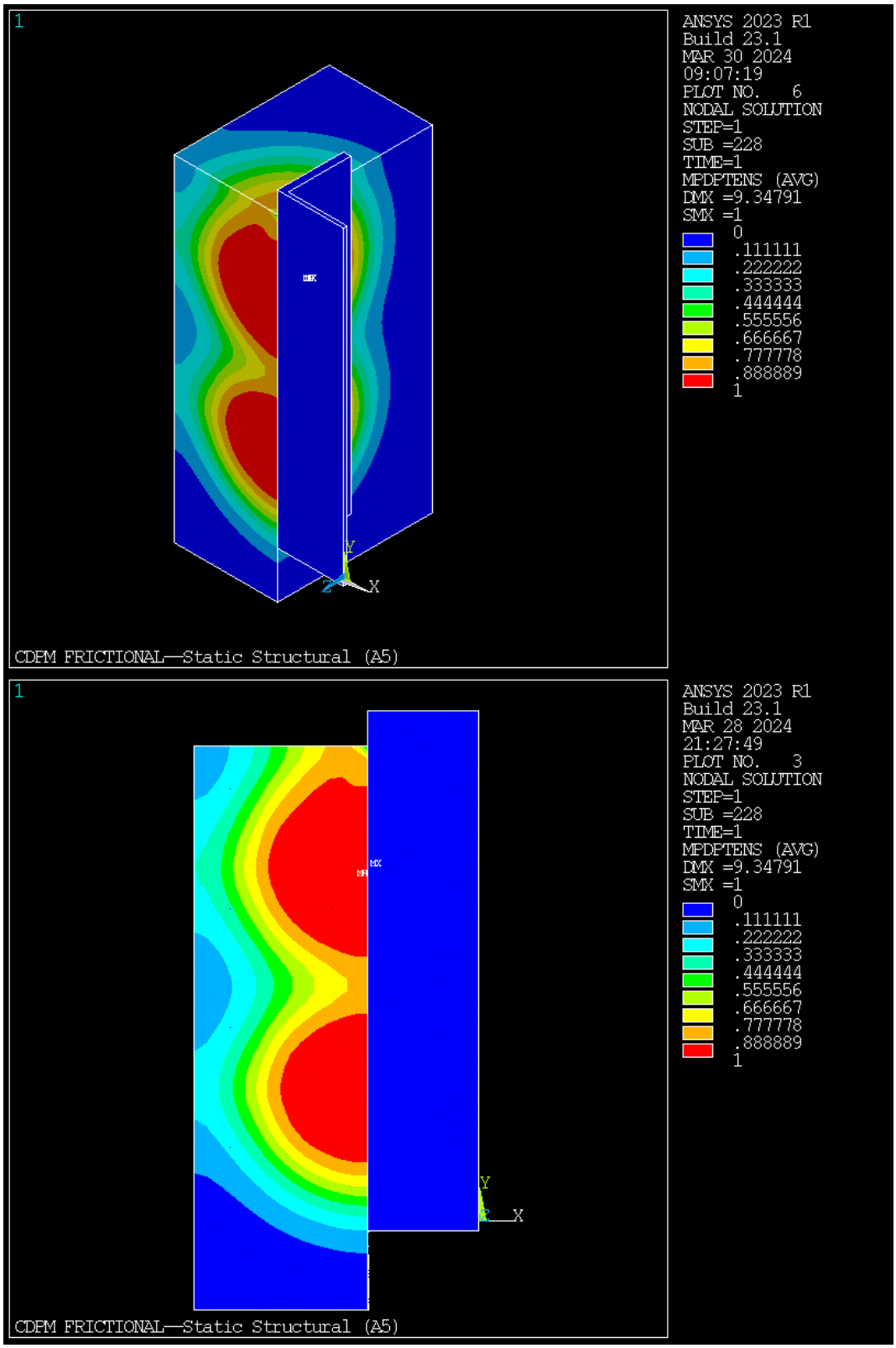

Fig. 4.11 Tension Damage for Perpendicular Headed Shear Stud

4.4.7 Force and Displacement Convergence

When a model has non-linear behaviour, it cannot be resolved directly. An iterative process must be utilized to identify the solution. A precise outcome is impossible to achieve, we can come close when the amount of energy inputted by loads and the energy put out by reactions in the model are approximately equal. The acceptable proximity to this precise balance is determined by the convergence criteria. Fig. 4.12 and 4.13 shows the force and displacement convergence of model during the iteration process.

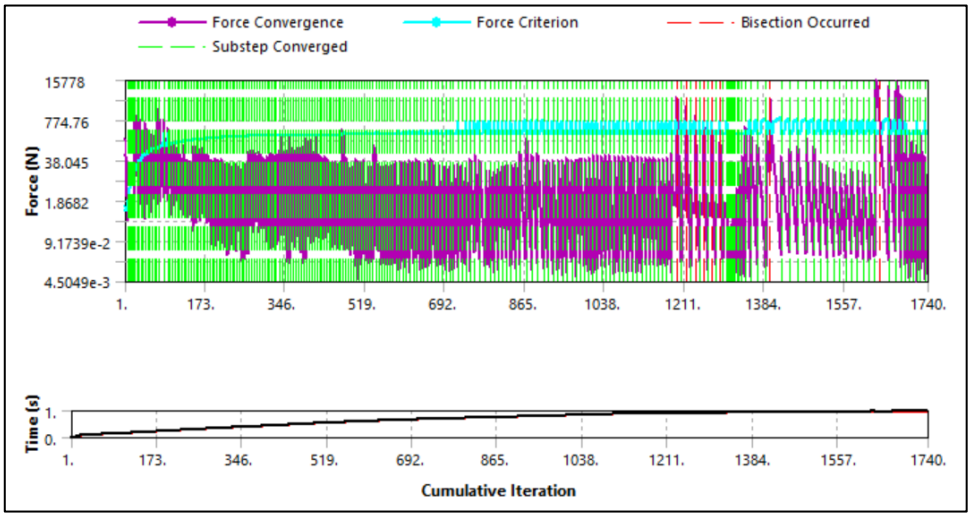

Fig. 4.12 Force Convergence for Perpendicular Headed Shear Stud

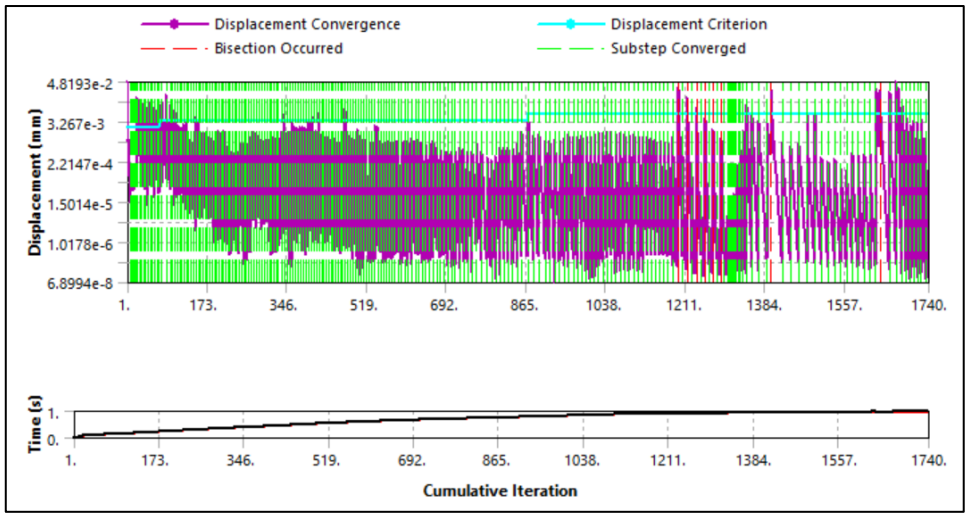

Fig. 4.13 Displacement Convergence for Perpendicular Headed Shear Stud

4.5 FINITE ELEMENT ANALYSIS RESULTS FOR 15 DEGREE INCLINED HEADED SHEAR STUD

Finite element analysis results such as load slip curve, stress, strain, damage for 15-degree inclined headed shear stud is shown in this section.

4.5.1 Load slip curve

Fig. 4.14 represents the load slip curve for 15-degree inclined headed shear stud. It seen from the curve that the ultimate shear resistance of a headed shear stud is 113.175 KN. When the shear stud placed at an angle of inclination 15 degree with respect to Y-axis and downward displacement (push) is applied to steel beam, the ultimate shear resistance of a headed shear stud is increased to 130.13 KN. But when steel beam is subjected to upward displacement (pull), the ultimate shear resistance of inclined headed shear stud reduced to 49.97 KN.

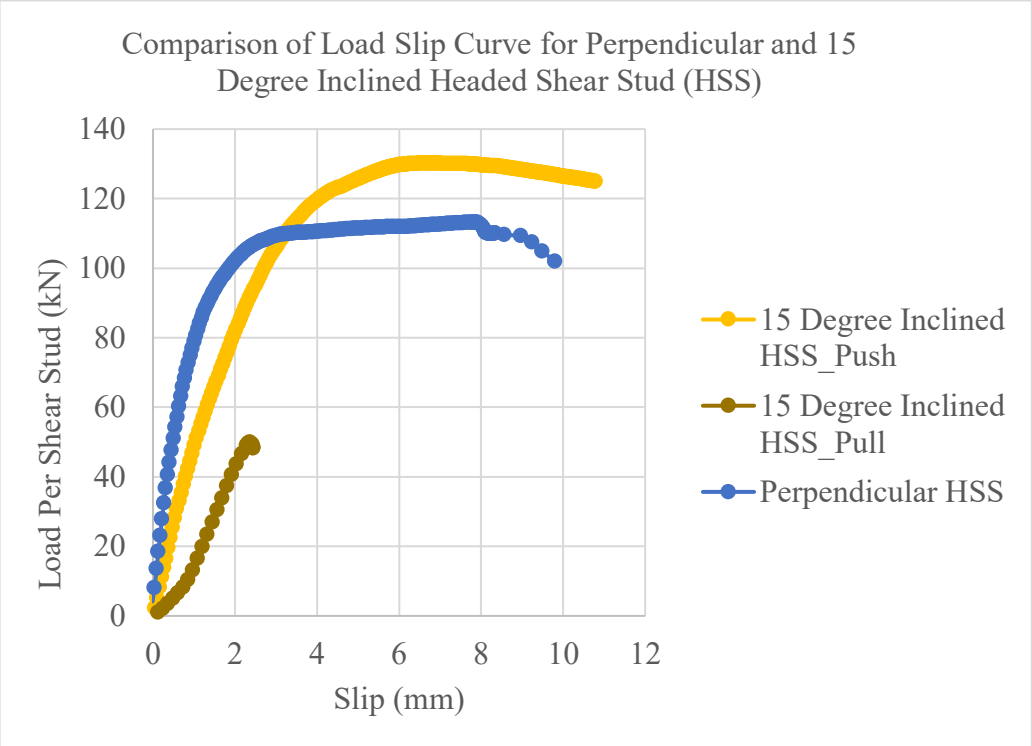

Fig. 4.14 Comparison of Load Slip Curve for Perpendicular and 15 Degree Inclined Headed Shear Stud (HSS)

4.5.2 Principal stress distribution at concrete slab

It is seen from the Fig. 4.15 that the concrete located just below the bottom half of the headed shear stud is in compression. Maximum compressive stresses are developed at the concrete slab part located at the bottom of the welded collar of HSS and concrete located just above the head of HSS. Concrete located just above the head of headed shear stud in compressed due to the component of internal force developed along the longitudinal axis of the headed shear stud.

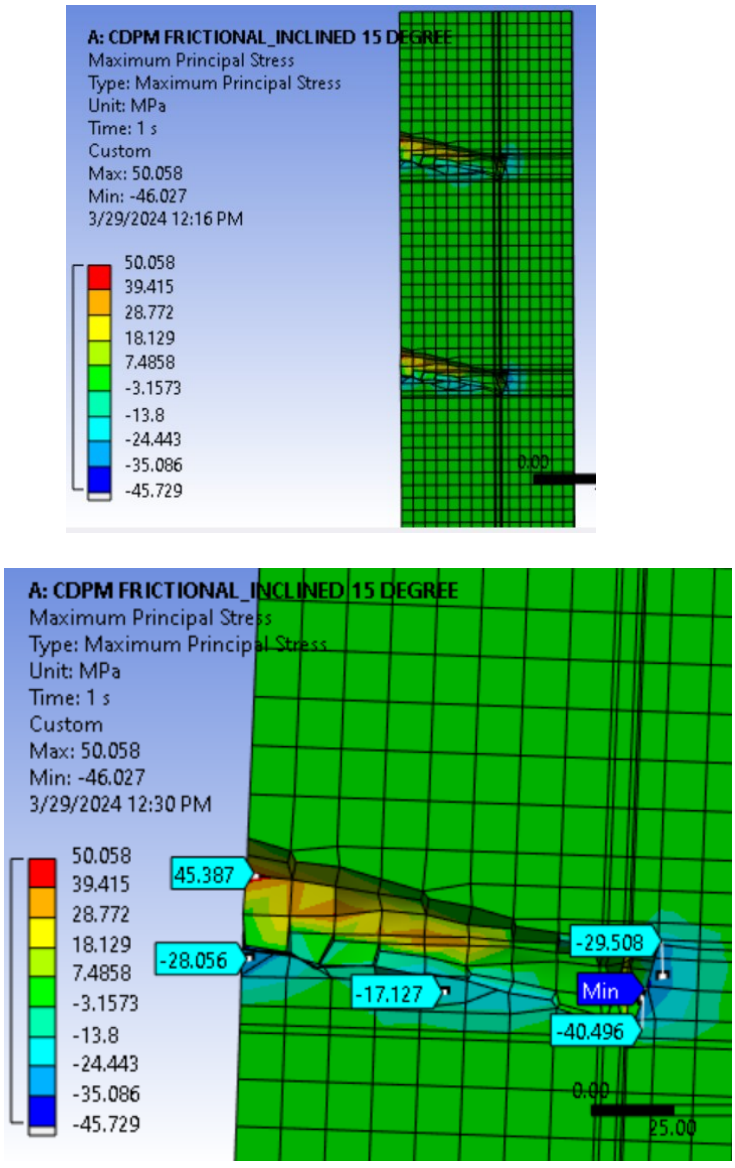

Fig. 4.15 Principal Stress Distribution in Concrete Slab for 15 Degree Inclined HSS

Fig. 4.16 indicates the factor of safety of concrete slab with respect to compressive strength of concrete slab. It is seen that the factor of safety of concrete slab part located

just below the welded collar of headed shear stud and just above the head of shear stud is less than 1.0, which represents the failure of concrete at that region. Factor of safety greater than 1.0 indicates that the material is safe from failure due to the application of load.

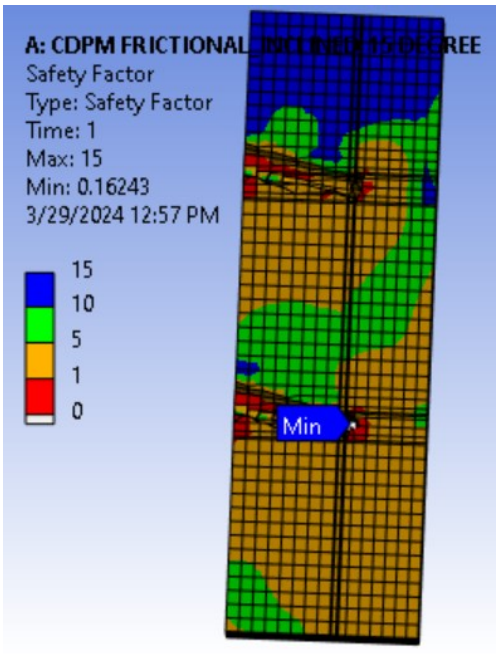

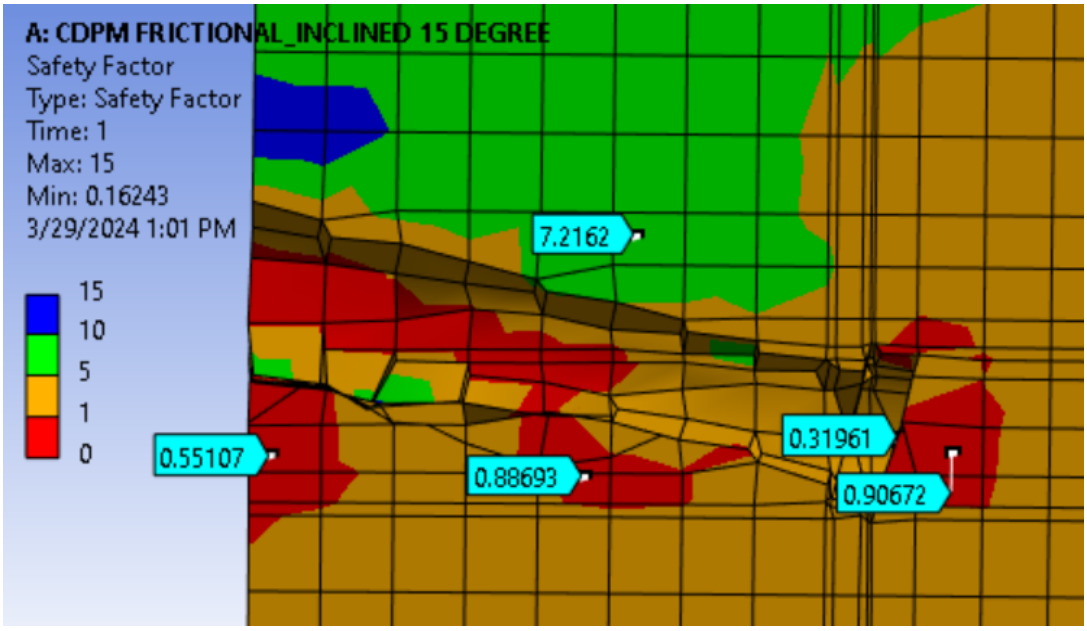

Fig. 4.16 Factor of Safety of Concrete Slab for 15-Degree Inclined Headed Shear Stud

4.5.3 Von Mises stress distribution at headed shear stud

Fig. 4.17 represents the distribution of von mises stress at different portion of the 15-degree inclined headed shear stud, it is seen that the maximum equivalent von mises stress is developed at the region of contact between steel beam and headed shear stud.

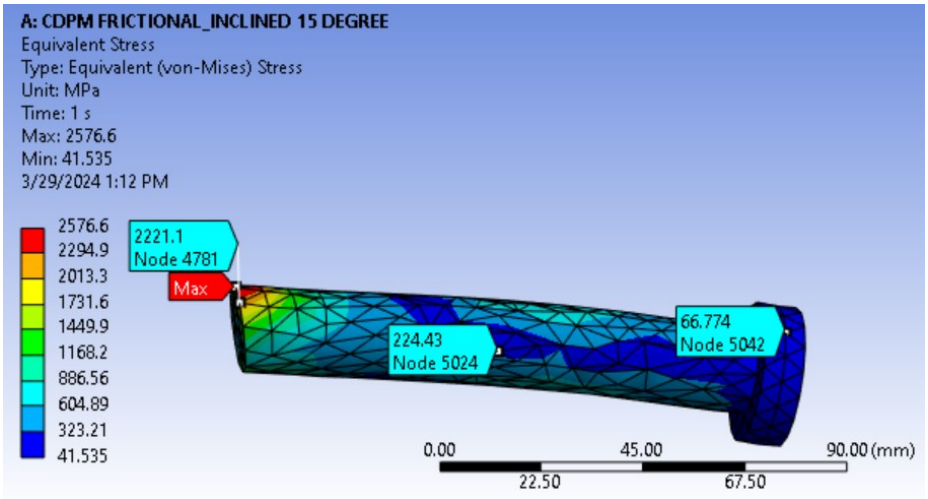

Fig. 4.17 Von Mises stress distribution at 15-degree inclined headed shear stud

Fig. 4.18 indicates the factor of safety of headed shear stud. It is seen that the factor of safety of headed shear stud part located at the region of contact point between steel beam and headed shear stud is less than 1.0, which represents the yielding of headed shear stud at that region. Factor of safety greater than 1.0 indicates that the material is safe from failure due to the application of load.

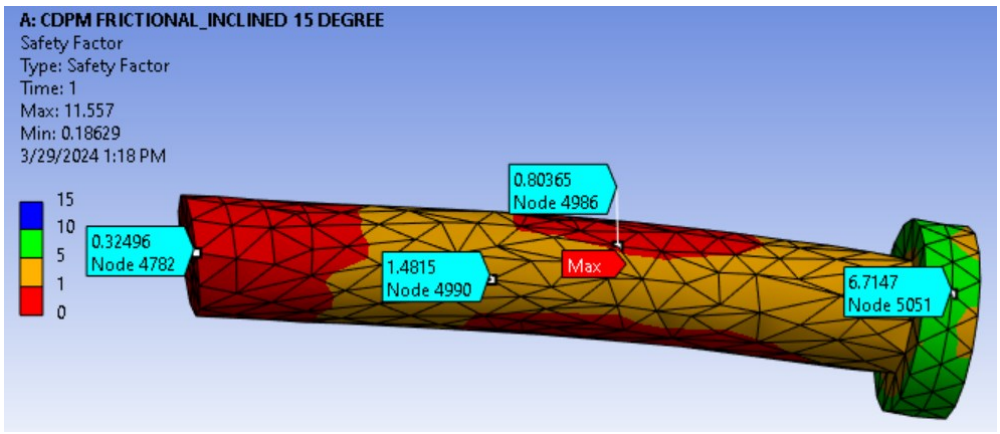

Fig. 4.18 Factor of Safety of 15-Degree Inclined Headed Shear Stud (HSS)

4.5.4 Shear Stress (X-Y Plane) distribution in concrete slab

Fig. 4.19 shows the distribution of shear stress in concrete slab along X-Y plane. Negative shear stress indicates downward movement and positive shear stress indicates upward movement.

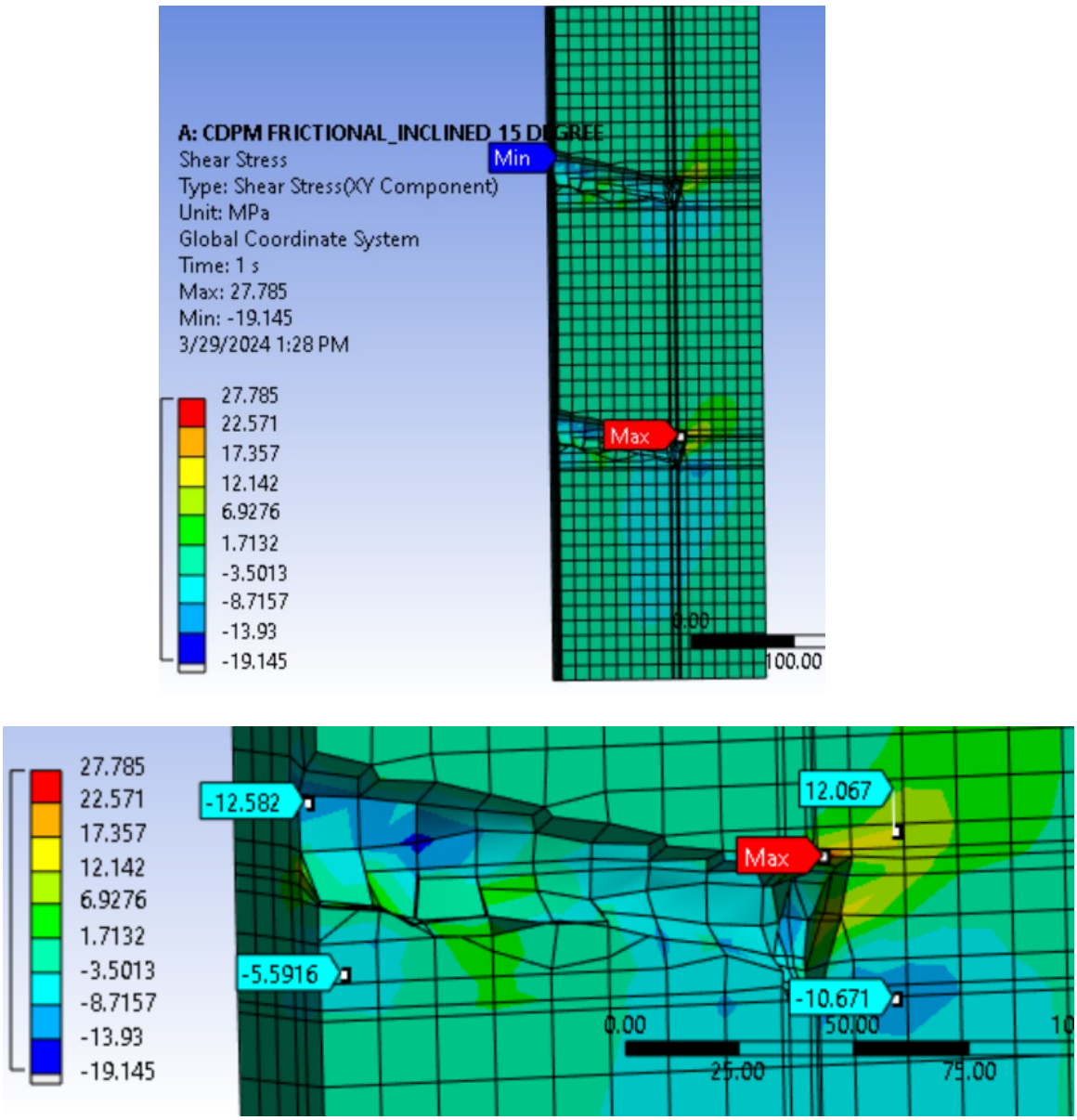

Fig. 4.19 Shear Stress (X-Y Plane) distribution in concrete slab

4.5.5 Shear Stress distribution in headed shear stud

Fig. 4.20 shows the distribution of shear stress in headed shear stud. It is seen from the Fig. 4.20 that the shear stress is maximum at the point where the headed shear stud

is connected with the steel beam while the shear stress is minimum at the head of the headed shear stud.

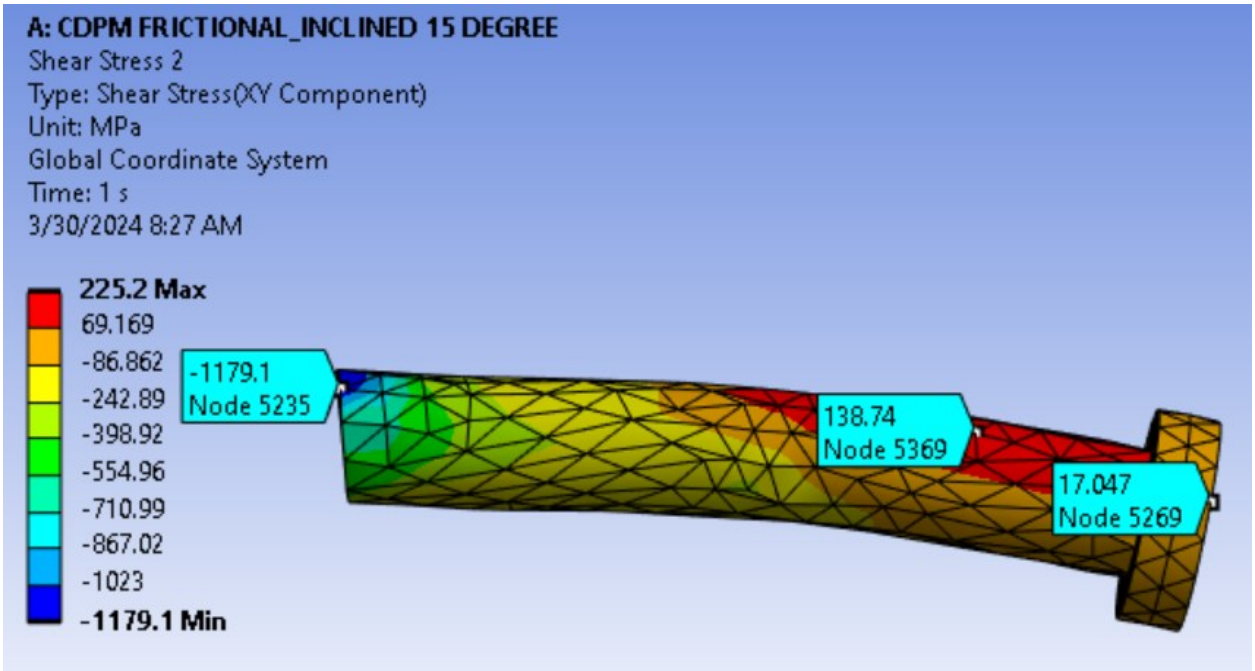

Fig. 4.20 Shear Stress (X-Y Plane) distribution in 15-Degree Inclined Headed Shear Stud

4.5.6 Damage Identification

Compression damage & tension damage of push out test specimen for 15-degree inclined headed shear stud is identified using following APDL command.

```
/SHOW,png
/ANG,1,
/VIEW,3,3,3,3 !Use these values to change the view
/gfile,600
SET,last !SET,Last = Outputs final result set
esel,s,ename,215
PLNSOL,MPDP,COMP
PLNSOL,MPDP,TENS
```

From the Fig. 4.21 and 4.22 it is seen that both the compression and tension damage occurred in the concrete slab near the location of headed shear stud due to maximum stress concentration.

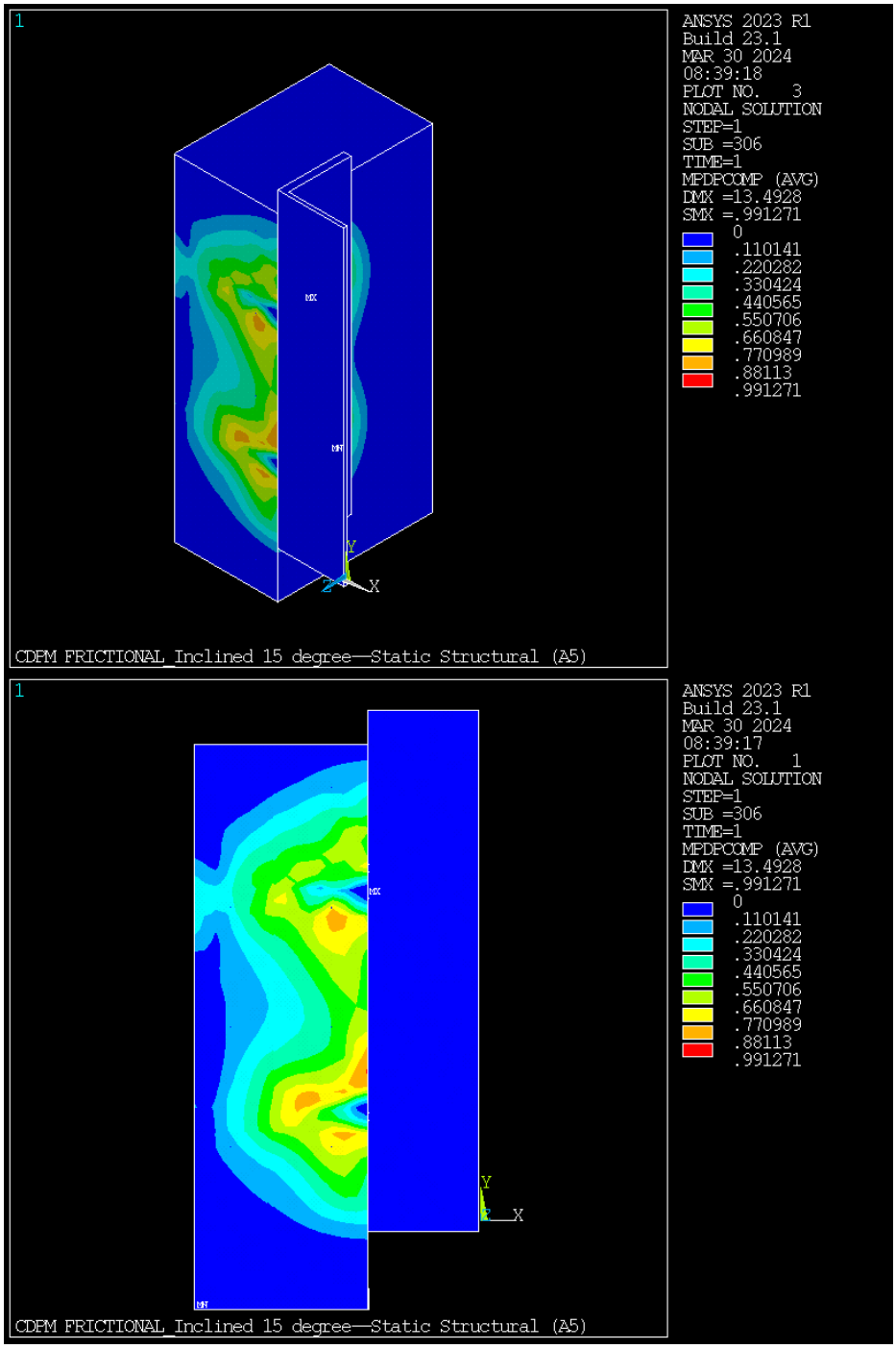

Fig. 4.21 Compression Damage for 15-Degree Inclined Headed Shear Stud

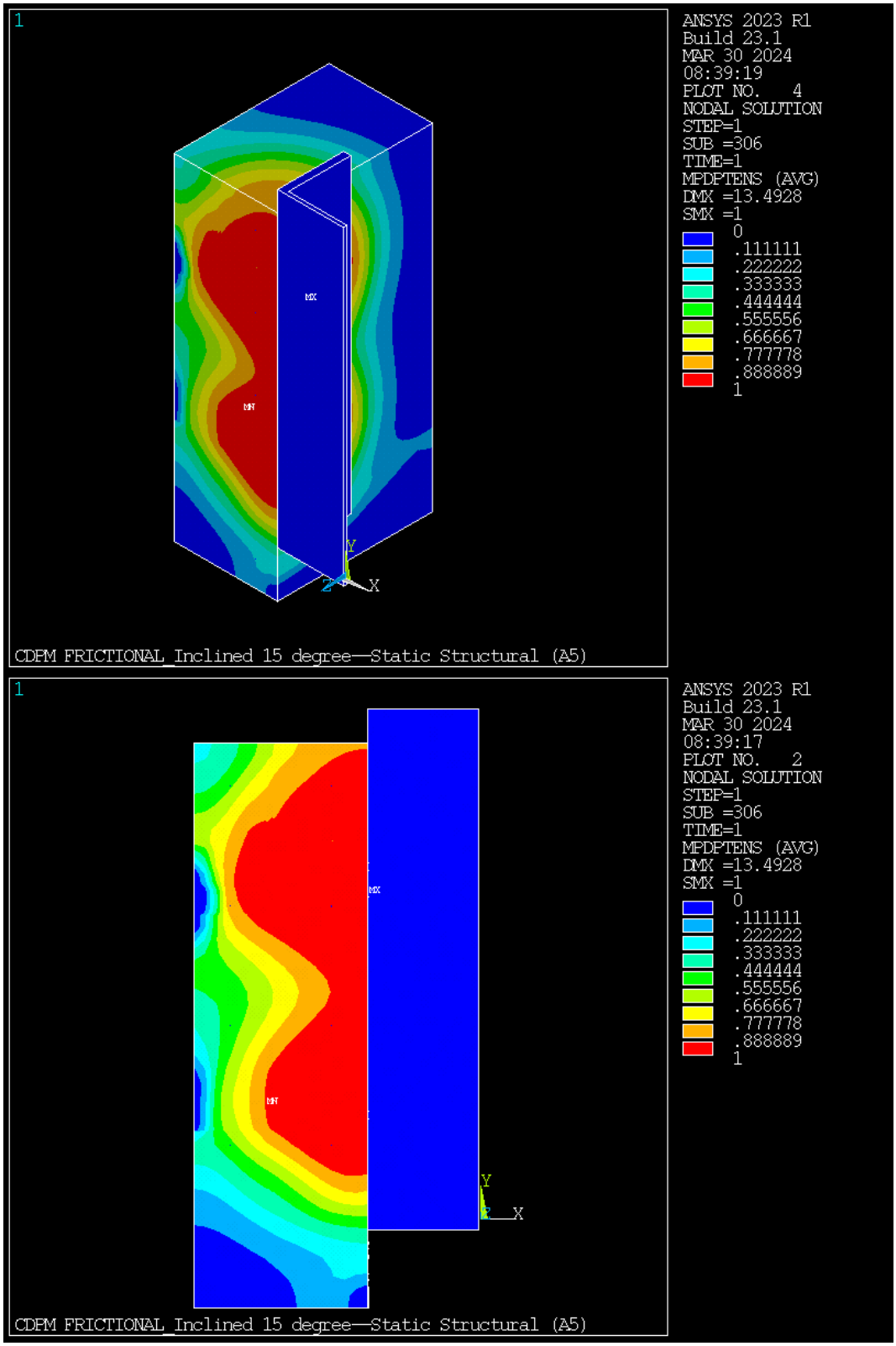

Fig. 4.22 Tension Damage for 15-Degree Inclined Headed Shear Stud

4.5.7 Force and Displacement Convergence

Fig. 4.23 and 4.24 shows the force and displacement convergence of push out test model for 15-degree inclined headed shear stud during the iteration process.

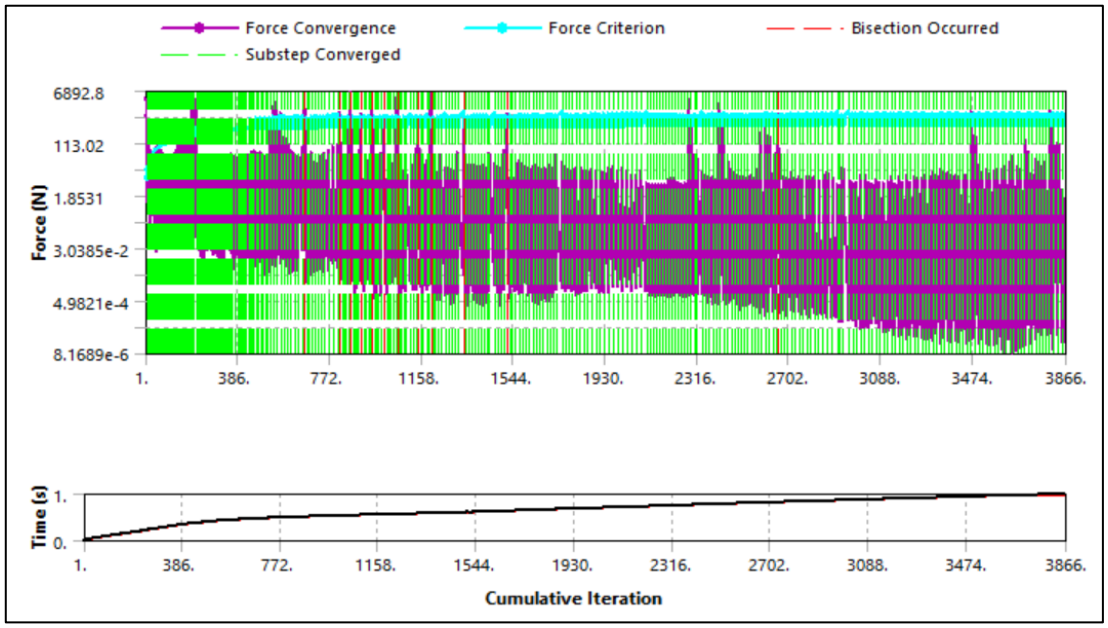

Fig. 4.23 Force Convergence for 15-Degree Inclined Headed Shear Stud

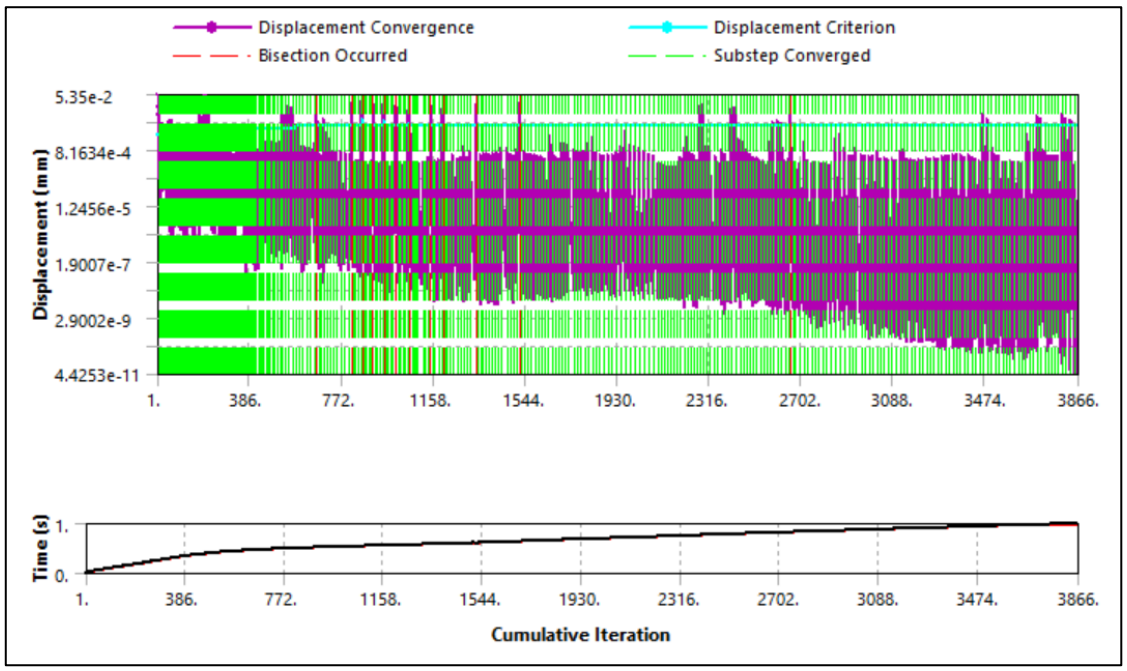

Fig. 4.24 Displacement Convergence for 15-Degree Inclined Headed Shear Stud

4.6 FE ANALYSIS RESULTS FOR 30 DEGREE INCLINED HEADED SHEAR STUD

Finite element analysis results such as load slip curve, stress, strain, damage for 30-degree inclined headed shear stud is shown in this section.

4.6.1 Load slip curve

Fig. 4.25 represents the load slip curve for 30-degree inclined headed shear stud. It seen from the curve that the ultimate shear resistance of a headed shear stud is 113.175 KN. When the shear stud placed at an angle of inclination 30 degree with respect to Y-axis and downward displacement (push) is applied to steel beam, the ultimate shear resistance of a headed shear stud is increased to 132.785 KN. But when steel beam is subjected to upward displacement (pull), the ultimate shear resistance of inclined headed shear stud reduced to 65.00 KN.

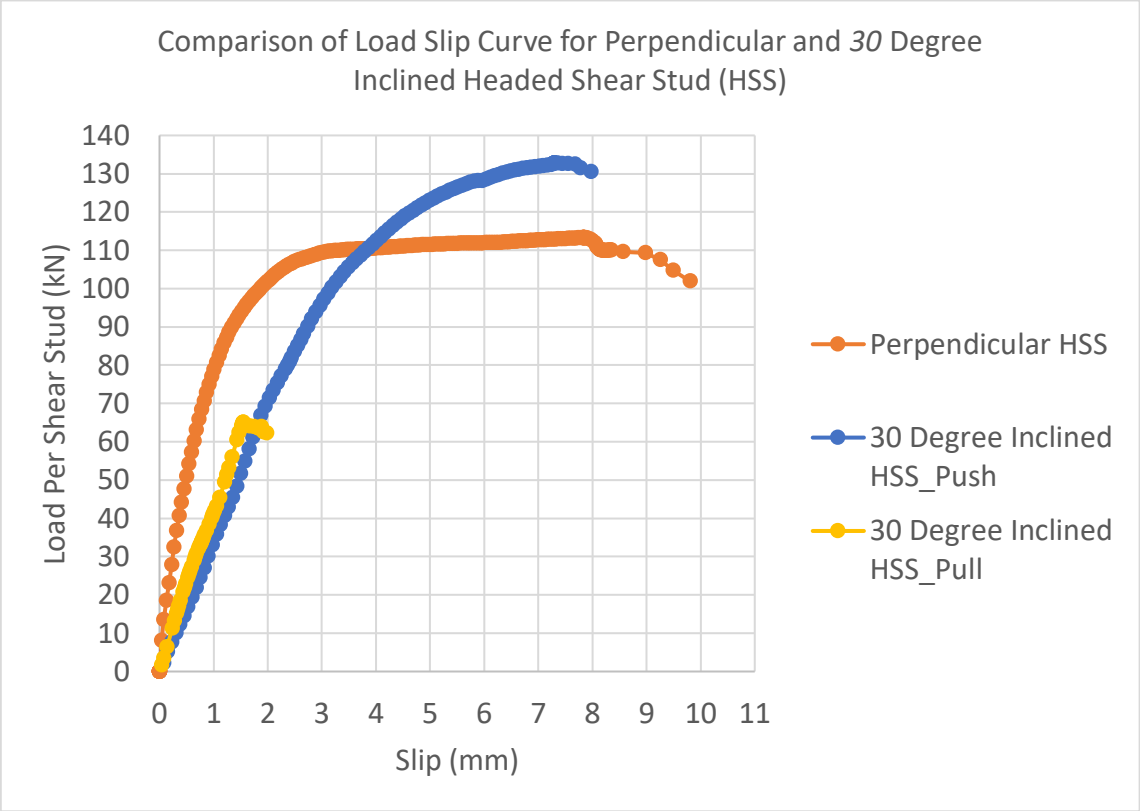

Fig. 4.25 Comparison of Load Slip Curve for Perpendicular and 30 Degree Inclined Headed Shear Stud (HSS)

4.6.2 Principal stress distribution at concrete slab

Fig. 4.26 shows that the concrete located just below the bottom half of the headed shear stud is in compression. Maximum compressive stresses are developed at the concrete slab part located just below the middle of the HSS and concrete located just above the head of HSS. Concrete located just above the head of headed shear stud in compressed due to the component of internal force developed along the longitudinal axis of the HSS.

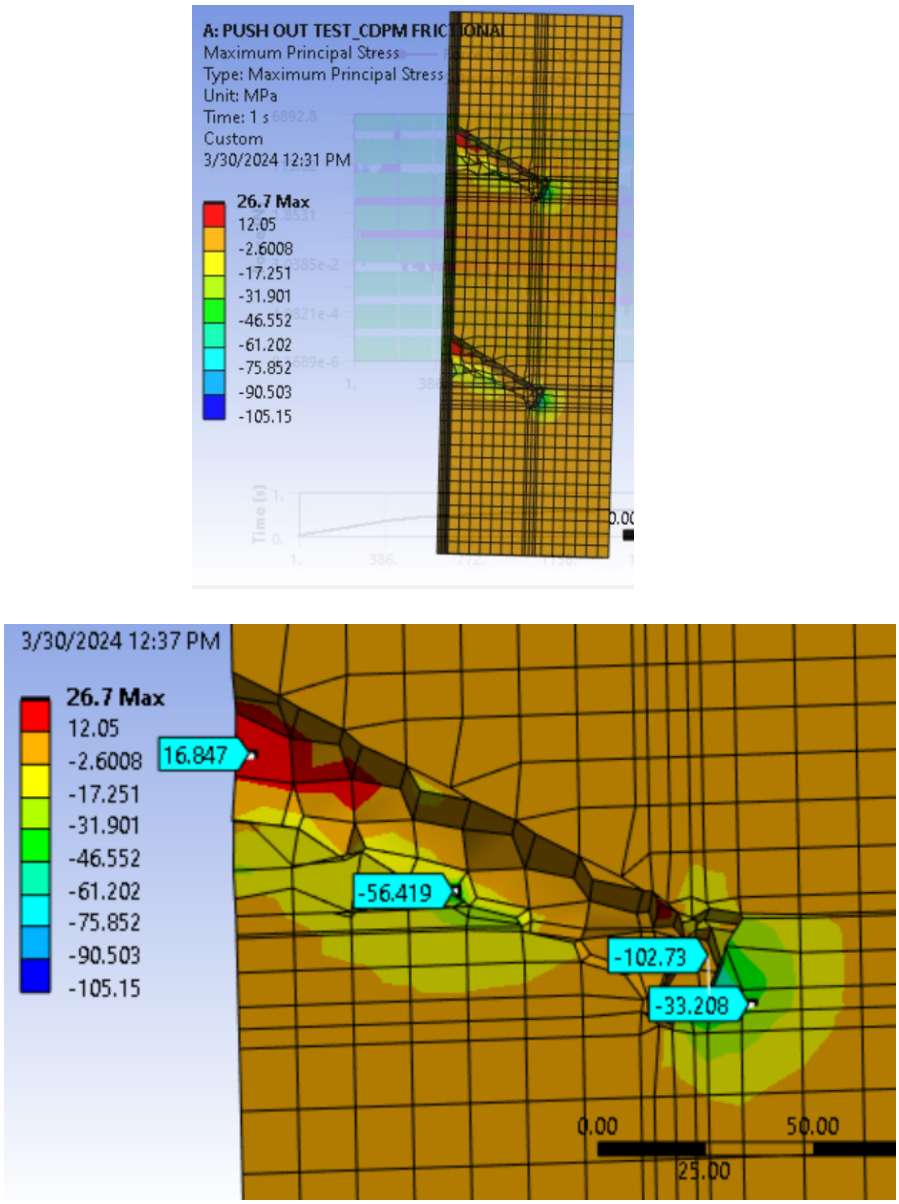

Fig. 4.26 Principal Stress Distribution in Concrete Slab for 30 Degree Inclined HSS

Fig. 4.27 indicates the factor of safety of concrete slab. The factor of safety of concrete slab part located just below the middle of the HSS and just above the head of HSS is less than 1.0, which represents the failure of concrete at that region. Factor of safety greater than 1.0 indicates that the material is safe from failure due to the application of load.

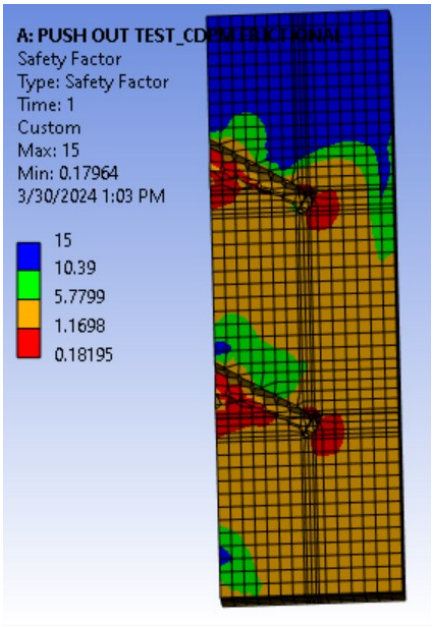

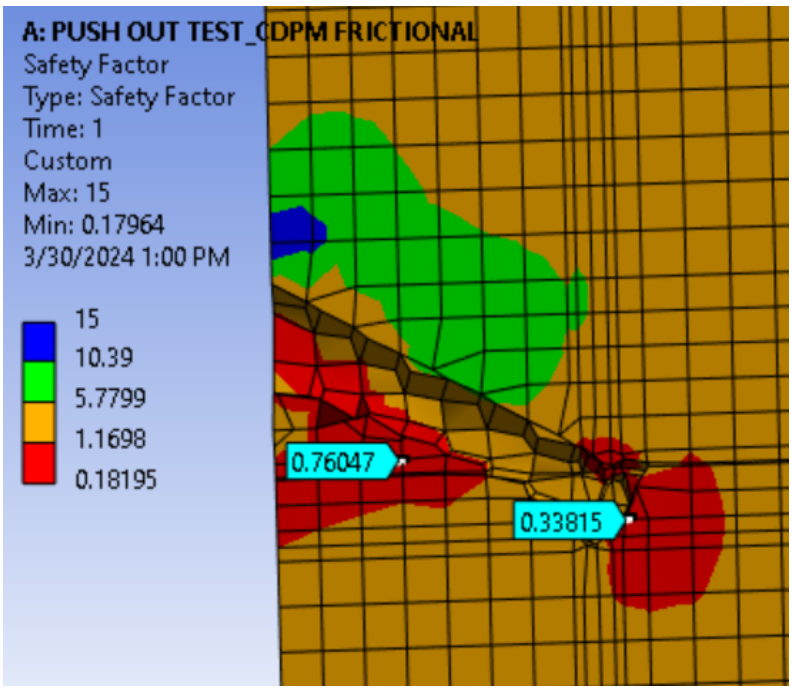

Fig. 4.27 Factor of Safety of Concrete Slab for 30-Degree Inclined Headed Shear Stud

4.6.3 Von Mises stress distribution at headed shear stud

Fig. 4.28 represents the distribution of equivalent von mises stress at different portion of the 30-degree inclined HSS, it is seen from the Fig. 4.28 that the maximum equivalent von mises stress is developed at the region of contact between steel beam and HSS

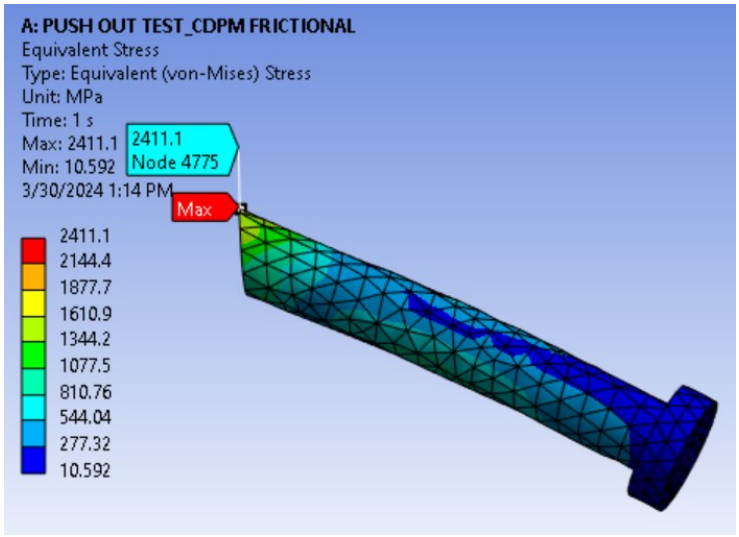

Fig. 4.28 Von Mises stress distribution at 30-degree inclined headed shear stud

Fig. 4.29 indicates the factor of safety of headed shear stud. It is seen that the factor of safety of HSS part located at the region of contact point between steel beam and HSS is less than 1.0, which represents the yielding of HSS at that region. Factor of safety greater than 1.0 indicates that the material is safe from failure due to the application of load.

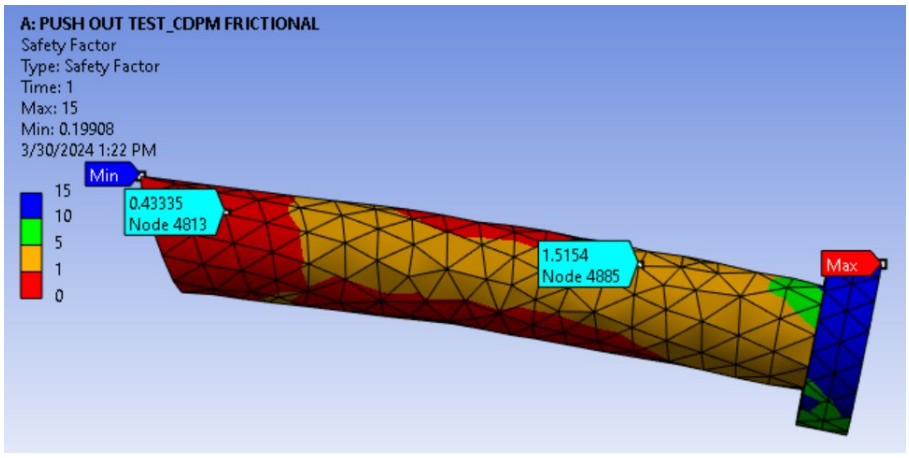

Fig. 4.29 Factor of Safety of 30-Degree Inclined Headed Shear Stud (HSS)

4.6.4 Shear Stress (X-Y Plane) distribution in concrete slab

Fig. 4.30 shows the distribution of shear stress in concrete slab along X-Y plane. Negative shear stress indicates downward movement and positive shear stress indicates upward movement.

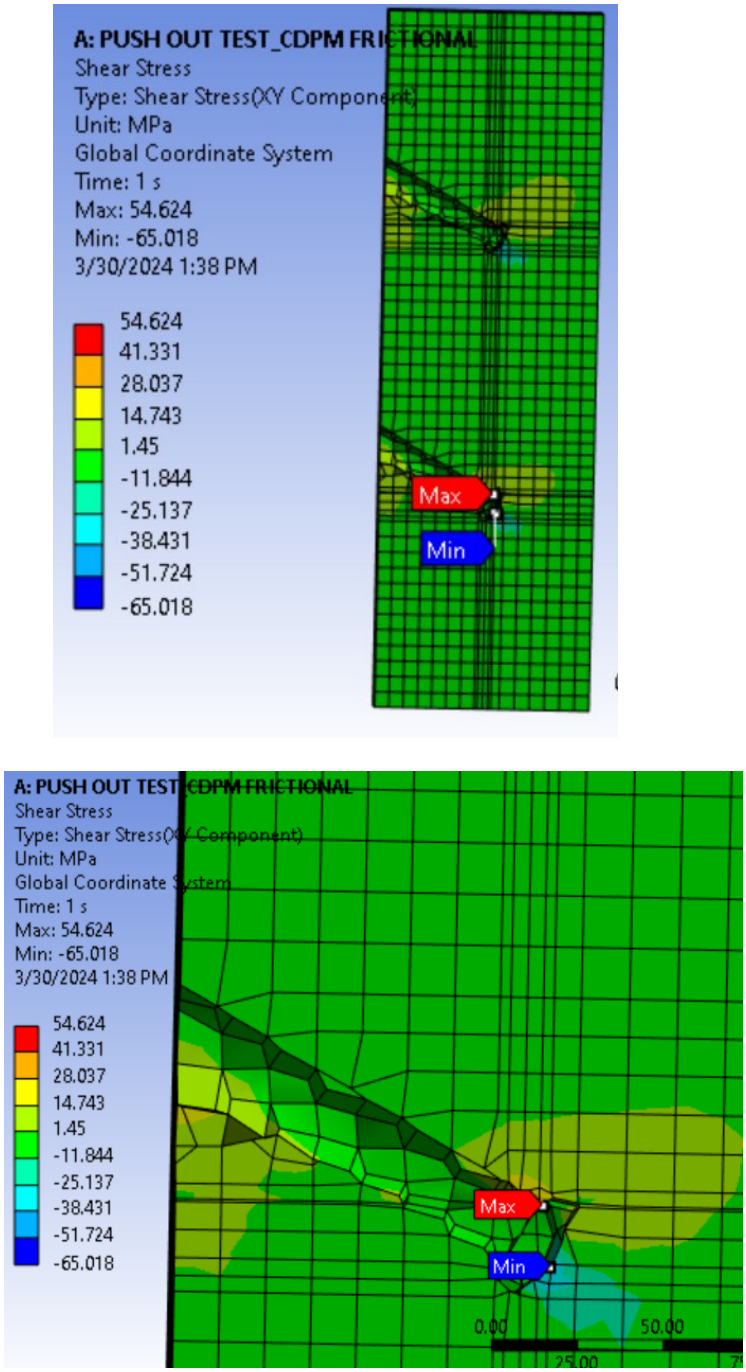

Fig. 4.30 Shear Stress (X-Y Plane) distribution in concrete slab

4.6.5 Shear Stress distribution in headed shear stud

Fig. 4.31 shows the distribution of shear stress in headed shear stud. It is seen from the Fig. 4.31 that the shear stress is maximum at the point where the headed shear stud is connected with the steel beam while the shear stress is minimum at the head of the headed shear stud.

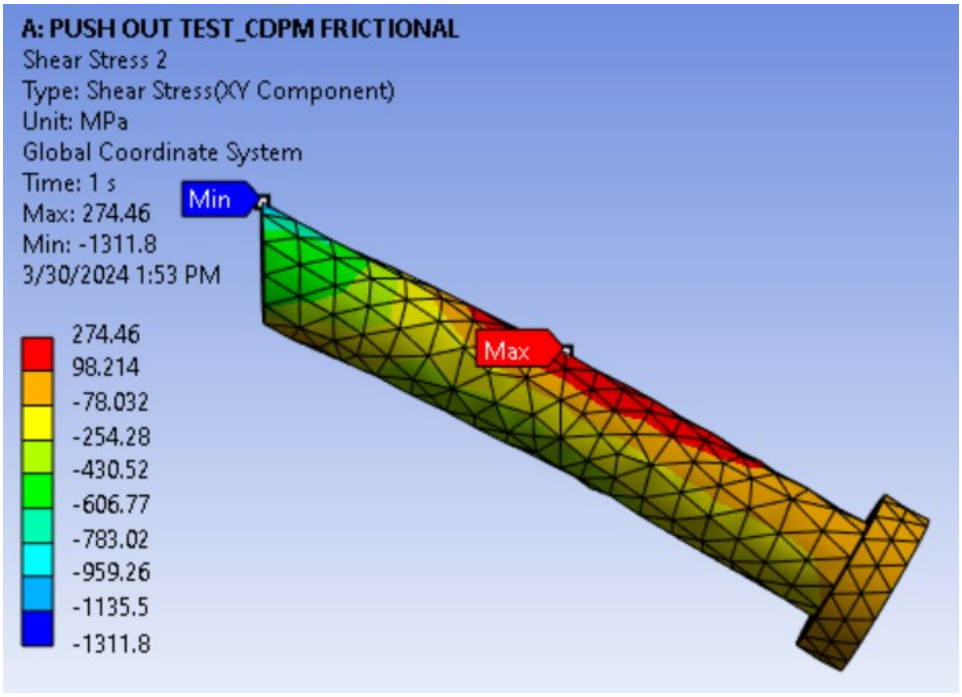

Fig. 4.31 Shear Stress (X-Y Plane) distribution in 30-Degree Inclined Headed Shear Stud

4.6.6 Damage Identification

Compression damage & tension damage of push out test specimen for 30-degree inclined headed shear stud is identified using following APDL command.

```
/SHOW,png
/ANG,1,
/VIEW,3,3,3,3 !Use these values to change the view
/gfile,600
SET,last !SET,Last = Outputs final result set
esel,s,ename,215
PLNSOL,MPDP,COMP
PLNSOL,MPDP,TENS
```

Fig. 4.32 and 4.33 indicate that both the compression and tension damage occurred in the concrete slab near the location of HSS due to the maximum stress concentration.

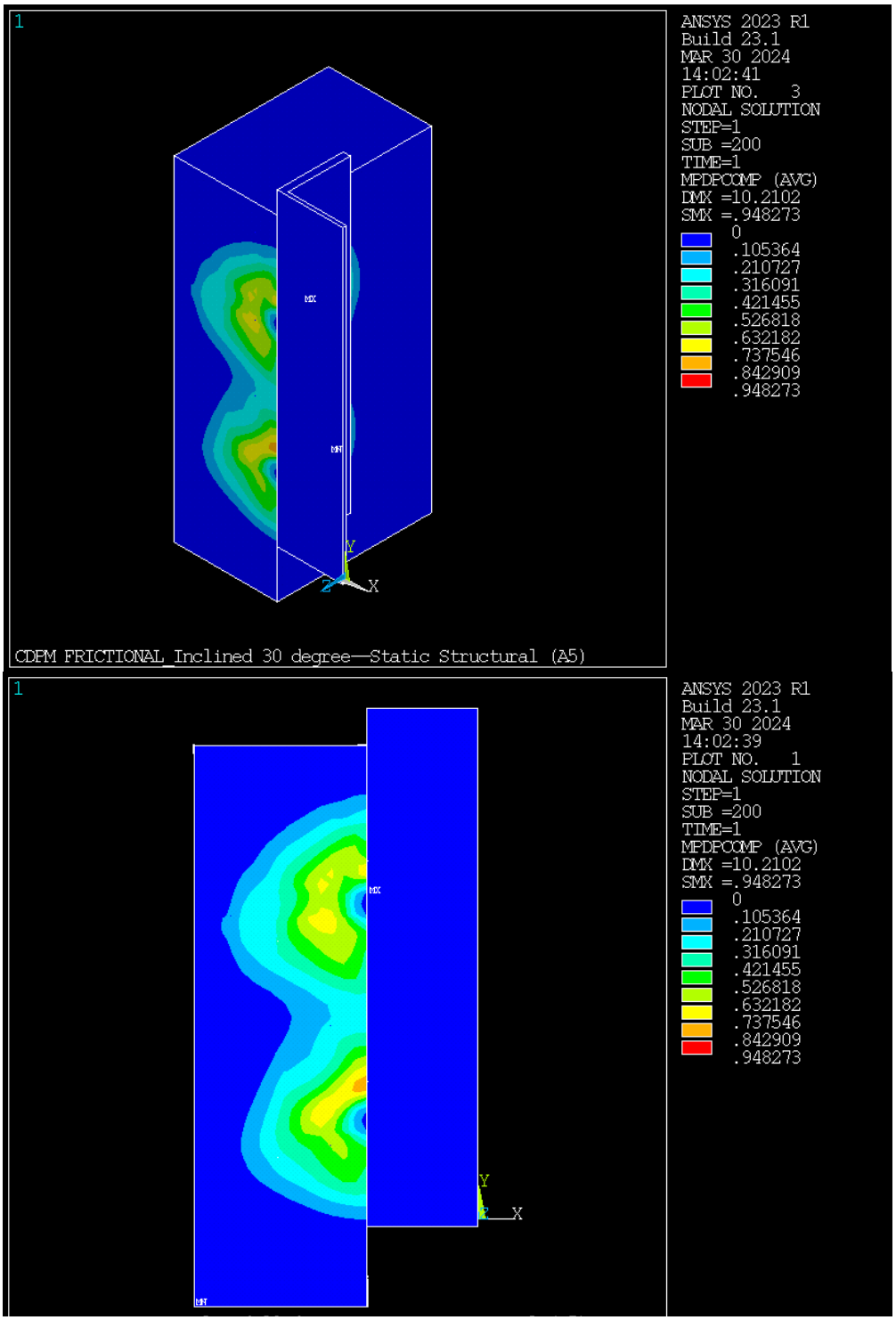

Fig. 4.32 Compression Damage for 30-Degree Inclined Headed Shear Stud

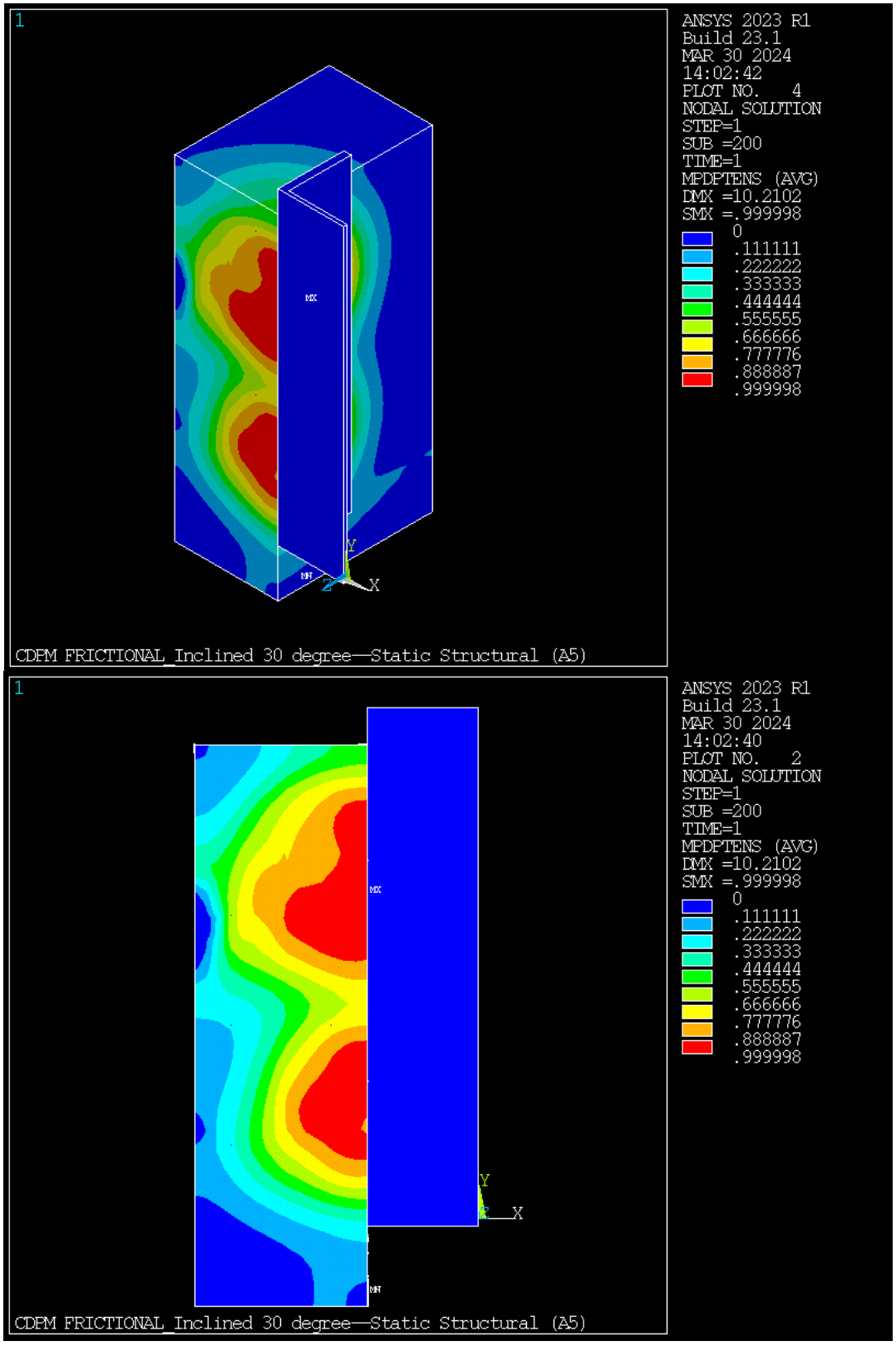

Fig. 4.33 Tension Damage for 30-Degree Inclined Headed Shear Stud

4.6.7 Force and Displacement Convergence

Fig. 4.34 and 4.35 shows the force and displacement convergence of push out test model for 30-degree inclined headed shear stud during the iteration process.

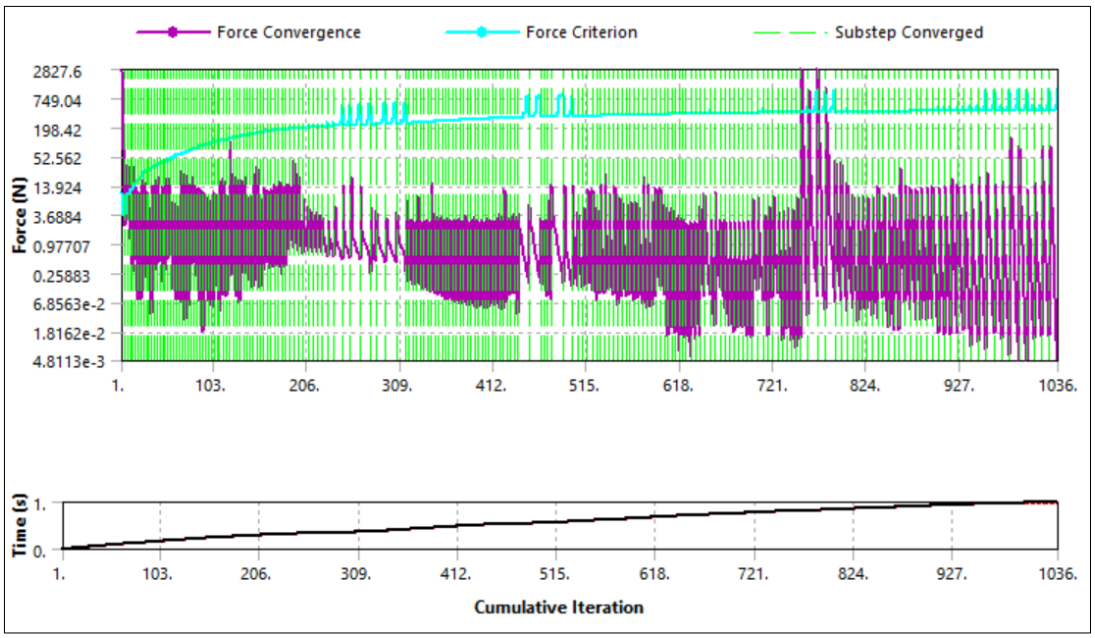

Fig. 4.34 Force Convergence for 30-Degree Inclined Headed Shear Stud

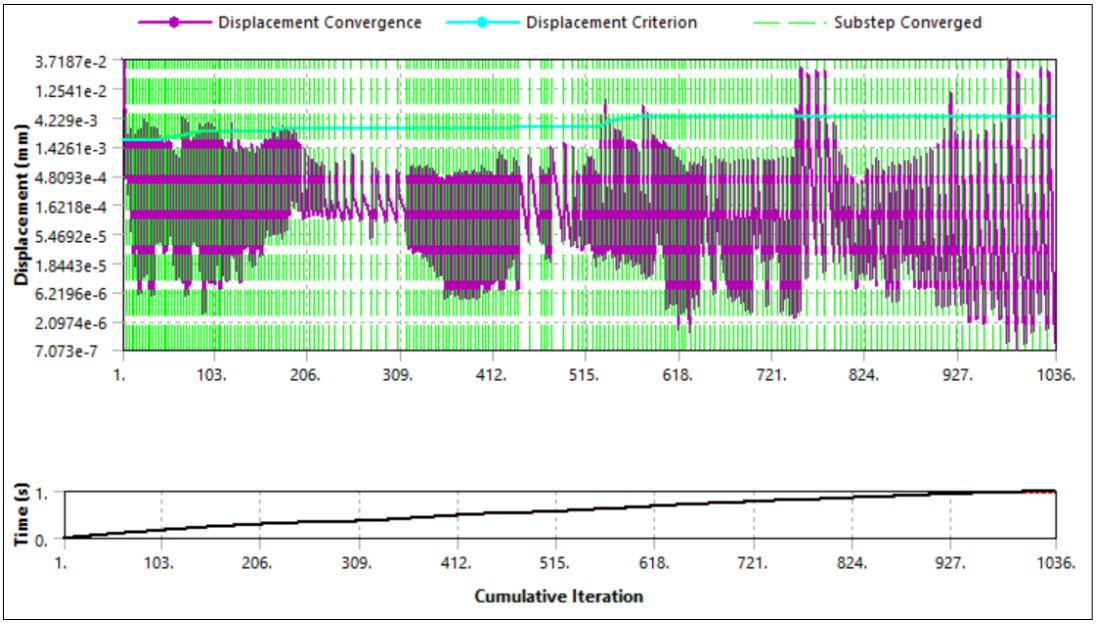

Fig. 4.35 Displacement Convergence for 30-Degree Inclined Headed Shear Stud

4.7 FE ANALYSIS RESULTS FOR 45 DEGREE INCLINED HEADED SHEAR STUD

Finite element analysis results such as load slip curve, stress, strain, damage for 30-degree inclined headed shear stud is shown in this section.

4.7.1 Load slip curve

Fig. 4.36 represents the load slip curve for 45-degree inclined headed shear stud. It seen from the curve that the ultimate shear resistance of a headed shear stud embedded in concrete and welded to the flange of steel beam is 113.175 KN. When the shear stud placed at an angle of inclination 45 degree with respect to Y-axis and downward displacement (push) is applied to steel beam, the ultimate shear resistance of a headed shear stud is increased to 140.335 KN. But when steel beam is subjected to upward displacement (pull), the ultimate shear resistance of inclined HSS reduced to 60.06 KN.

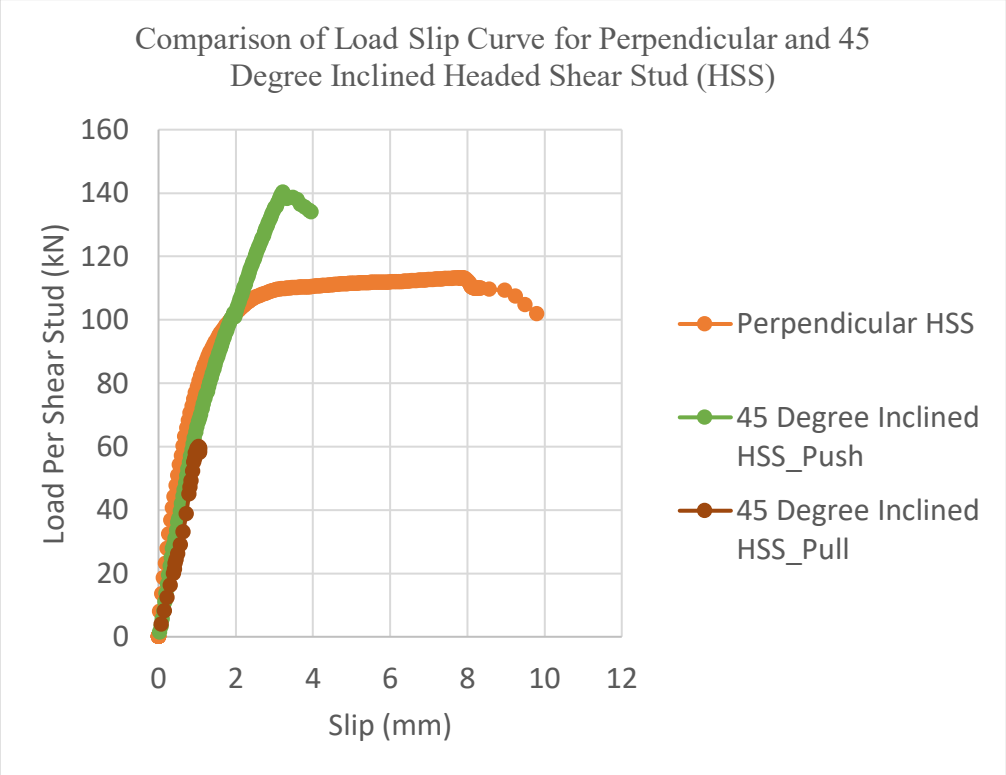

Fig. 4.36 Comparison of Load Slip Curve for Perpendicular and 45 Degree Inclined Headed Shear Stud (HSS)

4.7.2 Principal stress distribution at concrete slab

Fig. 4.37 shows that the concrete located just below the bottom half of the HSS is in compression. Maximum compressive stresses are developed at the concrete slab part located just below the middle of the headed shear stud and concrete located just above the head of headed shear stud. Concrete located just above the head of headed shear stud in compressed due to the component of internal force developed along the longitudinal axis of the headed shear stud.

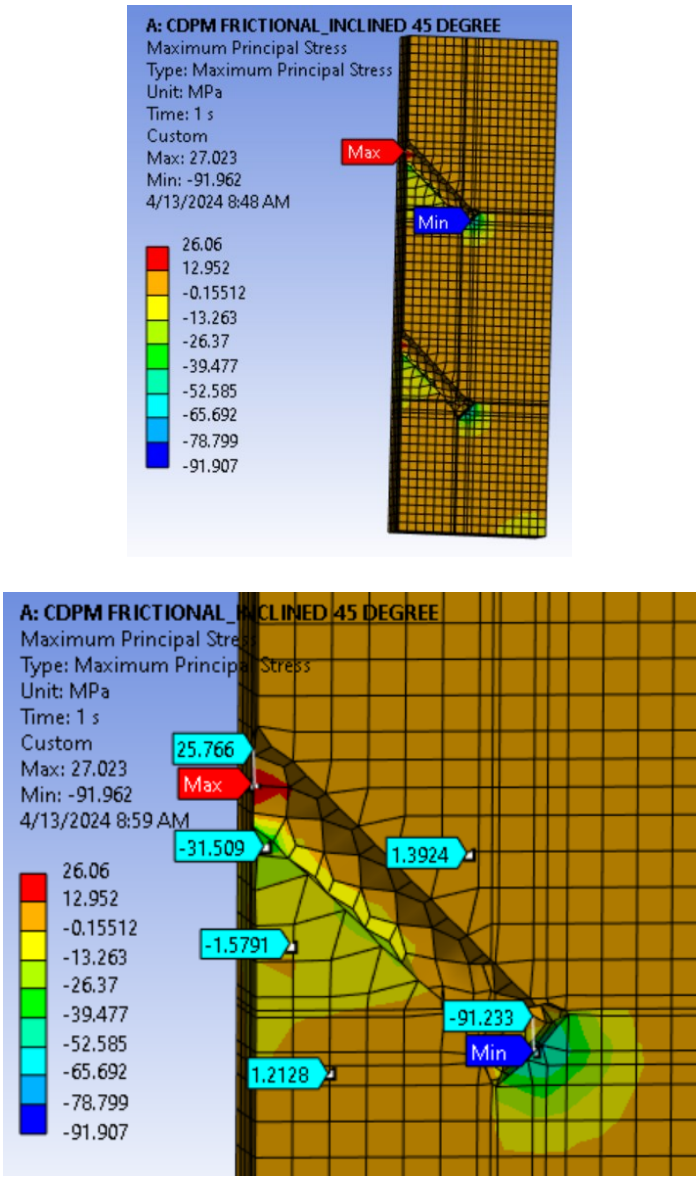

Fig. 4.37 Principal Stress Distribution in Concrete Slab for 45 Degree Inclined HSS

Fig. 4.38 indicates the factor of safety of concrete slab. The factor of safety of concrete slab part located just below the middle of the HSS and just above the head of HSS is less than 1.0, which represents the failure of concrete at that region. Factor of safety greater than 1.0 indicates that the material is safe from failure due to the application of load.

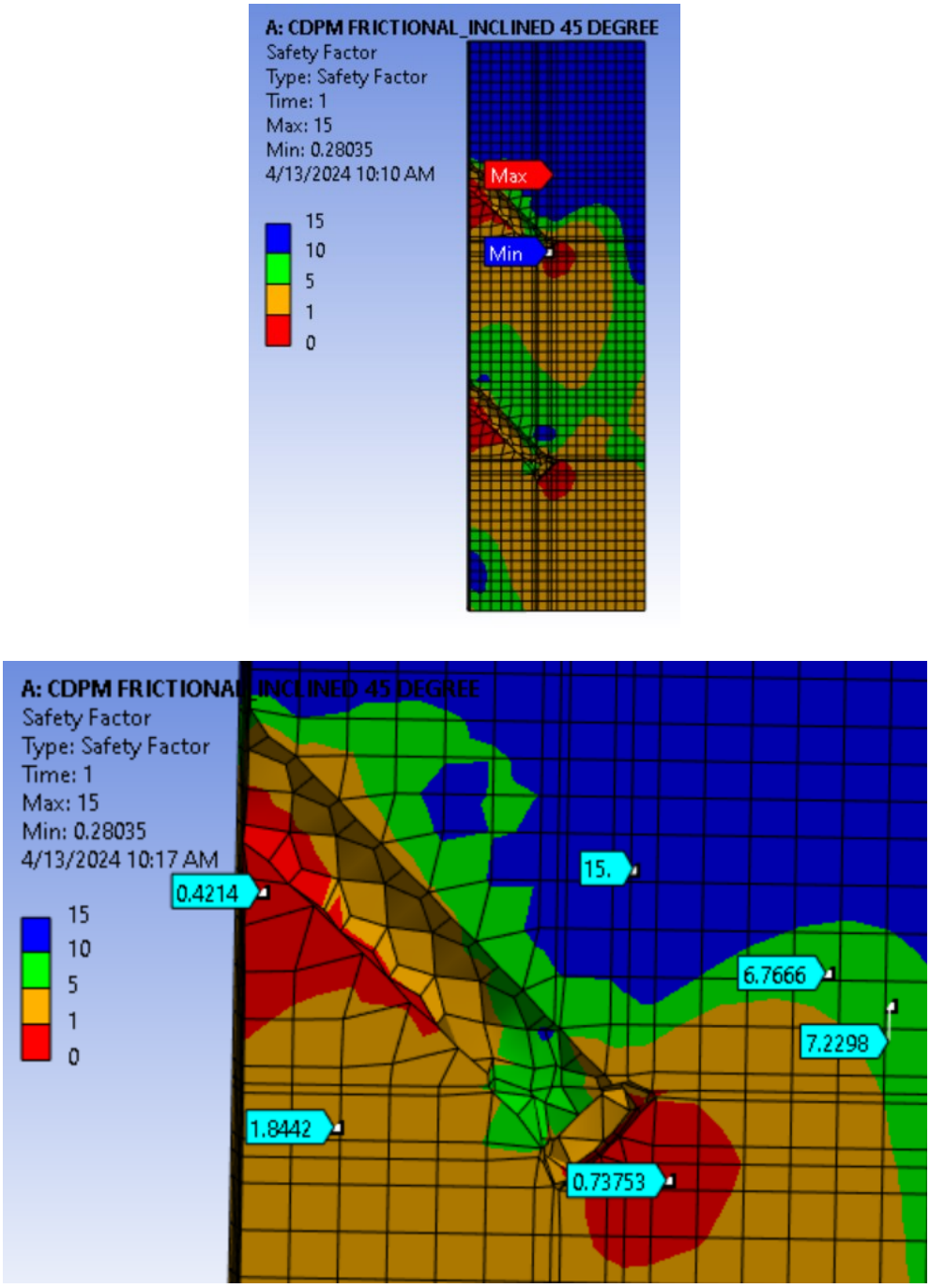

Fig. 4.38 Factor of Safety of Concrete Slab for 45-Degree Inclined Headed Shear Stud

4.7.3 Von Mises stress distribution at headed shear stud

Fig. 4.39 represents the distribution of equivalent von mises stress at different portion of the 45-degree inclined headed shear stud, it is seen from the Fig. 4.38 that the maximum equivalent von mises stress is developed at the region of contact between steel beam and headed shear stud.

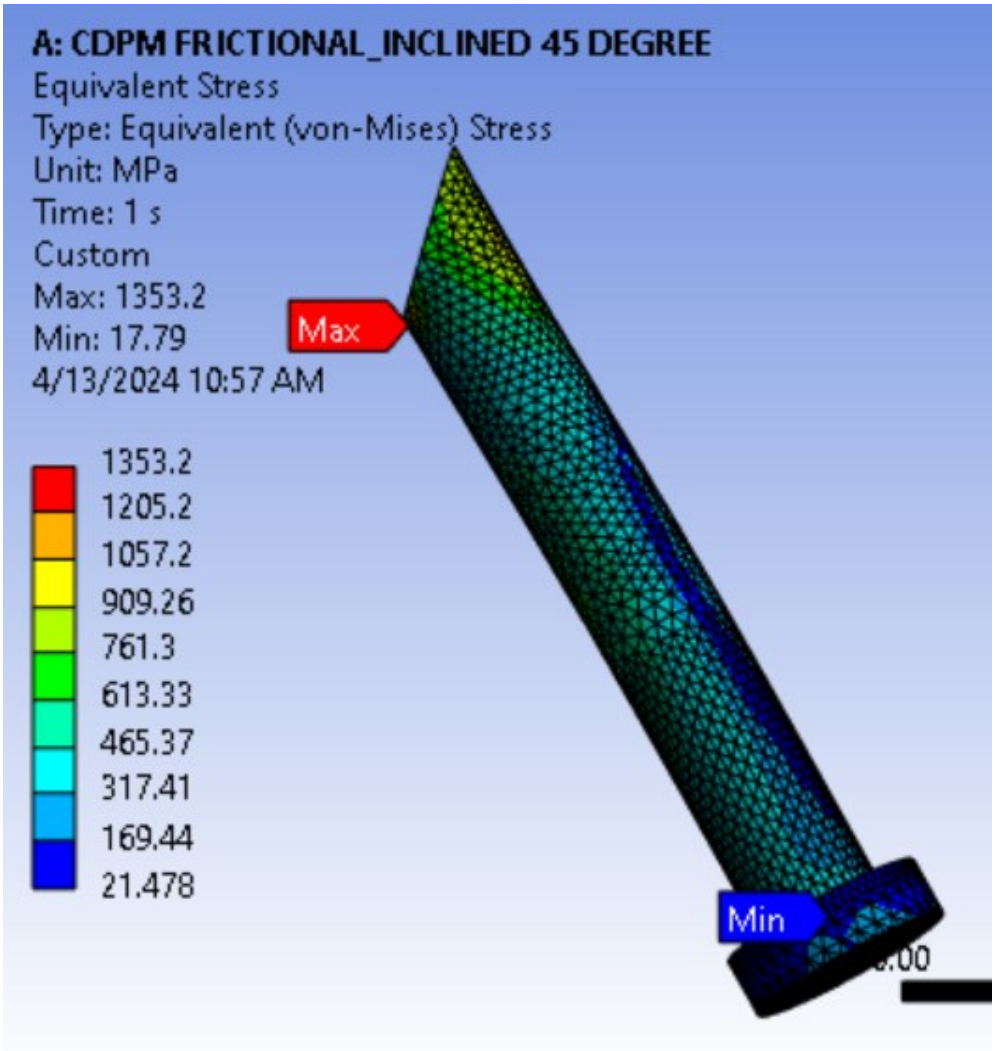

Fig. 4.39 Von Mises stress distribution at 45-degree inclined headed shear stud

Fig. 4.40 indicates the factor of safety of headed shear stud. It is seen that the factor of safety of headed shear stud part located at the region of contact point between steel beam and headed shear stud is less than 1.0, which represents the yielding of headed shear stud at that region. Factor of safety greater than 1.0 indicates that the material is safe from failure due to the application of load.

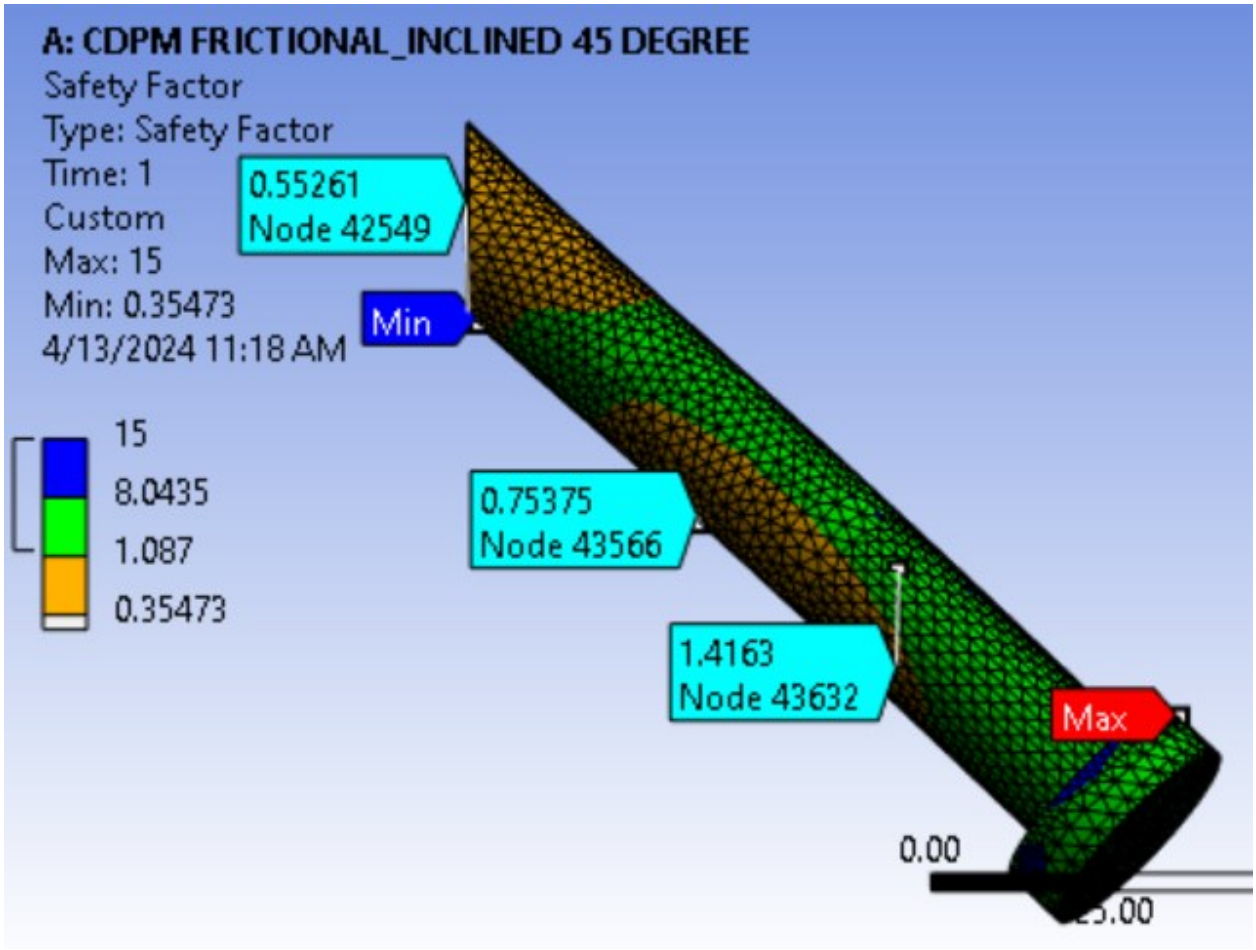

Fig. 4.40 Factor of Safety of 45-Degree Inclined Headed Shear Stud (HSS)

4.7.4 Shear Stress (X-Y Plane) distribution in concrete slab

Fig. 4.41 shows the distribution of shear stress in concrete slab along X-Y plane. Negative shear stress indicates downward movement and positive shear stress indicates upward movement

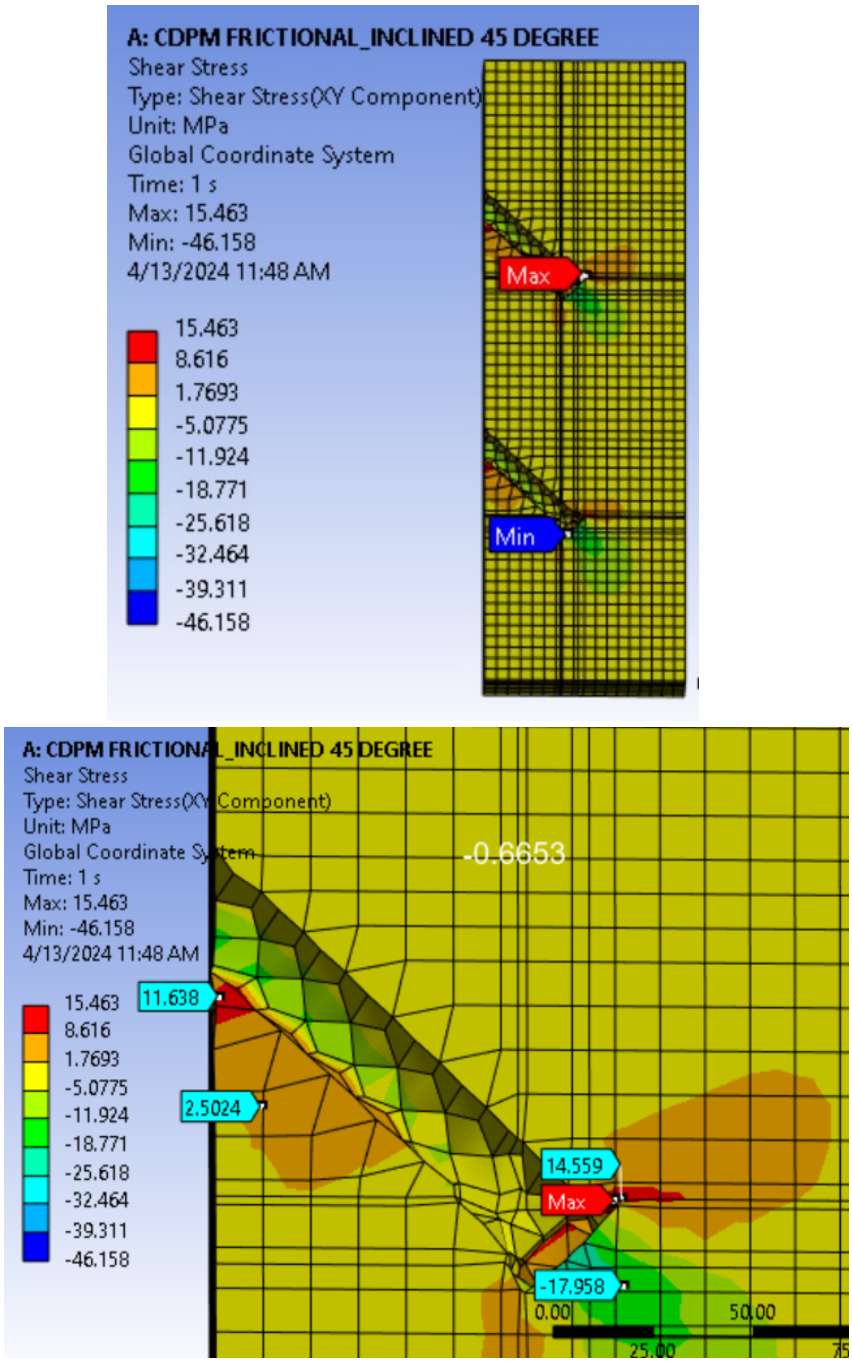

Fig. 4.41 Shear Stress (X-Y Plane) distribution in concrete slab

4.7.5 Shear Stress distribution in headed shear stud

Fig. 4.42 shows the distribution of shear stress in HSS. It is seen from the Fig. 4.42 that the shear stress is maximum at the point where the headed shear stud is connected with the steel beam while the shear stress is minimum at the head of the HSS.

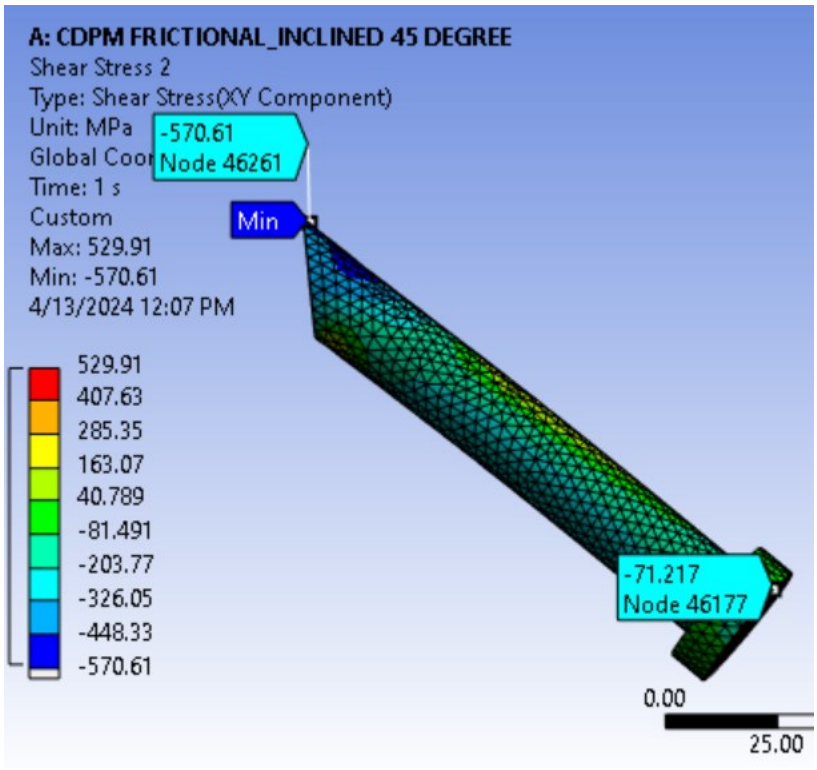

Fig. 4.42 Shear Stress (X-Y Plane) distribution in 45-Degree Inclined Headed Shear Stud

4.7.6 Damage Identification

Compression damage & tension damage of push out test specimen for 30-degree inclined headed shear stud is identified using following APDL command.

```
/SHOW,png
/ANG,1,
/VIEW,3,3,3,3 !Use these values to change the view
/gfile,600
SET,last !SET,Last = Outputs final result set
esel,s,ename,215
PLNSOL,MPDP,COMP
PLNSOL,MPDP,TENS
```

Fig. 4.43 and 4.44 represent that both the compression and tension damage occurred in the concrete slab near the location of the HSS due to the maximum stress concentration.

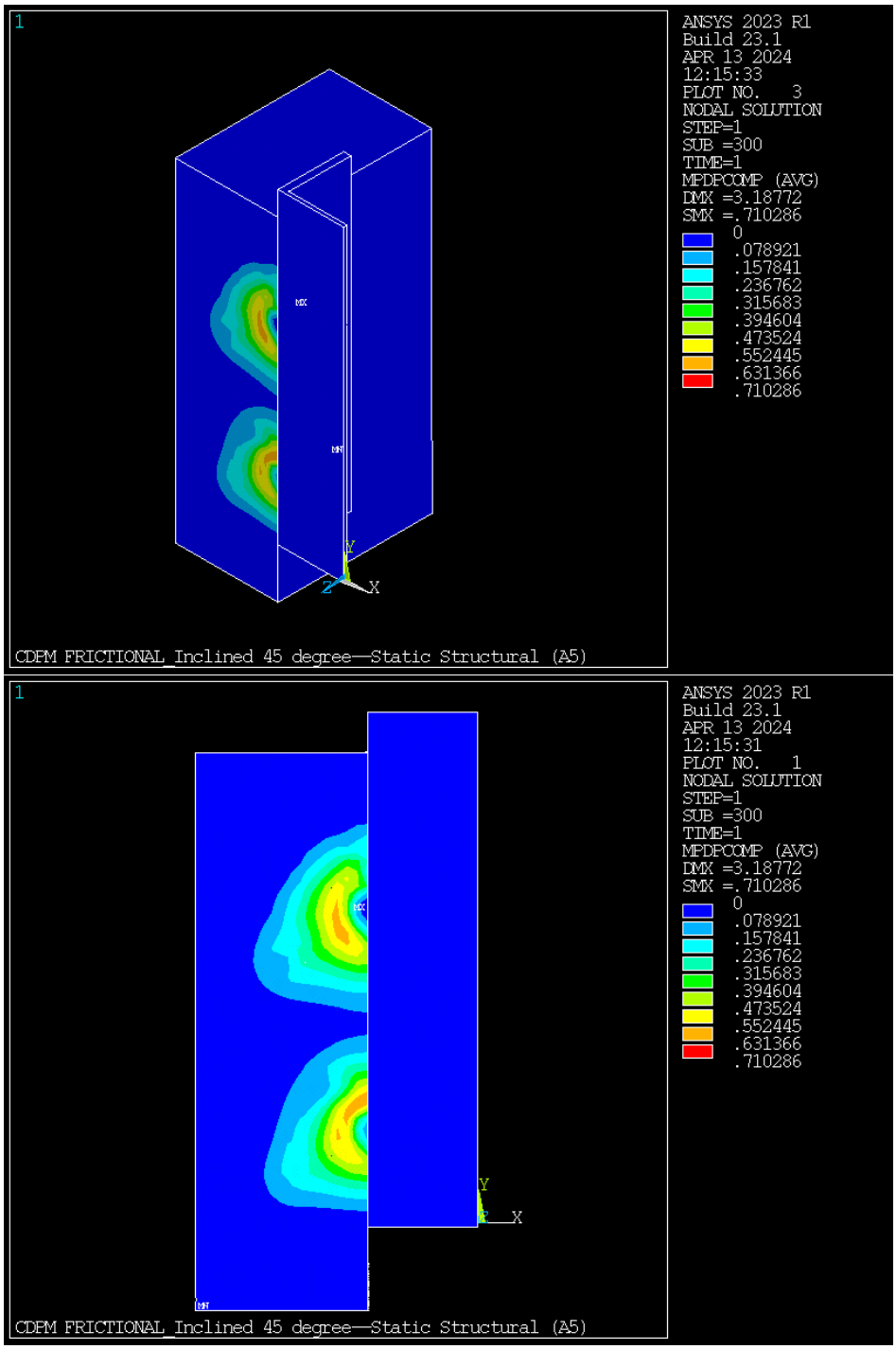

Fig. 4.43 Compression Damage for 45-Degree Inclined Headed Shear Stud

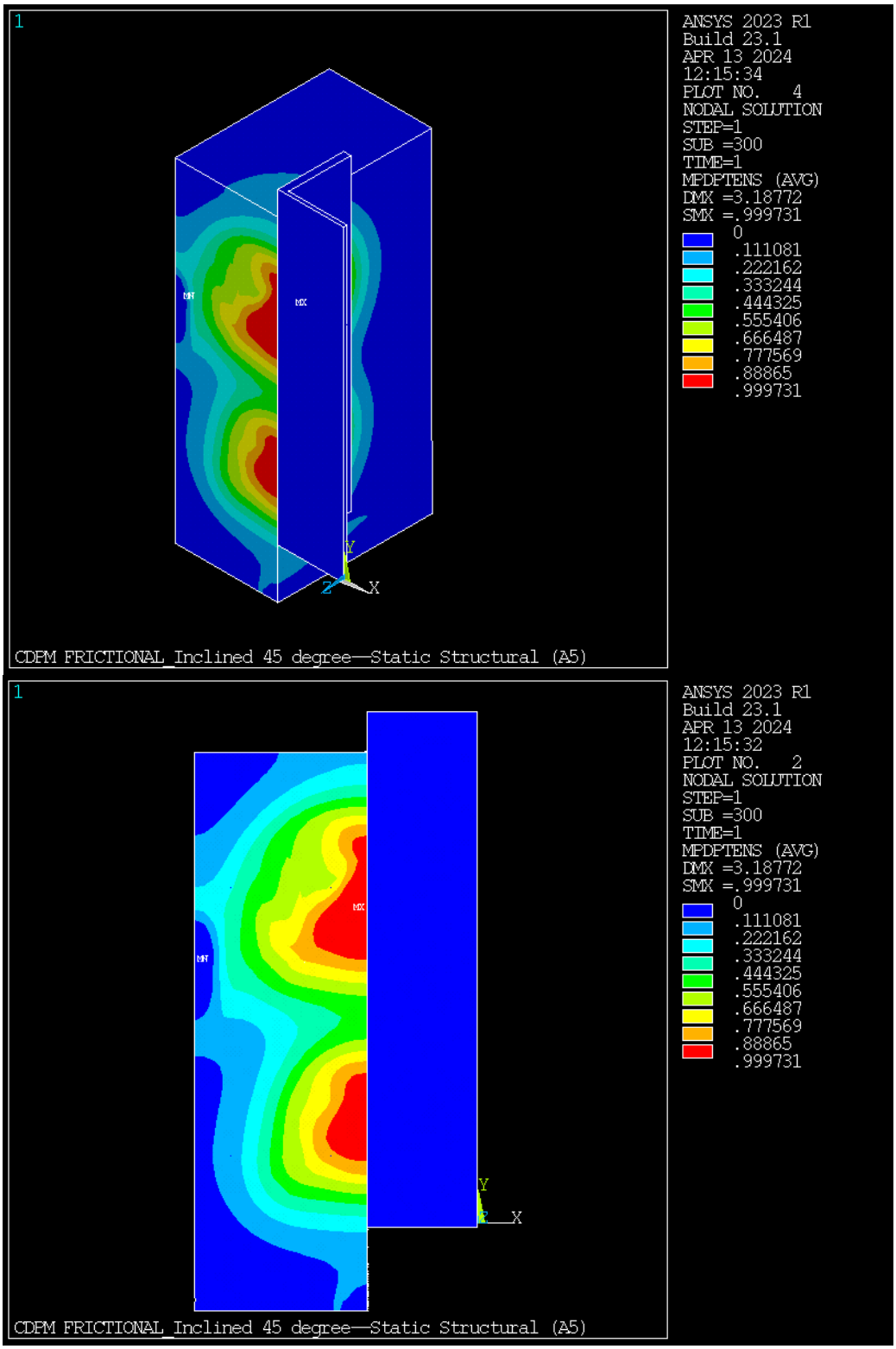

Fig. 4.44 Tension Damage for 45-Degree Inclined Headed Shear Stud

4.7.7 Force and Displacement Convergence

Fig. 4.45 and 4.46 shows the force and displacement convergence of push out test model for 45-degree inclined headed shear stud during the iteration process.

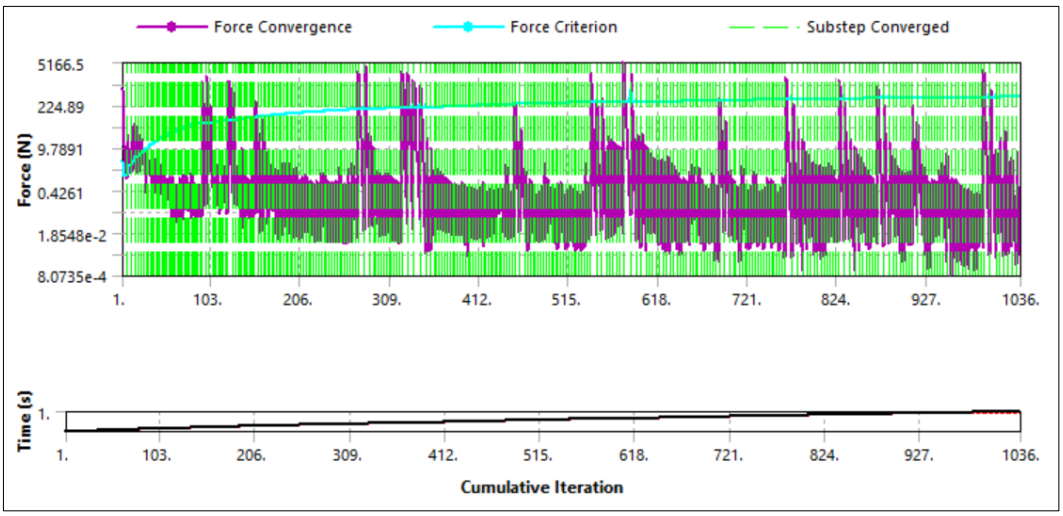

Fig. 4.45 Force Convergence for 45-Degree Inclined Headed Shear Stud

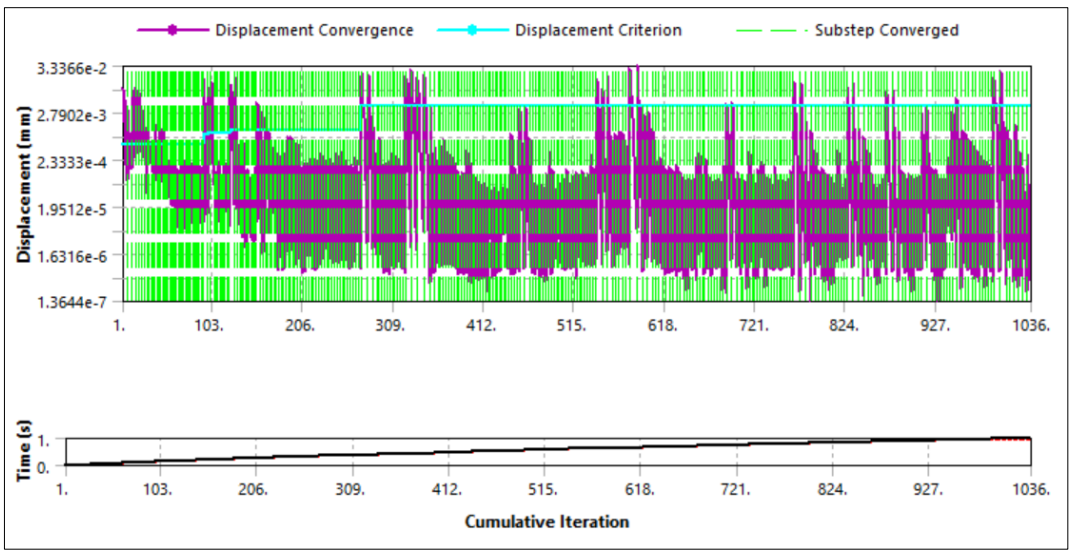

Fig. 4.46 Displacement Convergence for 45-Degree Inclined Headed Shear Stud

4.8 COMPARISON OF FE ANALYSIS RESULTS FOR PERPENDICULAR & INCLINED HEADED SHEAR STUD (HSS)

In this section finite element analysis results for perpendicular and different inclined headed shear stud are described.

4.8.1 Ultimate Shear Resistance & Maximum Displacement

Table 4.3, Fig. 4.47 & Fig. 4.48 show the maximum shear load carried by single headed shear stud and maximum displacement for perpendicular & inclined headed shear stud subjected to Downward (Push) & Upward (Pull) Displacement type Loading.

Table 4.3 Ultimate Shear Resistance & Maximum Displacement

Specimen	Maximum shear load per shear stud (KN)	Maximum Displacement (mm)	Failure Type
Perpendicular HSS	113.175	9.80	Concrete Failure
15 Degree Inclined HSS_Push	130.13	10.79	Concrete Failure
30 Degree Inclined HSS_Push	132.785	7.97	Concrete Failure
45 Degree Inclined HSS_Push	140.335	3.95	Concrete Failure
15 Degree Inclined HSS_Pull	49.97	2.44	Concrete Failure
30 Degree Inclined HSS_Pull	65.00	1.98	Concrete Failure
45 Degree Inclined HSS_Pull	60.06	1.07	Concrete Failure

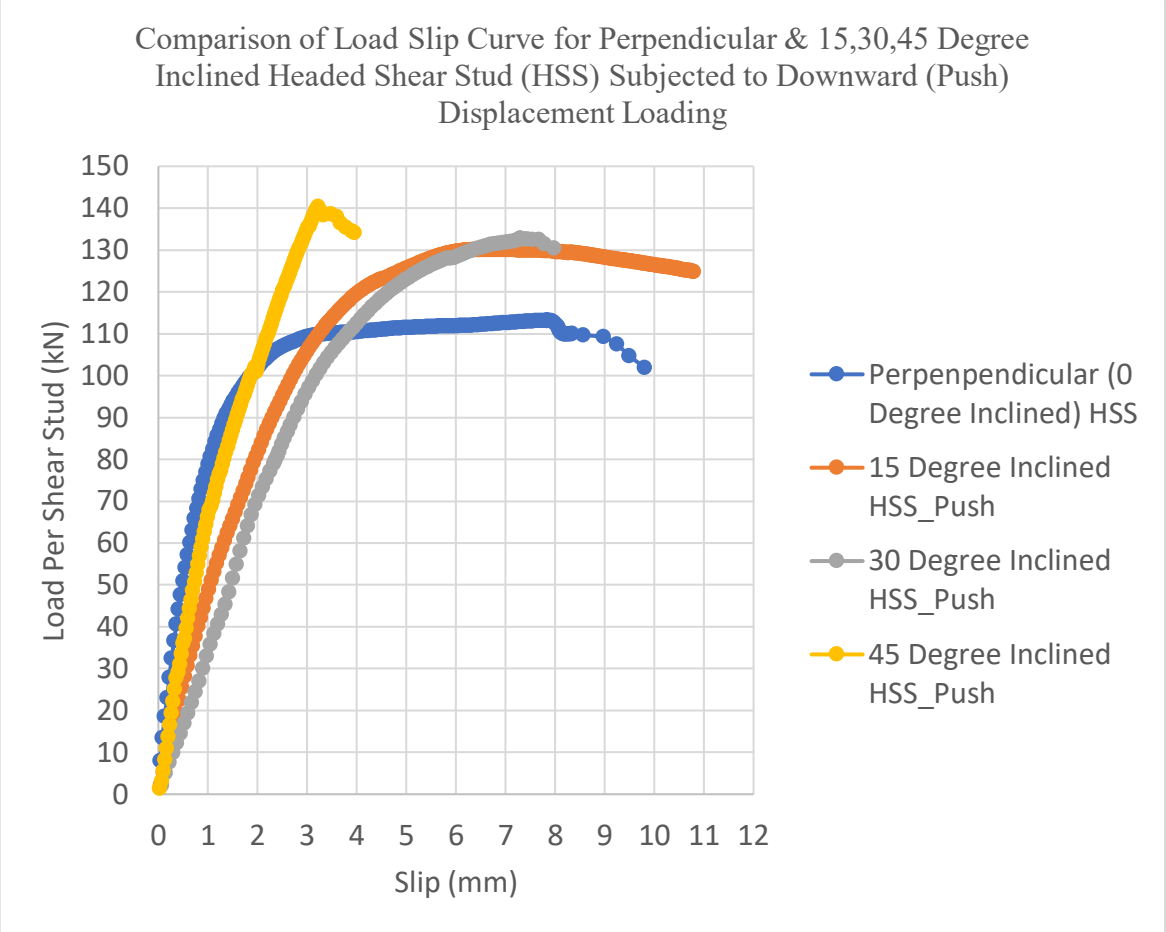

Fig. 4.47 Comparison of Load Slip Curve for Perpendicular & 15,30,45 Degree Inclined Headed Shear Stud (HSS) Subjected to Downward (Push) Displacement Loading

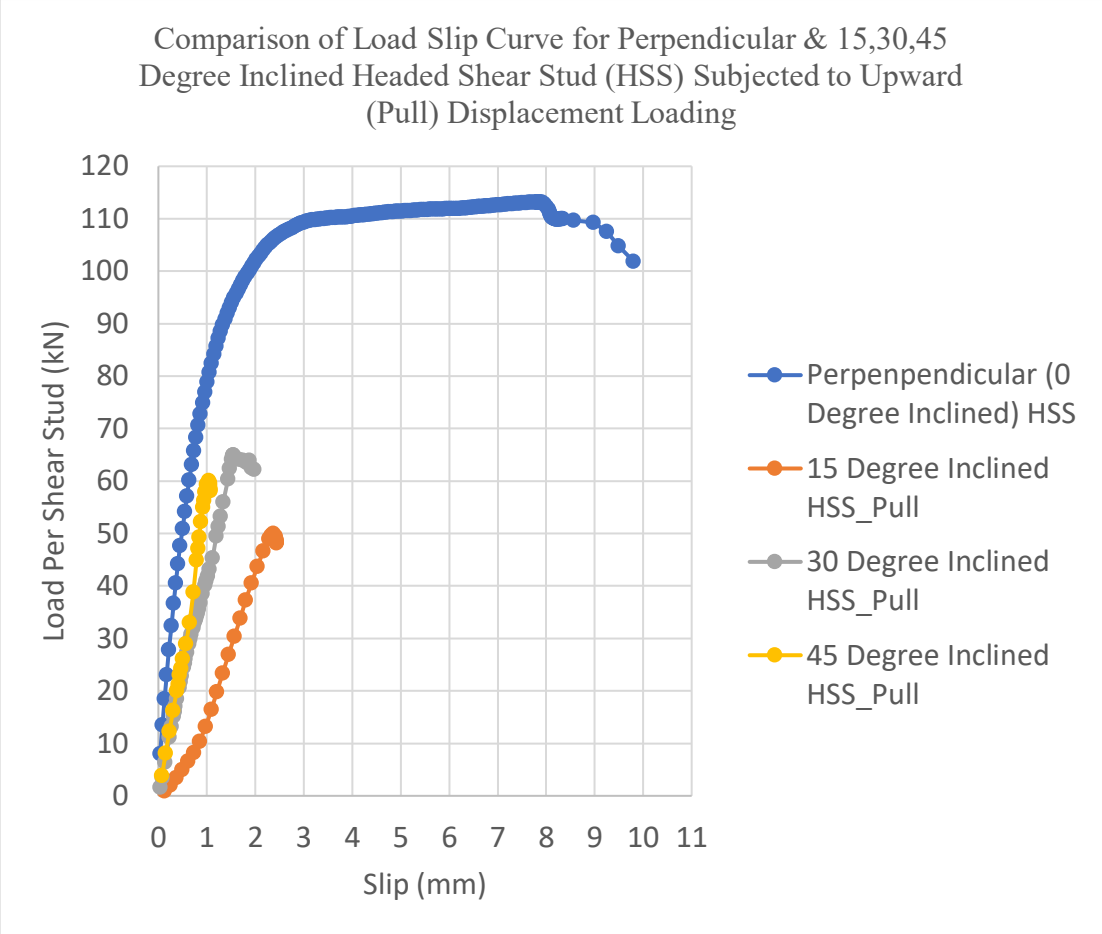

Fig. 4.48 Comparison of Load Slip Curve for Perpendicular & 15,30,45 Degree Inclined Headed Shear Stud (HSS) Subjected to Upward (Pull) Displacement Loading

4.8.2 Variation of Principal Stress in Concrete Slab

Fig. 4.49 to Fig. 4.52 show the variation of principal stress in concrete slab for perpendicular & different inclined headed shear stud. It is seen from the Fig. that the maximum compressive stress in concrete is generated below the stud shank for perpendicular headed shear stud but for inclined headed shear stud maximum compressive stress is generated at the concrete slab located at the top of the headed shear stud.

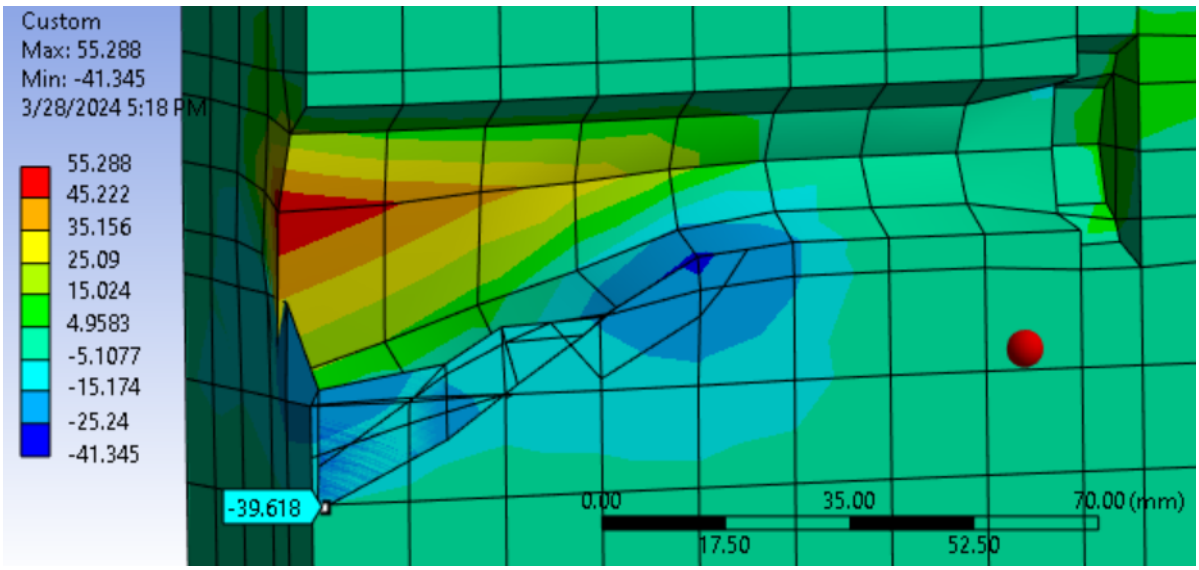

Fig. 4.49 Principal Stress Distribution in Concrete Slab for Perpendicular Headed Shear Stud (HSS)

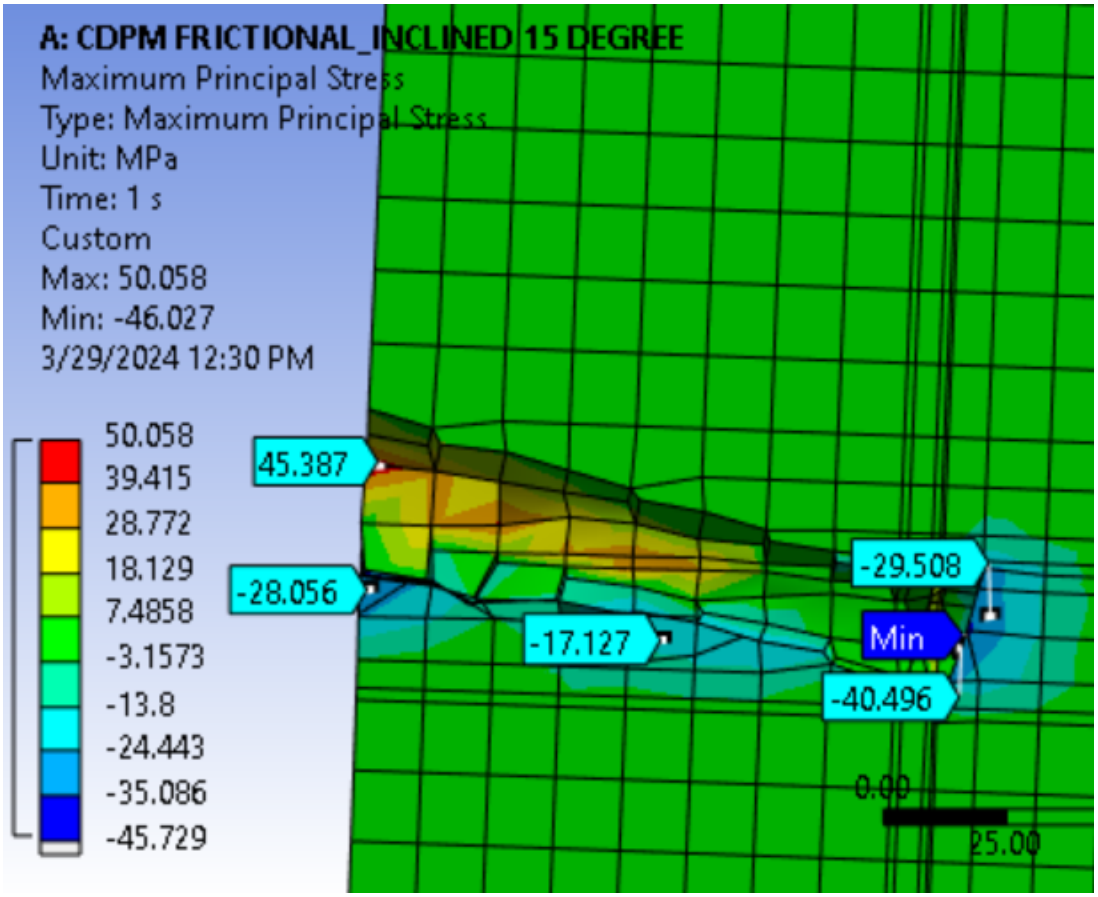

Fig. 4.50 Principal Stress Distribution in Concrete Slab for 15 Degree Inclined Headed Shear Stud (HSS)

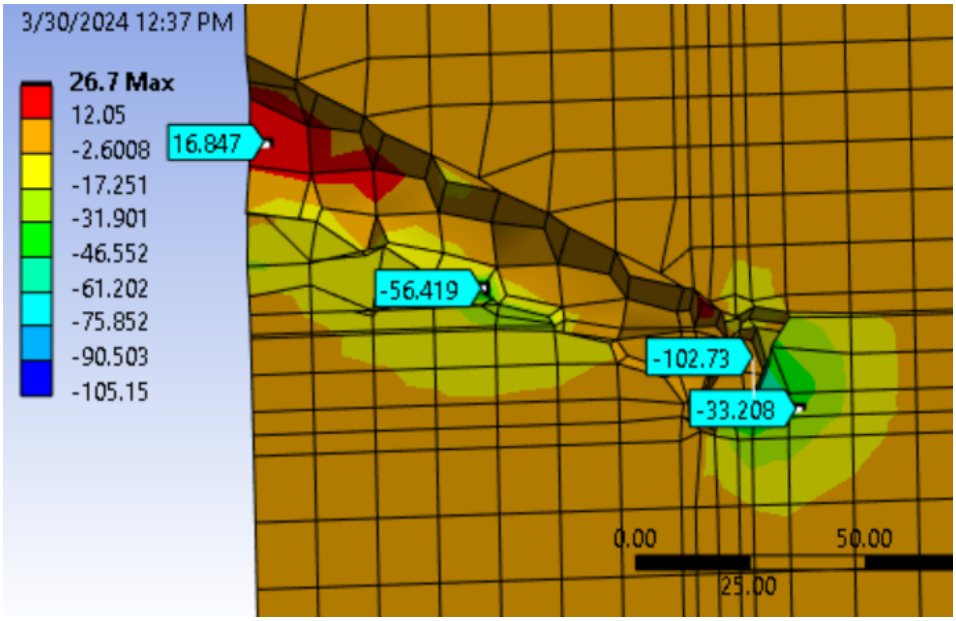

Fig. 4.51 Principal Stress Distribution in Concrete Slab for 30 Degree Inclined Headed Shear Stud (HSS)

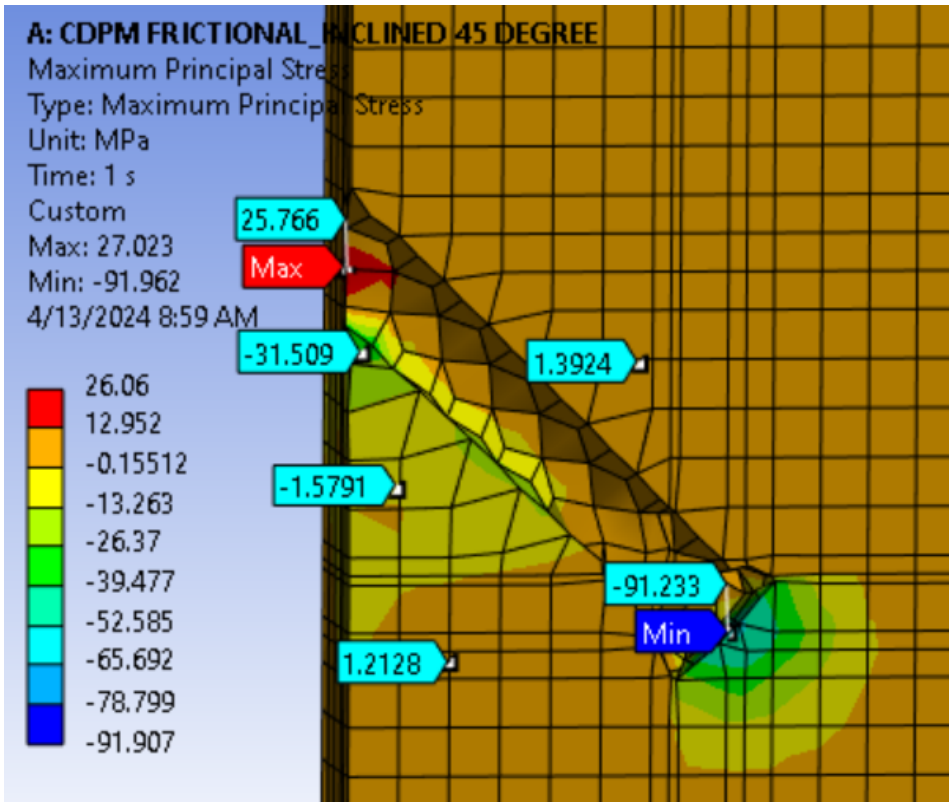

Fig. 4.52 Principal Stress Distribution in Concrete Slab for 45 Degree Inclined Headed Shear Stud (HSS)

4.8.3 Variation of Compression Damage of Concrete Slab

The damage caused by compression to concrete slab is depicted in Fig. 4.53. As can be observed from the Fig. 4.53, concrete's compressive stress is distributed more widely for a 15-degree inclined headed shear stud for which it's ductility is higher and less widely for a 45-degree inclined headed shear, so it is showing less ductility.

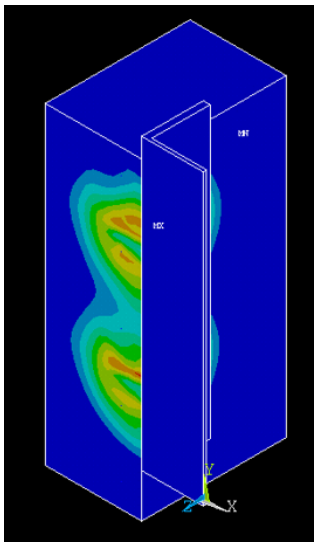

Perpendicular Headed Shear Stud

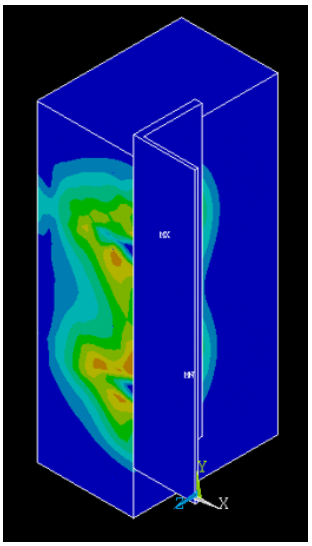

15- Degree Inclined Headed Shear Stud

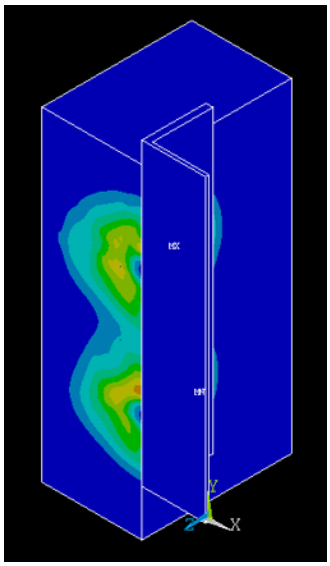

30-Degree Inclined Headed Shear Stud

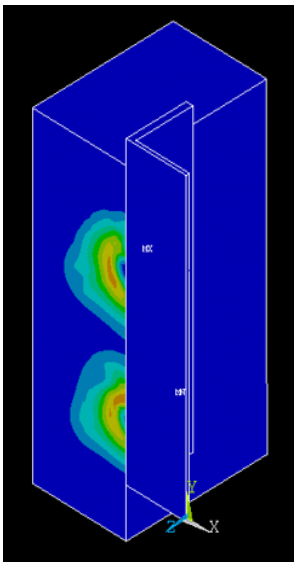

45-Degree Inclined Headed Shear Stud

Fig. 4.53 Variation of Compression Damage of Concrete Slab

Chapter 5: CONCLUSIONS & RECOMMENDATIONS

5.1 CONCLUSIONS

In this study numerical investigations of structural performance of inclined shear key in steel-composite construction is performed by standard push-out test according to Eurocode 4 using FEA software ANSYS. Followings are the conclusions from this numerical study

1. The ultimate shear load carried per shear stud, maximum slip & overall load-slip curve of the push-out test obtained from the finite element analysis is mostly identical with the test result conducted by Gattesco and Giuriani (1996) [51] for 19 mm diameter perpendicularly placed headed shear stud (HSS).
2. The ultimate shear resistance of a headed shear stud obtained from FE analysis is 113.175 KN, according to CSA S6-14, BNBC-2020 & AASHTO LRFD recommended design equations the ultimate shear resistance of a headed shear stud is 89.589 KN, 111.985 KN & 111.985 KN respectively. So, the numerical analysis result is very close to the BNBC-2020 & AASHTO LRFD but CSA S6-16 provides a conservative estimation of the ultimate shear strength of headed shear stud.
3. When the headed shear stud is inclined along the direction of loading as shown in Fig. 3.3.e, the ultimate shear load carried by a headed shear stud for 15-degree, 30-degree & 45-degree inclined headed shear stud is 130.13 KN, 132.785 KN & 140.335 KN respectively. So due to the inclination of the headed shear stud along the direction of loading, the ultimate shear load carrying capacity is increased by 15 %, 17.33 % & 24 % for 15, 30 & 45-degree inclination respectively.

4. When the headed shear stud is inclined opposite to the direction of loading as shown in Fig. 3.3.f, the ultimate shear load carried by a headed shear stud for 15-degree, 30-degree & 45-degree inclined headed shear stud is 49.97 KN, 65.00 KN & 60.06 KN respectively. So due to the inclination of the headed shear stud opposite to the direction of loading, the ultimate shear load carrying capacity is decreased by 56 %, 42.57 % & 46.93 % for 15, 30 & 45-degree inclination respectively.

5. When the headed shear stud is inclined along the direction of loading as shown in Fig. 3.3.e, maximum slip of a headed shear stud for 15-degree, 30-degree & 45-degree inclined headed shear stud is 10.79 mm, 7.97 mm & 3.95 mm respectively. So due to the inclination of the headed shear stud along the direction of loading, maximum slip value is increased for 15-degree & 30-degree and decreased for 45-degree inclination. As the minimum value of slip for ductile behaviour of headed shear stud is 6 mm as per the Eurocode-4, 15-degree & 30-degree inclined headed shear stud may be treated as ductile and 45-degree inclined headed shear stud may be considered as brittle.

6. When the headed shear stud is inclined opposite to the direction of loading as shown in Fig. 3.3.f, maximum slip of a headed shear stud for 15-degree, 30-degree & 45-degree inclined headed shear stud is 2.44 mm, 1.98 mm & 1.07 mm respectively. So due to the inclination of the headed shear stud opposite to the direction of loading, maximum slip value is decreased for all the headed shear studs. As the minimum value of slip for ductile behaviour of headed shear stud is 6 mm as per the Eurocode-4, headed shear stud inclined opposite to the direction loading may be considered as brittle.

7. Headed shear stud shall be welded to the flange surface very carefully. Only if the direction of loading is known, inclined shear keys may be a better choice for enhanced composite action of steel concrete composite structures.

5.2 RECOMMENDATIONS FOR FUTURE STUDY

Followings are the recommendations for future study related to this:

1. In this study only 19 mm diameter headed shear stud is considered. Performance of inclined headed shear stud having diameter larger or smaller than 19 mm may be investigated.
2. In the current study, only the numerical investigation is done. To verify the applicability of inclined headed shear stud in practical steel-concrete composite construction, detail experimental investigation may be done.
3. In this numerical study, push-out test specimen was prepared according to Eurocode 4 which contains total 8 nos. of headed shear stud on two sides. Future numerical and experimental study can be conducted considering BS5400 guideline for push-out test specimen which contain total 4 nos. of headed shear stud on two sides.
4. Structural performance of inclined shear can be investigated considering the variation of compressive strength of concrete and yield strength of headed shear stud.
5. Performance of inclined headed shear stud having larger embedment length in concrete can be investigated numerically and experimentally.

REFERENCES

[1] Lee, P. G., Shim, C. S., & Chang, S. P. (2005). Static and fatigue behavior of large stud shear connectors for steel–concrete composite bridges. Journal of constructional steel research, 61(9), 1270-1285.

[2] Shariati, M., Sulong, N. R., Shariati, A., & Kueh, A. B. H. (2016). Comparative performance of channel and angle shear connectors in high strength concrete composites: An experimental study. Construction and Building Materials, 120, 382-392.

[3] Deng, W., Xiong, Y., Liu, D., & Zhang, J. (2019). Static and fatigue behavior of shear connectors for a steel-concrete composite girder. Journal of Constructional Steel Research, 159, 134-146.

[4] Lungershausen, H. (1988). Zur Schubtragfähigkeit von Kopfbolzendübeln, Mitteilung Nr. 88-7.

[5] https://steelandtube.co.nz/specifiers/comflor

[6] https://www.nbmcw.com/product-technology/peb-steel-structures/composite-construction-in-pre-engineered-buildings.html

[7] Begum, M., SERAJUS, S. M., TAUHID, B. K. N., & Ahmed, W. (2013). Cost analysis of steel concrete composite structures in Bangladesh.

[8] Pelke, E., & Kurrer, K. E. (2015, June). On the evolution of steel-concrete composite construction. In Fifth International Congress on Construction History (pp. 107-116).

[9] https://www.escglobalgroup.com/post/steel-concrete-composite-construction

[10] Salmon, C. G., & Johnson, J. E. (2009). Steel structures: design and behavior: emphasizing load and resistance factor design. (No Title).

[11] Ollgaard, J. G., Slutter, R. G., & Fisher, J. W. (1971). Shear strength of stud connectors in lightweight and normal weight concrete, AISC Eng'g Jr., April 1971 (71-10). AISC Engineering journal, 55-34.

[12] Lee, P. G., Shim, C. S., & Chang, S. P. (2005). Static and fatigue behavior of large stud shear connectors for steel–concrete composite bridges. Journal of constructional steel research, 61(9), 1270-1285.

[13] Deng, W., Xiong, Y., Liu, D., & Zhang, J. (2019). Static and fatigue behavior of shear connectors for a steel-concrete composite girder. Journal of Constructional Steel Research, 159, 134-146.

[14] Liu, Y., Zhang, Q., Bao, Y., & Bu, Y. (2019). Static and fatigue push-out tests of short headed shear studs embedded in Engineered Cementitious Composites (ECC). Engineering Structures, 182, 29-38.

[15] Viest, I. M. (1956, April). Investigation of stud shear connectors for composite concrete and steel T-beams. In Journal Proceedings (Vol. 52, No. 4, pp. 875-892).

[16] Leonhardt, F., Andrä, W., Andrä, H. P., & Harre, W. (1987). Neues, vorteilhaftes Verbundmittel für Stahlverbund-Tragwerke mit hoher Dauerfestigkeit. Beton-und Stahlbetonbau, 82(12), 325-331.

[17] Oguejiofor, E. C., & Hosain, M. U. (1992). Behaviour of perfobond rib shear connectors in composite beams: full-size tests. Canadian Journal of Civil Engineering, 19(2), 224-235.

[18] Oguejiofor, E. C., & Hosain, M. U. (1994). A parametric study of perfobond rib shear connectors. Canadian Journal of Civil Engineering, 21(4), 614-625.doi:10.1139/l94-063.

[19] Oguejiofor, E. C., & Hosain, M. U. (1997). Numerical analysis of push-out specimens with perfobond rib connectors. Computers & Structures, 62(4), 617-624.

[20] Vellasco, P. D. S., De Andrade, S. A. L., Ferreira, L. T. S., & De Lima, L. R. O. (2007). Semi-rigid composite frames with perfobond and T-rib connectors Part 1: Full scale tests. Journal of Constructional Steel Research, 63(2), 263-279.

[21] Vianna, J. D. C., Costa-Neves, L. F., Vellasco, P. D. S., & De Andrade, S. A. L. (2009). Experimental assessment of Perfobond and T-Perfobond shear connectors' structural response. Journal of Constructional Steel Research, 65(2), 408-421.

[22] Ahn, J. H., Kim, S. H., & Jeong, Y. J. (2008). Shear behaviour of perfobond rib shear connector under static and cyclic loadings. Magazine of Concrete Research, 60(5), 347-357.

[23] Vianna, J. D. C., De Andrade, S. A. L., Vellasco, P. D. S., & Costa-Neves, L. F. (2013). Experimental study of Perfobond shear connectors in composite construction. Journal of Constructional Steel Research, 81, 62-75.

[24] Costa-Neves, L. F., Figueiredo, J. P., Vellasco, P. D. S., & da Cruz Vianna, J. (2013). Perforated shear connectors on composite girders under monotonic loading: An experimental approach. Engineering Structures, 56, 721-737.

[25] Rodrigues, J. P. C., & Laím, L. (2014). Experimental investigation on the structural response of T, T-block and T-Perfobond shear connectors at elevated temperatures. Engineering structures, 75, 299-314.

[26] Kim, S. H., Choi, K. T., Park, S. J., Park, S. M., & Jung, C. Y. (2013). Experimental shear resistance evaluation of Y-type perfobond rib shear connector. Journal of constructional steel research, 82, 1-18.

[27] Kim, S. H., Choi, J., Park, S. J., Ahn, J. H., & Jung, C. Y. (2014). Behavior of composite girder with Y-type perfobond rib shear connectors. Journal of Constructional Steel Research, 103, 275-289.

[28] Kim, S. H., Heo, W. H., Woo, K. S., Jung, C. Y., & Park, S. J. (2014). End-bearing resistance of Y-type perfobond rib according to rib width–height ratio. Journal of Constructional Steel Research, 103, 101-116.

[29] Kim, S. H., Park, S. J., Heo, W. H., & Jung, C. Y. (2015). Shear resistance characteristic and ductility of Y-type perfobond rib shear connector. Steel and Composite Structures, 18(2), 497-517.

[30] Kim, S. H., Kim, K. S., Park, S., Ahn, J. H., & Lee, M. K. (2016). Y-type perfobond rib shear connectors subjected to fatigue loading on highway bridges. Journal of Constructional Steel Research, 122, 445-454.

[31] Kim, S. H., Kim, K. S., Lee, D. H., Park, J. S., & Han, O. (2017). Analysis of the shear behavior of stubby Y-type perfobond rib shear connectors for a composite frame structure. Materials, 10(11), 1340.

[32] Kim, S. H., Park, S., Kim, K. S., & Jung, C. Y. (2017). Generalized formulation for shear resistance on Y-type perfobond rib shear connectors. Journal of Constructional Steel Research, 128, 245-260.

[33] Kopp, M., Wolters, K., Claßen, M., Hegger, J., Gündel, M., Gallwoszus, J., ... & Feldmann, M. (2018). Composite dowels as shear connectors for composite beams–Background to the design concept for static loading. Journal of Constructional Steel Research, 147, 488-503.

[34] Seidl, G., Petzek, E., & Băncilă, R. (2013). Composite dowels in bridges-efficient solution. Advanced Materials Research, 814, 193-206.

[35] Hechler, O., Berthellemy, J., Lorenc, W., Seidl, G., & Viefhues, E. (2011). Continuous shear connectors in bridge construction. In Composite construction in steel and concrete VI (pp. 78-91).

[36] Dudziński, W., Pękalski, G., Harnatkiewicz, P., Kopczyński, A., Lorenc, W., Kożuch, M., & Rowiński, S. (2011). Study on fatigue cracks in steel-concrete shear connection with composite dowels. Archives of Civil and Mechanical Engineering, 11(4), 839-858.

[37] Lorenc, W., Kożuch, M., & Rowiński, S. (2014). The behaviour of puzzle-shaped composite dowels—Part I: Experimental study. Journal of Constructional Steel Research, 101, 482-499.

[38] Shariati, M., Ramli Sulong, N. H., Shariati, A., & Khanouki, M. A. (2016). Behavior of V-shaped angle shear connectors: experimental and parametric study. Materials and Structures, 49, 3909-3926.

[39] Balasubramanian, R., & Rajaram, B. (2016). Study on behaviour of angle shear connector in steel-concrete composite structures. International Journal of Steel Structures, 16, 807-811.

[40] Hicks, S., Cao, J., McKenzie, C., Chowdhury, M., & Kaufusi, R. (2016). Evaluation of shear connectors in composite bridges (No. 602).

[41] Deng, W., Gu, J., Liu, D., Hu, J., & Zhang, J. (2019). Study of single perfobond rib with head stud shear connectors for a composite structure. Magazine of Concrete Research, 71(17), 920-934.

[42] Gu, J. C., Liu, D., Deng, W. Q., & Zhang, J. D. (2019). Experimental study on the shear resistance of a comb-type perfobond rib shear connector. Journal of Constructional Steel Research, 158, 279-289.

[43] Bangladesh National Building Code (BNBC)-2020

[44] Slutter, R. G., & Driscoll, G. C. (1961, May). Research on Composite Desing at Lehigh University Proceedings. In National Engineering Conference, AISC.

[45] Mainstone, R. J., & Menzies, J. B. (1967). SHEAR CONNECTORS IN STEEL-CONCRETE COMPOSITE BEAMS FOR BRIDGES. I. STATIC AND FATIGUE TESTS ON PUSH-OUT SPECIMENS. Concrete, 1(9), 291-+.

[46] Hallam, M. W. (1976). The behaviour of stud shear connectors under repeated loading (Vol. 281, No. Resh Rpt.).

[47] Oehlers, D. J., & Foley, L. (1985). The fatigue strength of stud shear connections in composite beams. Proceedings of the Institution of Civil Engineers, 79(2), 349-364.

[48] Prakash, A., Anandavalli, N., Madheswaran, C. K., & Lakshmanan, N. (2012). Modified push-out tests for determining shear strength and stiffness of HSS stud connector-experimental study. International Journal of Composite Materials, 2(3), 22-31.

[49] Mia, M. M., & Bhowmick, A. K. (2019, June). A finite element-based approach for fatigue life prediction of headed shear studs. In Structures (Vol. 19, pp. 161-172). Elsevier.

[50] Nguyen, H. T., & Kim, S. E. (2009). Finite element modeling of push-out tests for large stud shear connectors. Journal of Constructional Steel Research, 65(10-11), 1909-1920.

[51] Gattesco, N., & Giuriani, E. (1996). Experimental study on stud shear connectors subjected to cyclic loading. Journal of Constructional Steel Research, 38(1), 1-21.

[52] ENV, D. (1994). 2: 2001," Eurocode 4: Design of Composite Steel and Concrete Structures," Part 2: Composite Bridges.

[53] AASHTO LRFD. Bridge design specifications. 3rd ed. American Association of State Highway and Transportation Officials; 2004

[54] Zreid, I., & Kaliske, M. (2014). Regularization of microplane damage models using an implicit gradient enhancement. International Journal of Solids and Structures, 51(19-20), 3480-3489.

[55] Zreid, I., & Kaliske, M. (2016). An implicit gradient formulation for microplane Drucker-Prager plasticity. International Journal of Plasticity, 83, 252-272.

[56] Zreid, I., & Kaliske, M. (2018). A gradient enhanced plasticity–damage microplane model for concrete. Computational Mechanics, 62(5), 1239-1257.

[57] Ansys® ANSYS Mechanical APDL, Release 23 R2 July 2023, Help System, Element Reference, ANSYS, Inc.

[58] Alhusban, M., & Parvin, A. (2022). Finite Element Analysis of Axially Loaded RC Walls with Openings Strengthened Using Textile Reinforced Mortar for Sustainable Structures. Buildings, 12(11), 1993.

[59] ANSYS®. Academic Research Mechanical Release 18; Help System; ANSYS, Inc.: Canonsburg, PA, USA, 2018. Available online: http://www.ansys.com

[60] Rabbat, B. G., & Russell, H. G. (1985). Friction coefficient of steel on concrete or grout. Journal of Structural Engineering, 111(3), 505-515.

[61] Baltay, P., & Gjelsvik, A. (1990). Coefficient of friction for steel on concrete at high normal stress. Journal of Materials in Civil Engineering, 2(1), 46-49.

[62] https://help.solidworks.com/2021

[63] https://ansyshelp.ansys.com

APPENDICES

A 1.1 Coupled Damage-Plasticity Microplane Model APDL Code Input in ANSYS

```
! === Start Code ===

! This means these commands will be carried out during pre-processing
/PREP7

! Step 1: Define elastic properties of material
E = 24000! Young's Modulus, MPa
nu = 0.2 ! Poisson's Ratio, unitless

! Step 2: Define microplane model properties
fc = 26  ! Uniaxial compressive strength, MPa
fb = 29.9! Biaxial compressive strength, MPa(estimate as 1.15*fc if unknown)
ft = 2.6 ! Tensile strength, MPa(estimate as 0.1*fc if unknown)
Rt = 1   ! Tension cap hardening constant, unitless  (typically = 1)
D = 40000! Compressive hardening constant, MPa^2
           (typically between 1e4 and 50e4)
sigma_cv = -19.93! Int. of comp. cap and DP yield, MPa
                  (always negative, approximately -2/3*fb or lower)
Rc = 2! Compression cap ratio constant, unitless(typically = 2)
gamma_t = 0! Tensile damage threshhold, unitless(typically = 0)
gamma_c = 2e-5! Compressive damage threshhold, unitless
                (typically between 1e-5 to 10e-5)
beta_t = 9000! Tension damage evolution, unitless(typically 1.5*beta_c)
beta_c = 6000! Compression damage evolution, unitless
               (typically between 1000 and 10000)


! Step 3: Define nonlocal parameters c and m
c = 1500! Nonlocal range parameter,mm^2(element size should be < 0.5*sqrt(c))
m = 2.5 ! Over-nonlocal parameter, unitless(typically 1 to 3)

! Step 4: Select element type
element = 215! Element type number (Linear = 215, Quadratic = 216)

! Assign Elastic Properties
MP,EX,conc,E       ! Assign Young's Modulus
MP,NUXY,conc,nu    ! Assign Poisson's Ratio

! Assign microplane properties for coupled damaged-plasticity (MPLANE-DPC)
TB,MPLANE,conc,,,DPC
TBDATA,1,fc,fb,ft,Rt,D,sigma_cv
TBDATA,7,Rc,gamma_t,gamma_c,beta_t,beta_c

! Assign nonlocal properties to microplane model (MPLANE-NLOCAL)
TB,MPLANE,conc,,,NLOCAL
TBDATA,1,c,m
```

```
! Define coupled elements (this code assumes ITYPE = matid, which should be
in almost all cases)
itype = conc

et,itype,element
keyopt,itype,18,2! Element needs 2 nonlocal parameters for keyopt(18)

! Switch element type of those that are assigned Concrete
esel,s,mat,,conc
emodif,all,type,itype

! To check that everything worked out, print the element list
allsel
etlist,all

! Now proceed to the solution and output all results
/SOLU
outres,aeso,all

! Setting minimum number of equilibrium iteration to 50
neqit,50
```